

AMERICAN UNIVERSITY OF BEIRUT

INVESTIGATING THE ANTICANCER POTENTIAL OF
NOVEL THERAPEUTICS USING 3D MODEL SYSTEMS OF
COLON CANCER

by
ALISSAR ATEF MONZER

A Dissertation
submitted in partial fulfillment of the requirements
for the degree of Doctor of Philosophy
to the Department of Biology
of the Faculty of Arts and Sciences
at the American University of Beirut

Beirut, Lebanon
January 2022

AMERICAN UNIVERSITY OF BEIRUT

INVESTIGATING THE ANTICANCER POTENTIAL OF
NOVEL THERAPEUTICS USING 3D MODEL SYSTEMS OF
COLON CANCER

by
ALISSAR ATEF MONZER

Approved by:



Dr. Rabih Talhouk, Professor
Department of Biology

Chair



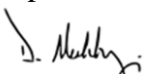
Dr. Hala Muhtasib, Professor
Department of Biology

Advisor



Dr. Wassim Abou-Kheir, Associate Professor
Department of Anatomy, Cell Biology & Physiological Sciences

Co-advisor



Dr. Deborah Mukherji, Associate Professor
Department of Internal Medicine

Member

Tamara Abou-Antoun

Dr. Tamara Abou-Antoun, Associate Professor
School of Pharmacy, LAU

External Member



Dr. Ihab Younis, Associate Teaching Professor
Biological Sciences Program, CMU-Q

External Member

Date of dissertation defense: January 27, 2022

AMERICAN UNIVERSITY OF BEIRUT

DISSERTATION RELEASE FORM

Student Name: Monzer Alissar Atef
Last First Middle

I authorize the American University of Beirut, to: (a) reproduce hard or electronic copies of my dissertation; (b) include such copies in the archives and digital repositories of the University; and (c) make freely available such copies to third parties for research or educational purposes:

- As of the date of submission
- One year from the date of submission of my dissertation.
- Two years from the date of submission of my dissertation.
- Three years from the date of submission of my dissertation.



Alissar Monzer February 6, 2022
Signature Date

ACKNOWLEDGMENTS

When attempting to explain my journey to my PhD dissertation, I am filled with many emotions. Looking back over the years, I am reminded of the challenges I have faced, the experiences I have gained and the lessons I have learned.

My journey has been filled with significant wins and life-changing losses. Regardless of what has occurred, I have been truly blessed and fortunate throughout this journey. I have built relationships that will last a lifetime, created memories that bring warmth to my heart, and gained knowledge and wisdom that will shape my life and future to come. I would like to express my sincerest gratitude to the following individuals who have made it possible for me to be here.

To my key advisors: Dr. Hala Muhtasib and Dr. Wassim Abou-Kheir. Dr. Hala Muhtasib, your immense knowledge has been a key attribute in my professional growth and dissertation. Thank you for your never-ending compassion, empathy and care. Your feedback has helped me to succeed and forced me to set my standards of work high.

Dr. Wassim Abou-Kheir, from the moment we met, you created a positive influence in my life. You have brought light into my life during dark times. Thank you for believing in me, guiding me and pushing me to become the best version of myself. Your compassion, encouragement and support will be forever remembered and cherished. I am so thankful to have had an amazing mentor like you in my life. Forever I will be grateful.

Second, I would like to express my gratitude for the committee members: Dr. Deborah Mukherji, Dr. Tamara Abou-Antoun, Dr. Ihab Younis, and Dr. Rabih Talhouk, for their valuable input and meticulous remarks and questions. Thank you for the time spent in reviewing this dissertation.

HM and WAK lab members, past and present, thank you for your love, support and friendship over the years, I will forever cherish our time and memories together. You have become my second family, not through blood but choice. While our next steps in life may be in varying directions, our bond will flourish and hold us together forever. Some of us will be lucky and end up in sunny destinations like my partner in crime, Farah Ballout.

I must make a special thank you to Kevork, Farah, Samar, Maya and Amani. Your assistance and resourcefulness have been instrumental in my research. Thank you for all of your help in the past year.

To my family, I dedicate this work. My beautiful mother Sana, because of you, I have the vision to reach for my dreams, and the grit to push through the challenges that come

my way. I could never even hope to express just how much appreciation I hold in my heart for you.

My brother Rafaat, thank you for inspiring me to pursue my ambitions and pushing me to work hard towards my goal. You are the driving force behind my success.

My sister Meera, there is no adequate way to express my gratitude to the sister who is always there, always kind, and always generous. You are a pure shining ray of sunshine in my life. I do not know what I would do without you. Thank you.

To my husband Michael, thank you for your unconditional love and support. Thank you for always believing in me, even when I did not believe in myself. Thank you for pushing me to become the best version of myself. You are not only my husband but are my backbone, my partner, my blessing and a piece of my heart.

To all my relatives, friends and colleagues, your love and support have not gone unnoticed! Thank you for believing in me and supporting me! Without you, I would not have made it here. There are truly not enough thank yous!

Lastly but most importantly, I would like to dedicate this accomplishment to my father. You are the one who believed in me and pushed me to pursue my PhD. While I am truly at a loss for words when I attempt to express what you mean to me. Everything you have taught me in life has brought me to this moment. From day one, you have been my mentor, my backbone, my love, my support and my forever hero! Your lessons and wisdom will forever provide me guidance to any challenge or obstacle that comes my way. I am internally grateful for the sacrifices that you have made in return for my success. If it was not for you, I would not have made it to this milestone and I would not have become the person I am today. While your absence brings pain, my heart remains full with your imprint. This accomplishment is both of our dream. You are my biggest supporter and I owe you all of my success. I know you are smiling and sharing my success. I am truly blessed beyond measures to call you my father. I will love you forever and always!

In the dedication of ATEF MONZER, this one is for YOU!

ABSTRACT OF THE DISSERTATION OF

Alissar Atef Monzer

for Doctor of Philosophy
Major: Cell and Molecular Biology

Title: Investigating the Anticancer Potential of Novel Therapeutics Using 3D Model Systems of Colon Cancer

Background:

Chemotherapy for colorectal cancer (CRC), the second leading disease of cancer-related mortality, has so far revealed partial success. Cancer stem cells (CSCs) in CRC, which are spared by many chemotherapeutics, have tumorigenic capacity and are believed to be the reason behind cancer relapse. The inadequate response to 5-fluorouracil (5FU), the first-line therapy for advanced CRC, might be caused by surviving CSCs. So far, there have been no effective drugs to target colon CSCs. The identification of novel therapeutics that simultaneously target CSCs and chemo-resistant cells is a major challenge and is of high importance for successful cancer treatment. Quinones and imipridone have shown promising effect on targeting different types of cancer. However, research on the effects of DIQ, ONC201 and ONC206 to target CSCs in CRC is very limited.

Objective: The overall aim of this thesis is to investigate the anticancer activities and targeting mechanism(s) of three novel therapeutics, diiminoquinone DIQ, and the imipridone DRD2 antagonists ONC201 and ONC206, against human colon cancer cells with stem-like properties both in 2D and in 3D using colonosphere cultures and patient-derived organoids. Our first aim was to assess the toxicity of DIQ, ONC201 and ONC206 to non-tumorigenic colon FHS cells and their ability to target colon cancer stem cells in HCT116 and HT29 cells. In this aim, we used 3D sphere-formation assays to enrich cancer stem cells (CSCs) in the human colorectal cancer cell lines and determine mechanism(s) of DIQ and ONC206 for targeting colon cancer self-renewal capacity. The second aim was to establish three-dimensional patient-derived colon cancer organoid cultures and assess the effect of DIQ, ONC201 and 206 on them.

Methods: We first assessed the safety of DIQ, ONC201 and ONC206 on non-tumorigenic FHS74Int cells in comparison to their anticancer activity against colon cancer HCT116 and HT29 cells. Cell cycle analysis and reactive oxygen species (ROS) production in response to DIQ, ONC201 and ONC206 were investigated using propidium iodide and dihydroethidium staining, respectively. Invasion and migration ability of DIQ, ONC201 and ONC206 were assessed using wound healing and transwell invasion assays, respectively. Then, we tested their efficacy on sphere formation, sphere

size, and self-renewal capacity of spheres derived from colon cancer cell lines grown in 3D setting for up to 5 generations. Immunofluorescent analysis and western blot were used to determine the mechanism of action. For the second aim, we established colon cancer patient derived organoids from fresh tissue samples from consented patients with different stages of CRC undergoing colectomy at the American University of Beirut Medical Center (AUBMC, Beirut, Lebanon) according to appropriate Institutional Review Board (IRB) approval guidelines. Patient organoid model was used to assess DIQ, ONC201 and ONC206 response in comparison to 5FU. The effects of DIQ, ONC201 and ONC206 on organoids growth were evaluated by quantifying the number of organoids formed (OFC) and calculating the average size (diameters). Colon patient-specific organoids were characterized using immunofluorescent staining. Statistical analysis was performed using Graphpad prism 7.

Results: Our results showed that DIQ, ONC201 and ONC206 significantly inhibited cell proliferation, migration, and invasion in HCT116 and HT29 cell lines. DIQ, ONC201 and ONC206 treatments induced apoptosis along with an accumulation of HCT116 and HT29 cancer cells in the sub-G1 region and an increase in ROS in both CRC cell lines. DIQ, ONC201 and ONC206 significantly reduced sphere-forming and self-renewal ability of colon cancer HCT116 and HT29 stem/progenitor cells by eradication of the propagated spheres at sub-toxic doses up to generation 5 (G5). Mechanistically, DIQ and ONC206 targeted CSCs by reducing the proliferation marker Ki67 and CRC stem cell markers CD44, CD133 and CK19, as well as inducing DNA damage through decreasing gamma-H2AX (γ -H2AX) expression and downregulating the main components of stem cell-related β -catenin, AKT and ERK oncogenic signaling pathways. Potently, DIQ, ONC201, and ONC206 displayed a highly significant decrease in both the count and the size of the organoids derived from colon cancer patients as compared to control and 5FU conditions.

Conclusion: This study represents the first documentation of the molecular mechanism of the novel anticancer therapeutics DIQ, ONC201 and ONC206 via targeting CSCs, findings that will certainly have therapeutic implications for colon cancer patients.

TABLE OF CONTENTS

ACKNOWLEDGEMENTS.....	1
ABSTRACT.....	3
ILLUSTRATIONS.....	9
TABLES.....	13
ABBREVIATIONS.....	14
INTRODUCTION.....	17
A. Colorectal Cancer.....	17
1. Colon Cancer Epidemiology.....	17
2. Colon Anatomy and Function.....	19
3. Colorectal Cancer Initiation and Progression	20
4. Stages and Treatments of Colorectal Cancer.....	22
B. Cancer Stem Cells.....	24
1. Overview.....	24
2. Colorectal Cancer Stem Cells.....	25
3. Targeting Colorectal Cancer Stem Cells	28
C. Three-Dimensional Models for Colorectal Cancer Stem Cells.....	30
1. Overview of Three-Dimensional Models.....	30
2. Sphere Model.....	30
3. Patient-Derived Organoid Model	32
4. Advantages of Three-Dimensional Models Versus Two-Dimensional Models..	34
5. Limitations of 3D Models.....	36
D. Diiminoquinone DIQ.....	37
1. Overview.....	37

2. Anticancer activity of Quinones in Colorectal Cancer.....	39
E. Impiridone DRD2 Antagonists.....	41
1. ONC201	41
a. Anticancer Activity of ONC201 in Colorectal Cancer.....	43
2. ONC206.....	43
F. Aim of the Study.....	45
METHODS.....	47
A. Cell Culture Conditions.....	47
B. Drug Preparation and Treatment.....	47
C. MTT Cell Proliferation Assay.....	48
D. Trypan Blue Exclusion Assay.....	48
E. Wound Healing Assay.....	49
F. Transwell Invasion Assay.....	49
G. Reactive Oxygen Species.....	50
H. Cell Cycle Analysis.....	50
I. Annexin V- PI Staining	51
J. Sphere Formation Assay	51
K. Sphere Propagation Assay	52
L. 3D Imaging of Colonospheres.....	52
M. Western Blot Analysis.....	53
N. Ethical Consideration.....	54
O. Tissue Processing and Organoid Culture	55
P. Passaging of the Newly Established Organoids	56
Q. Cell Line-Derived Organoids.....	57
R. Immunofluorescence and Morphological Analysis of Organoids	57

S. Animal Experiments	58
T. Microscope Imaging	59
U. Statistical Analysis.....	59
RESULTS.....	62
A. Effect of DIQ, ONC201 and ONC206 Compounds on the Cell Proliferation of Human Non-Tumorigenic and Colorectal Cancer Cell Lines in 2D <i>in vitro</i> Models.....	62
B. Effect of DIQ, ONC201 and ONC206 on Migration and Invasion Ability of Colorectal Cancer Cells.....	70
C. Effect of DIQ, ONC201 and ONC206 on Cell Cycle and Apoptosis in Colorectal Cancer Cells.....	73
D. Effect of DIQ, ONC201 and ONC206 on the Production of Reactive Oxygen Species (ROS) in Colorectal Cancer Cells.....	77
E. DIQ, ONC201 and ONC206 Effects on the Expression of the Survival, Proliferation, and Stem Cell Markers in Colorectal Cancer Cells	78
F. Establishing DIQ, ONC201 and ONC206 Effects on an Enriched Population of Human Colorectal Cancer Stem Cells in 3D.....	82
1. Effect of DIQ, ONC201 and ONC206 on HCT116 and HT29 Sphere Counts and Sizes	82
2. DIQ and ONC206 Effect on Proliferation, Epithelial and Stem Cell Markers Expression in 3D Colonospheres.....	90
3. DIQ has Anti-Tumor Potential in NOD-SCID Mice Injected with HCT116 Spheres.....	99
G. Assessment of the Effect of DIQ, ONC201 and ONC206 Treatments on the Established Colon Cancer Patient Derived Organoids.....	100
1. Organoids as Models for DIQ, ONC201 and ONC206 Assessment.....	100
2. DIQ, ONC201 and ONC206 Assessment on Cell-Derived Organoids from Colorectal Cancer Cell Lines	109
3. DIQ Assessment on Patient-Derived Organoids from a Different Solid Tumor Prostate Cancer.....	112

DISCUSSION..... 116

BIBLIOGRAPHY..... 127

ILLUSTRATIONS

Figure

1.	GLOBOCAN estimates of incidence and mortality worldwide for colorectal cancer in 185 countries	18
2.	Mechanism of colorectal cancer progression	21
3.	Colorectal cancer stages	24
4.	From carcinogenesis to tumor resistance via cancer stem cells.....	25
5.	Normal and colorectal cancer stem cells.....	27
6.	Signaling pathways involved in resistance of CSCs to therapy.....	29
7.	Organoid culture model for both basic and translational research.....	33
8.	Chemical structure of DIQ.....	37
9.	Chemical structure of ONC201 and ONC206.....	41
10.	DIQ, ONC201 and ONC206 reduce the proliferation of HCT116 CRC cell lines in a time and dose-dependent manner.....	64
11.	DIQ, ONC201 and ONC206 reduce the proliferation of HT29 CRC cell lines in a time and dose-dependent manner.....	65
12.	DIQ, ONC201 and ONC206 reduce the viability of HCT116 CRC cell lines in a time and dose-dependent manner.....	66
13.	DIQ, ONC201 and ONC206 reduce the viability of HT29 CRC cell lines in a time and dose-dependent manner.....	67
14.	The inhibitory effects of DIQ, ONC201 and ONC206 were accompanied with considerable changes in cell morphology and confluency.....	68
15.	DIQ, ONC201 and ONC206 have relatively limited toxicity on the proliferation of FHS74Int cell line.....	69
16.	DIQ, ONC201 and ONC206 have relatively limited toxicity on the viability of FHS74Int cell line.....	70

17.	DIQ, ONC201, and ONC206 reduce the migration of HCT116 colorectal cancer cells.....	71
18.	DIQ, ONC201, and ONC206 reduce the migration of HT29 colorectal cancer cells.....	72
19.	DIQ and ONC206 reduce the invasion of HCT116 and HT29 colorectal cancer cells.	73
20.	DIQ induces an accumulation of HCT116 and HT29 cancer cells in the sub-G1 region and apoptosis.....	75
21.	ONC201 induces an accumulation of HCT116 and HT29 cancer cells in the sub-G1 region and apoptosis	76
22.	ONC206 induces an accumulation of HCT116 and HT29 cancer cells in the sub-G1 region and apoptosis.....	77
23.	ROS production in HCT116 and HT29 cells as detected by dihydroethidium (DHE) staining.	78
24.	DIQ alters the expression of the survival, proliferation, and stem cell markers in 2D colorectal cells	80
25.	ONC206 alters the expression of the survival, proliferation, and stem cell markers in 2D colorectal cells	81
26.	DIQ reduces the sphere-forming and self-renewal ability of HCT116 colorectal cancer stem/progenitor cells	84
27.	DIQ reduces the sphere-forming and self-renewal ability of HT29 colorectal cancer stem/progenitor cells	85
28.	ONC201 reduces the sphere-forming and self-renewal ability of HCT116 colorectal cancer stem/progenitor cells	86
29.	ONC201 reduces the sphere-forming and self-renewal ability of HT29 colorectal cancer stem/progenitor cells	87
30.	ONC206 reduces the sphere-forming and self-renewal ability of HCT116 colorectal cancer stem/progenitor cells	88
31.	ONC206 reduces the sphere-forming and self-renewal ability of HT29 colorectal cancer stem/progenitor cells	89
32.	DIQ, ONC201 and ONC206 are not targeting non-tumorigenic FHS74Int cells.....	90

33.	DIQ reduces the expression of the cytokeratin epithelial markers, CK8 and CK19, and the stem cell marker CD44 in 3D colonospheres.....	92
34.	DIQ reduces the expression of the proliferation marker Ki67 and increases the DNA damage marker γ -H2AX in 3D colonospheres.....	93
35.	ONC206 reduces the expression of the cytokeratin epithelial markers, CK8 and CK19, and the stem cell marker CD44 in 3D colonospheres....	94
36.	ONC206 reduces the expression of the proliferation marker Ki67, and increases the DNA damage marker γ -H2AX in 3D colonospheres.....	95
37.	DIQ induces apoptosis and inhibits proliferation in colorectal cancer stem/progenitor cells.....	97
38.	ONC206 induces apoptosis and inhibits proliferation in colorectal cancer stem/progenitor cells.....	98
39.	DIQ reduces tumor growth in NOD-SCID mice.....	99
40.	Establishment and characterization of patient-derived organoids from colon cancer patient 1.....	103
41.	DIQ reduces the growth of the patient-derived organoids from colon cancer patient 1.....	104
42.	DIQ reduces the growth of the patient-derived organoids from colon cancer patient 2.....	105
43.	Establishment and characterization of patient-derived organoids from colon cancer patient 3.....	106
44.	DIQ, ONC201 and ONC206 reduce the growth of patient-derived organoids from colon cancer patient 3.....	107
45.	DIQ, ONC201 and ONC206 reduce the growth of the patient-derived organoids from colon cancer patient 4.....	108
46.	DIQ, ONC201 and ONC206 reduce the growth of the patient-derived organoids from colon cancer patient 5.....	109
47.	The morphology of the cell-derived organoids from HCT116 and HT29 cells upon DIQ, ONC201 and ONC206 treatments.....	110
48.	DIQ, ONC201 and ONC206 reduce the growth of the cell-derived organoids from HCT116 cells.	111

49.	DIQ, ONC201 and ONC206 reduce the growth of the cell-derived organoids from HT29 cells.	112
50.	DIQ reduces the growth of the patient-derived organoids from different prostate cancer patients.....	114
51.	DIQ reduces the growth of the patient-derived organoids from different prostate cancer patients.	115

TABLES

Table

1.	Comparison of 2D versus 3D culture methods.....	36
2.	Anticancer agents that belong to the quinone family.....	40
3.	List of components and their respective concentrations used in human colorectal organoids culture medium.....	56
4.	List of components and their respective concentrations used in human prostate organoids culture medium.....	56
5.	List of primary and secondary antibodies used in immunofluorescent staining.....	60
6.	List of primary and secondary antibodies used in western blot experiments.....	60
7.	Colorectal cancer patients' clinical and histopathologic characteristics	61

ABBREVIATIONS

2D: Two-Dimension
3D: Three-Dimension
5FU: 5-Fluorouracil
ABC: ATP-Binding Cassette
AC: Adenocarcinoma
ALDH1: Aldehyde Dehydrogenase 1
APC: Adenomatous Polyposis Coli
ATF: Activating Transcription Factor
AUB: American University of Beirut
AUBMC: American University of Beirut Medical Center
Bcl-2: B-cell Lymphoma 2
BMP: Bone Morphogenetic Protein
BSA: Bovine Serum Albumin
CHOP: C/EBP Homologous Protein
ClpP: Caseinolytic Protease P
CK8: Cytokeratin 8
COX2: Cyclo-Oxygenase 2
CRC: Colorectal Cancer
CSCs: Cancer Stem Cells
DAB: Diaminobenzidine
DAPI: 4', 6-Diamidino-2-Phenylindole
DIQ: Diiminoquinone
DRD2: Dopamine D2 Receptor
ECL: Enhanced Chemiluminescence
ECM: Extracellular Matrix
EGFR: Epidermal Growth Factor Receptor
EMT: Epithelial-Mesenchymal Transition
FABP5: Fatty Acid-Binding Protein 5
FBS: Fetal Bovine Serum
FGF: Fibroblast Growth Factor

G: Generation
H&E: Hematoxylin and Eosin
HCT116: Human Colorectal Cell Line
HMGA1: High Mobility Group Protein A1
IC₅₀: Half-Maximal Inhibitory Concentration
ID: Inhibitors of Differentiation
IF: Immunofluorescence
IHC: Immunohistochemistry
IRB: Institutional Review Board
ISC: Intestinal Stem Cells
ISR: Integrated Stress Response
Lgr5: Leucine-Rich Repeat-Containing G-Protein-Coupled Receptor
MAC: Mucinous Adenocarcinoma
MAPK: Mitogen-Activated Protein Kinase
MSI: Microsatellite Instability
MTT: 3-(4, 5-dimethylthiazol-2-yl)-2, 5-diphenyltetrazolium bromide
NAC: N-acetylcysteine
NF-κB: Nuclear Factor Kappa
NGS: Normal Goat Serum
NOD-SCID: Non-Obese Diabetic Severe Combined Immunodeficiency
NOG: Noggin
NK: Natural Killer
OD: Optical Density
OFC: Organoids Forming Count
PARP: Poly [ADP-ribose] Polymerase
PBS: Phosphate Buffered Saline
PCNA: Proliferating Cell Nuclear Antigen
PFA: Paraformaldehyde
PI: Propidium Iodide
PPAR: Peroxisome Proliferator-Activated Receptor
P/S: Penicillin-Streptomycin
RI: ROCK Inhibitor

ROCK: Rho-Associated Kinase
ROS: Reactive Oxygen Species
SEC: Serous Endometrial Cancer
SEM: Standard Error Mean
SFU: Sphere Formation Unit
Shh: Sonic Hedgehog
SRCC: Signet-Ring Cell Carcinoma
TGF- β : Transforming Growth Factor-Beta
TNF- α : Tumor Necrosis Factor α
TRAIL: TNF-Related Apoptosis-Inducing Ligand
TQ: Thymoquinone
VEGF: Vascular Endothelial Cell Growth Factor
XIAP: X-Linked Inhibitor of Apoptosis Protein

CHAPTER I

INTRODUCTION

A. Colorectal cancer

1. Colon Cancer Epidemiology

Cancer ranks as a leading cause of death worldwide before the age of 70 years in both males and females in 112 countries worldwide, accounting for nearly 10 million deaths and an estimated 19.3 million new cases in 2020 [1].

Colorectal cancer (CRC) is the third most common worldwide in 2020 in terms of incidence of cancer (1.93 new million cases) in men and women, and the second most common cause of cancer death in 2020 reaching 935,000 deaths according to the global cancer statistics 2020 [1] (Figure 1). These statistics of CRC represent about one in 10 cancer cases and deaths. Many factors influence the risk of developing CRC including age, sex, race and ethnicity, dietary patterns, and lifestyle factors [2]. The incidence rates of CRC are rising in individuals younger than 50 [3]. Primary prevention and early screening remain the key strategies to lessen the growing global burden of colorectal cancer [2].

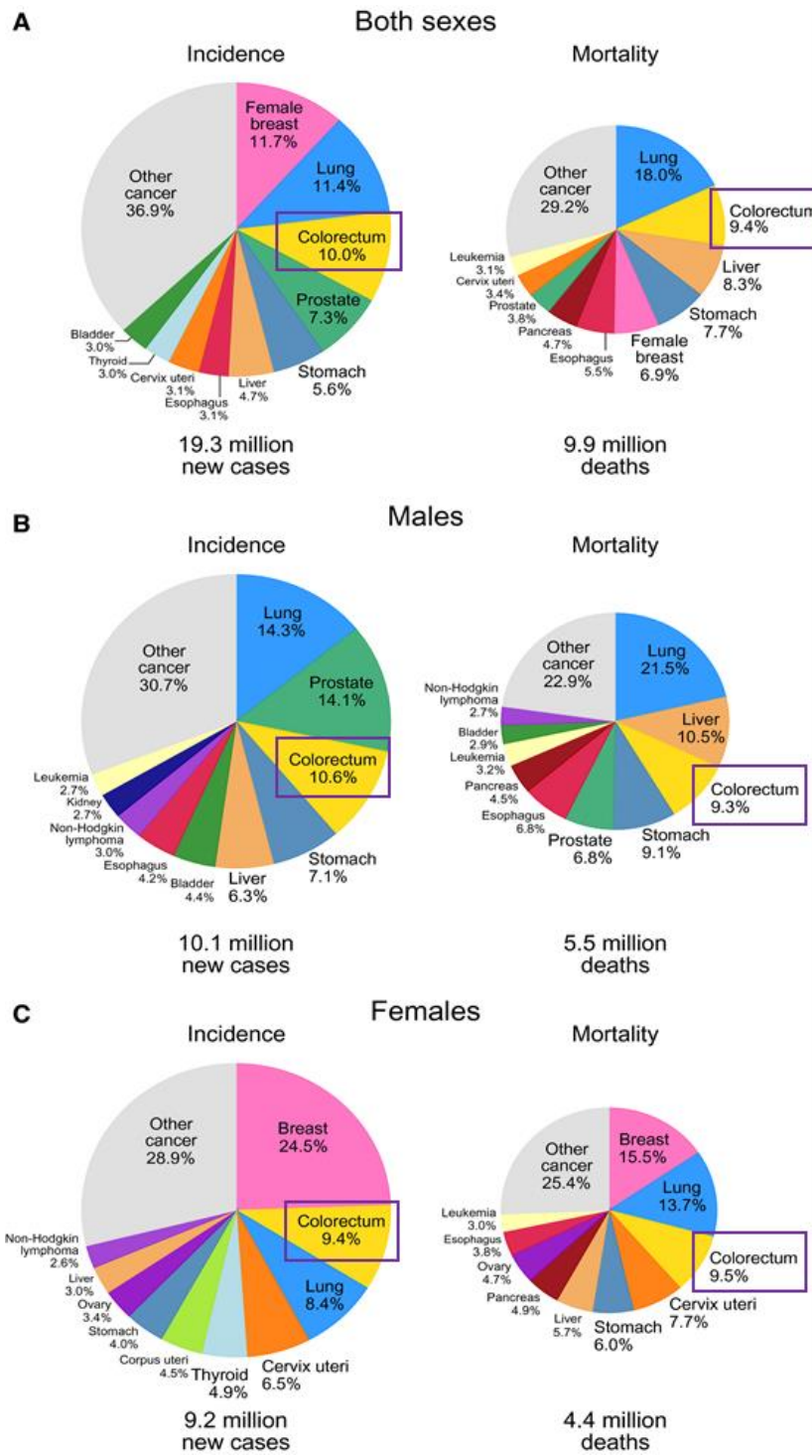


Figure 1. GLOBOCAN estimates of incidence and mortality worldwide for colorectal cancer in 185 countries. Distribution of incidence and mortality for the top 10 most common cancers in 2020 for (A) Both Sexes, (B) Men, and (C) Women according to global cancer statistics 2020 [Adapted and modified from [1]].

2. Colon Anatomy and Function

The colon is the longest part of the large intestine. The colon is a U-shaped tube made of muscle and connected at one end to a shorter tube called rectum. Together, the colon and rectum are about 2 meters (6.5 feet) long. Its main function is to receive almost completely digested food from the cecum, absorb water, vitamins and nutrients, form stool and feces, and propel them toward the rectum for elimination [2, 3]. The ascending, transverse, descending and the sigmoid colon are the four different parts of the colon. The colon starts with the ascending colon, and ends with the sigmoid colon that is connected to the rectum [2]. The colon wall is made up of four multiple layers ordered from the lumen outward as follows: the mucosa, submucosa, muscular layer, and serosa. These muscular layers contribute to the motility of the large intestine [4].

The intestinal epithelium is the most rapid self-renewing tissue of adult mammals characterized by its highest turnover rate of five to seven-day turnover time in humans [5]. The epithelium of the intestine is composed of differentiated villi and proliferating crypts. It is made up of five major differentiated epithelial cells, including enterocyte, goblet, enteroendocrine, Paneth and tuft cells. All these cells are derived from intestinal stem cells (ISCs), which are located at the bottom of the crypts. Such ISCs are characterized by two basic features: self-renewal and multipotency [6]. Proliferating progenitors called transit-amplifying (TA) cells allocated in the ISC niche are vigorously produced by the ISCs. The ISC niche is involved in providing crucial key biochemical structures and signals for polarity, growth, and physical strength of ISC. The epithelial-mesenchymal crosstalk is crucial for the maintenance of the functional stem cell niche, thus retaining a balance of stem cell quiescence and activity of ISCs [6]. Paneth cells are very crucial in leucine-rich repeat-containing G protein-coupled

receptor 5+ (Lgr5+) stem cell niche within intestinal crypts [7]. The direct cell contact between Lgr5+ stem cells and Paneth cells (stem cell niche) regulates and determines the self-renewal and proliferation potential of Lgr5+ stem cells both *in vitro* and *in vivo* [8]. Inefficient culture and inability to control the fate of Lgr5+ stem cells were reported in the absence of Paneth cells [9]. Wnt, bone morphogenetic protein (BMP), hedgehog, and Notch control and regulate the ISCs function [10, 11]. Wnt signaling, which mainly functions in the crypt base, is more likely involved in determining fate of stem cells and transit-amplifying cells in the intestinal epithelium. Notch signaling mainly controls daughter cell fate determination in the TA compartment. EGF, Noggin, and R-spondin1 are essential requirements in the crypt culture system. For example, R-spondins are the major drivers of crypt self-renewal by enhancing Wnt signaling. Removal of the BMP antagonist Noggin decreases Lgr5+ ISCs [12].

Specific molecular markers of stem cells are not yet known. Thus, there is a major challenge toward the full characterization and isolation of stem cells. Multiple markers of the adult ISCs, such as Lgr5, Bmi1, were specified in different gene expression and lineage tracing studies [13, 14]. Some markers that might correlate with the stem cell tumorigenic phenotype were proposed to characterize CRC stem cells too [15, 16] (Figure 5).

3. Colorectal Cancer Initiation and Progression

Cancer development is a multistep process that starts with tumor initiation, followed by tumor promotion, and culminates with tumor progression. Colon cancer represents a unique model. It arises primarily from polyps and might progress into adenomas, which are characterized by their malignant potential. CRC is associated with

one or a combination of mutations and chromosomal and microsatellite instability (MIS) [17, 18] (Figure 2).

CRC initiation was triggered by mutations of the adenomatous polyposis coli (APC) gene. APC gene is a tumor suppressor gene that is involved in the Wnt signaling pathway [17].

Tumor promotion and progression are accompanied by additional mutations at the level of KRAS, p53 and SMAD4, stimulating the amplification of growth rate of the adenoma and leading to consequent tumor invasion and metastasis [17].

Mutations at the level of TP53 occur mainly at later stages of CRC development in 50-70% of carcinomas. DNA damage, DNA repair and apoptosis are sensed by the key player p53 protein [17]. p53 loss causes an enhancement of tumor progression, failure of apoptotic mechanisms, and the induction of the epithelial–mesenchymal transition [17].

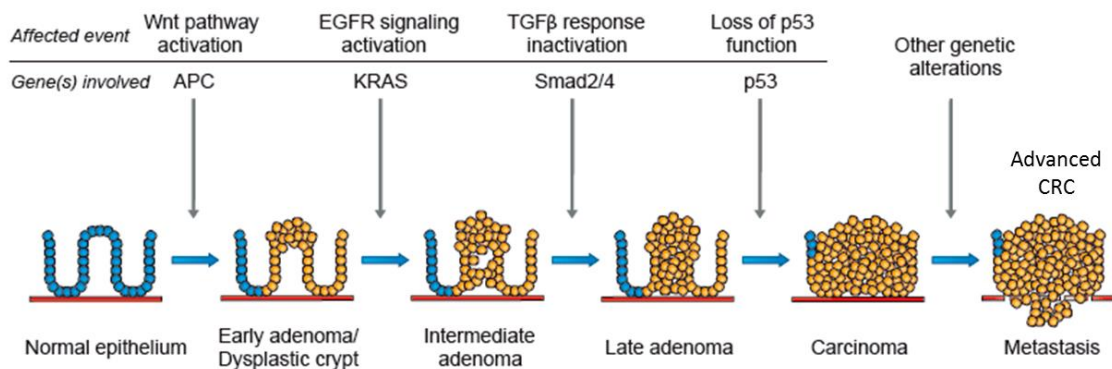


Figure 2. Mechanism of colorectal cancer progression. This model represents the observed clinicopathological changes along with genetic abnormalities in the progression of chromosomally unstable CRC. All possible mutations during CRC development are shown in the above figure. SMAD4: SMAD family member 4; TGFβ: transforming growth factor-β; EGFR: Epidermal growth factor receptor [Adapted and modified from <http://syscol-project.eu/about-syscol/>].

4. Stages and Treatments of Colorectal Cancer

Clinically, CRCs are usually subdivided into proximal or right-sided, and distal or left-sided depending on the origin of the colon section. Proximal or right-sided CRCs are the colon sections originating from proximal to the splenic flexure (cecum, ascending colon and transverse colon), whereas distal or left-sided CRCs tumors arise distally from descending colon and sigmoid colon. Rectal cancers arise 15 cm within the anal sphincter and cause higher rates of loco-regional relapse and lung metastases, whereas colon cancers spread towards the liver region and have a better prognosis [19]. Most colon cancers are classified as adenocarcinomas and are subdivided into low-grade and high-grade colorectal tumors. Adenocarcinomas of the colon are represented by three major subtypes, namely classical adenosquamous adenocarcinoma (CA), mucinous adenocarcinoma (MAC), and signet-ring cell carcinoma (SRCC) [19].

Colorectal cancer is diagnosed after the onset of symptoms, or through screening colonoscopy, or using noninvasive stool-based testing, such as occult blood tests. Regular screening can prevent CRC. The focus of contemporary research is directed towards minimally invasive surgical techniques, limit treatment-related toxicities, and promote the personalization of therapy. Following surgical removal, CRC is classified into four different stages [20-22] (Figure 3). Stage 0 represents the earliest stage of the cancer, which is known as carcinoma *in situ* or intramucosal carcinoma. In this stage, the cancer has not grown past the mucosa of the colon or rectum. Surgery is the standard treatment at this stage. Stage I colon cancer is confined to the lining of the colon with the appearance of small tumorigenic nodules, where the tumor has penetrated the muscular layer of the colon but did not reach any adjacent organs or local lymph nodes. Approximately 90% of stage I CRC patients do not experience a cancer

relapse and are cured with surgery alone. Stage II CRC has spread past the colon wall into the abdominal cavity but did not invade any of the local lymph nodes. Surgery is the first line of treatment in stage II CRC. Systemic adjuvant therapy is recommended for the “high-risk” stage II patients due to the risk of cancer recurrence after the surgery. Adjuvant chemotherapy incorporates a variety of treatments such as 5-fluorouracil (5FU) and leucovorin, or capecitabine if a high chance of recurrence exists. Stage III CRC has reached the abdominal cavity and has invaded the regional lymph nodes. Contribution of systemic adjuvant therapy, preferably with a combination of fluoropyrimidine and oxaliplatin, is recommended for all resected stage III patients to reduce the risk of colon cancer recurrence and improve survival. Stage IV CRC is characterized by the metastasis of the advanced disease to other distant organs, mainly liver and lungs. Surgery by itself is not enough at this stage, and chemotherapy regimens or even radiation are recommended [20-23].

Colorectal cancers can be classified into local invasion depth (T stage), lymph node involvement (N stage) and presence of distant metastases (M stage). These stages are combined into an overall stage definition, which represents the basis for therapeutic decisions [21, 22].

Current medical treatment of CRC includes a wide array of systemic therapies, which include chemotherapeutic (e.g 5FU), targeted therapy (such as epidermal growth factor receptor (EGFR) and (VEGFR) inhibitors), in addition to immunotherapy [24, 25].

Colorectal Cancer Stages

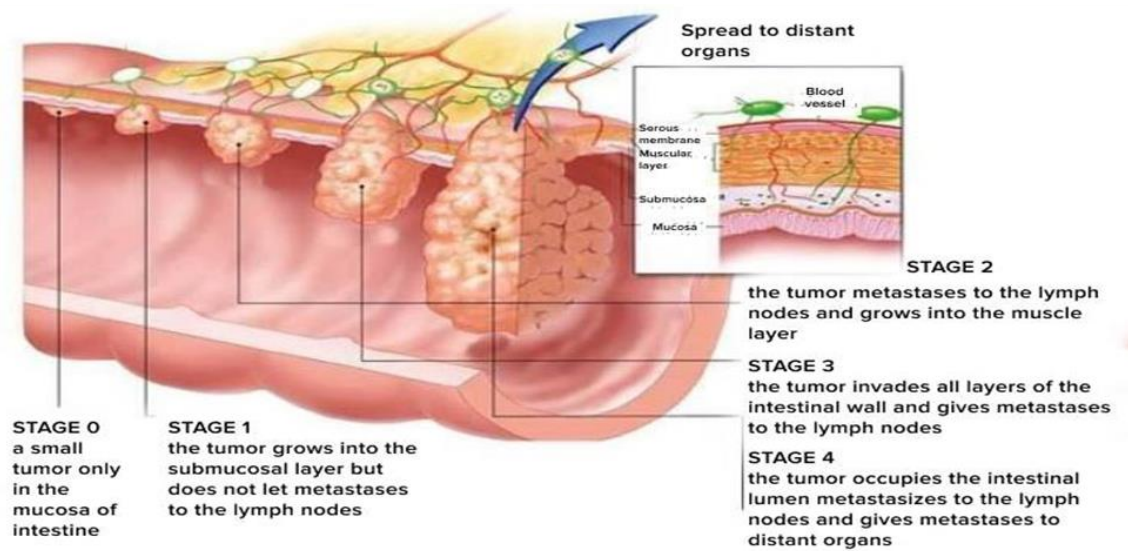


Figure 3. Colorectal cancer stages. CRC is classified into four different stages. Stage 0 represents the earliest stage of the cancer. In stages 1, 2 and 3, CRC does not metastase to distant organs. Stage 4 is characterized by the metastasis of the advanced disease to other distant organs. [Adapted and modified from <https://medtour.help/disease/colorectal-cancer-rectal-cancer>].

B. Cancer Stem Cells

1. Overview

Like normal pluripotent stem cells, cancer stem cells (CSCs) are long-lived, and show quiescent potentials in a dormant state [26]. CSCs are characterized by their self-renewal, pluripotency, and tumor expansion potential of differentiated cell populations with altered molecular and cellular phenotypes [27, 28]. This small subpopulation of cells is associated with tumor invasion and metastasis, resistance to therapy, cancer relapse and poor prognosis in patients [28] (Figure 4). They are responsible for angiogenic induction and apoptotic resistance. CSCs are present within solid tumors; therefore targeting this population holds hope for treatment response [29].

CSCs express distinctive arrays of stem cell marker genes, such as Lgr5, Oct4, Sox2, Nanog, c-kit, ABCG2, and ALDH, which make them vulnerable to therapies targeting multiple cellular pathways [26, 30]. In addition, it is not possible to develop a ‘pan-CSC’-targeting mechanism due to the absence of known universal markers for CSCs [31, 32]. The stem cell niche is composed of fibroblasts, endothelia, and inflammatory cells. It is involved in the maintenance and promotion of CSCs into more aggressive and invasive potentials

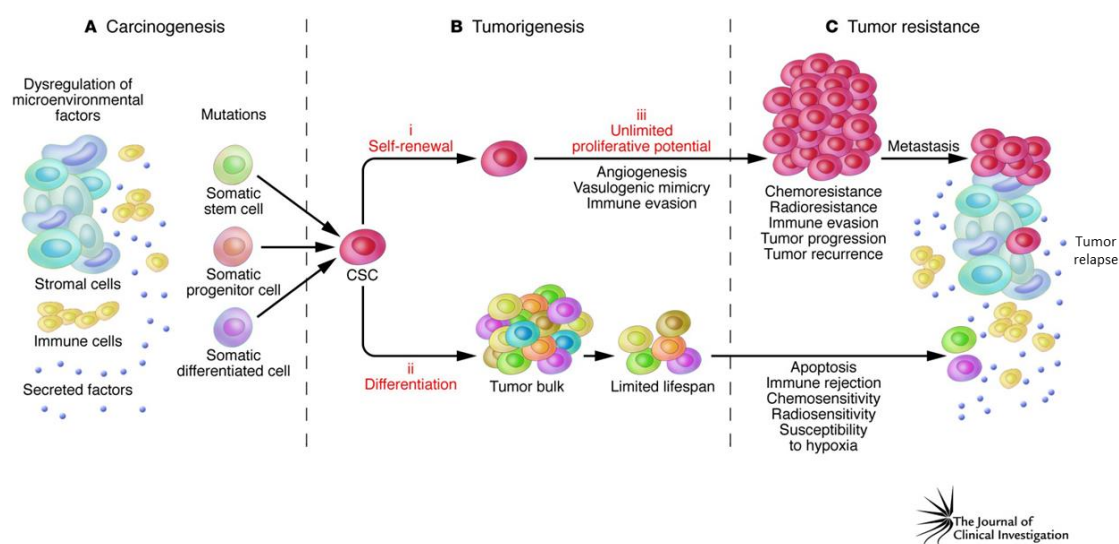


Figure 4. From carcinogenesis to tumor resistance via cancer stem cells. Neoplastic progression, tumor recurrence, and metastasis are driven by CSCs. (A) Tumors can arise from somatic cells undergoing genetic mutations and affected by the dysregulation of microenvironmental factors. (B) CSCs are posited to be exclusively capable of driving tumorigenesis through their self-renewal and differentiation abilities. (C) CSCs can induce increased resistance to chemotherapeutic agents and/or ionizing radiation, and mediate immune rejection. [Adapted and modified from [29]].

2. Colorectal Cancer Stem Cells

Using flow cytometric analysis and spheroid cultures, specific surface markers have been identified and correlated to CRC phenotype including, CD133, CD44, CD34, CD24, epithelial-specific antigen (ESA), CD166, CD29, Lgr5 and ALDH [16].

However, most of the CSC surface markers identified so far are also expressed in normal ISCs, thus not allowing their potential use as therapeutic targets for treating cancer (Figure 5).

Among these specific colon surface biomarkers, CD133, which identifies a colon cancer–initiating cell (CC-IC) population in human tumors, is considered to be a key CSC marker in CRC. Human colorectal CSCs were first isolated based on CD133 expression [33, 34]. CD133, which is also expressed in normal colon tissue, accounts for approximately 2.5% of colorectal cancer tumor cells that could have derived from oncogenic transformation of normal colonic stem cells [35]. The use of CD133 as an effective marker of colorectal CSCs has been supported by many studies. Notably, tumor formation that resembled the original malignancy took place rapidly in immunodeficient mice injected in CD133+ cancer cells, whereas CD133- cells did not [33, 34]. Consistent with a CSC phenotype, CD133+ colorectal tumors were found to be resistant to radiotherapy and chemotherapy.

Another known CSC marker, CD44, regulates adhesion, differentiation, and migration. CD44+ colorectal CSCs display aggressive proliferation, more colony formation, and chemo- and radio-resistance as compared to CD44 negative cells. In HCT116 colon cancer cells, knockdown of CD44 with short hairpin RNA (shRNA) led to the reduction in cell proliferation, migration and invasion [36]. Some data argue against the specificity of CD44 for colonic stem cells since CD44 was expressed not only in the stem cell compartment at the crypt bottom but also in cells within the proliferative compartment. Thus, questioning whether CD44 is a specific CRC stem marker remains to be determined.

Lgr5 is another reported marker for colorectal CSCs mainly during the initiation of tumorigenesis. Interestingly, CRC resistance and relapse were prevented by the combination targeting of both Lgr5+ cells and differentiated cancer cells. The Lgr5 expression is related to 5FU resistance and colorectal cancer relapse [37]. Lgr5-expressing cells are able to generate long-term crypt-villus organoids with all differentiated cell lines.

Although CD44, CD133, and Lgr5 are relatively good colorectal CSC markers, the possibility of other CSCs markers in the colon still exists. More specific stem cell markers are needed to enable targeting them at a premalignant stage.

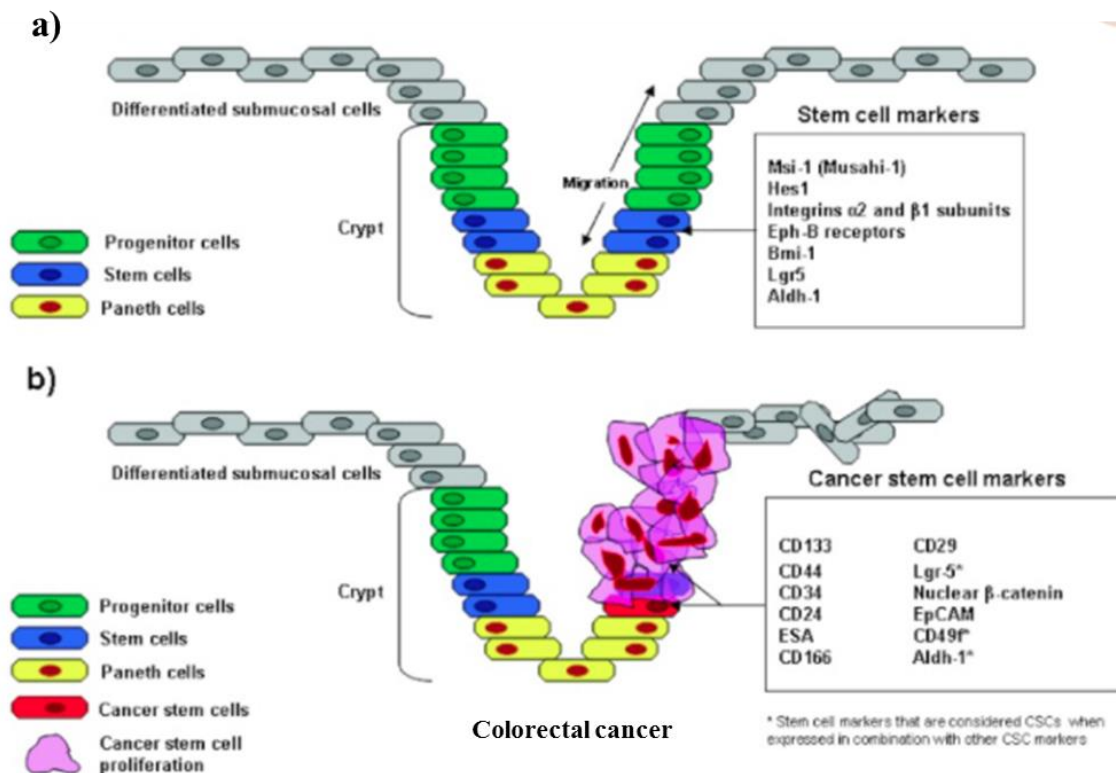


Figure 5. Normal and colorectal cancer stem cells. Some markers that might exist in ISC (a) and CRC (b) stem cells. Some markers in CRC, such as Lgr5, CD44, CD133, might correlate with the stem cell tumorigenic phenotype [Adapted and modified from [15]].

3. Targeting Colorectal Cancer Stem Cells

Although 5FU is the mainstay backbone of chemotherapy treatment for metastatic CRC, it causes many side effects and toxicity [38]. Most CRC patients die of metastasis due to the resistance of their disease to standard therapies. Around 75% of patients with metastatic CRC receiving chemotherapy develop recurrence within 18 months [39]. The presence of chemotherapy-resistant CSCs is one of the most key causes of tumor recurrence. There is a high need for significant identification of novel therapeutics targeting chemo-resistant and cancer stem cells in CRC.

Different strategies aim to sensitize CSCs including the use of differentiation-inducing agents, inhibitors of survival pathways, immune therapy, triple-target therapeutic strategies, targeting proteins such as CD133, CD44, or EpCAM by antibody-directed therapy, as well as targeting ABCG2 which are ATP-binding drug efflux pumps by ATP-competitors [40]. It is believed that there are no effective drugs to target CSCs.

Multiple signaling systems are involved in resistance of CSCs to therapy (Figure 6). Three major signaling pathways contribute to stem cell development, tumorigenicity, and oncogenesis: the Notch, sonic hedgehog (Shh) and Wnt signaling [41, 42]. These pathways control the balance between proliferation, differentiation, migration, and renewal of CSCs. It is widely accepted that the Wnt/ β -catenin pathway is the most relevant signaling pathway for CRC development; it plays a key role in colorectal tumorigenesis and is involved in the process of epithelial to mesenchymal transition (EMT) and invasion. This pathway is mechanistically responsible for drug resistance of colon CSCs [41]. Blocking the Wnt/ β -catenin pathway in CD133+ colon cancer cells led to the reversal of their resistance to 5FU [43]. Increasing evidence

shows that these three embryonic pathways can interact with other oncogenic signaling pathways, such as those involving the MAPK, PI3K, AKT, ERK and EGF, which are aberrantly activated in many human cancers [44-46]. Thus, identifying drugs that target these oncogenic pathways would make a solid rationale for the targeted therapy of cancers. Indeed, studies have shown that AKT and ERK are overexpressed in human CRC [45]. Therefore, these developmental pathways could be considered important therapeutic targets for suppressing CSC self-renewal and proliferation, and tumorigenicity.

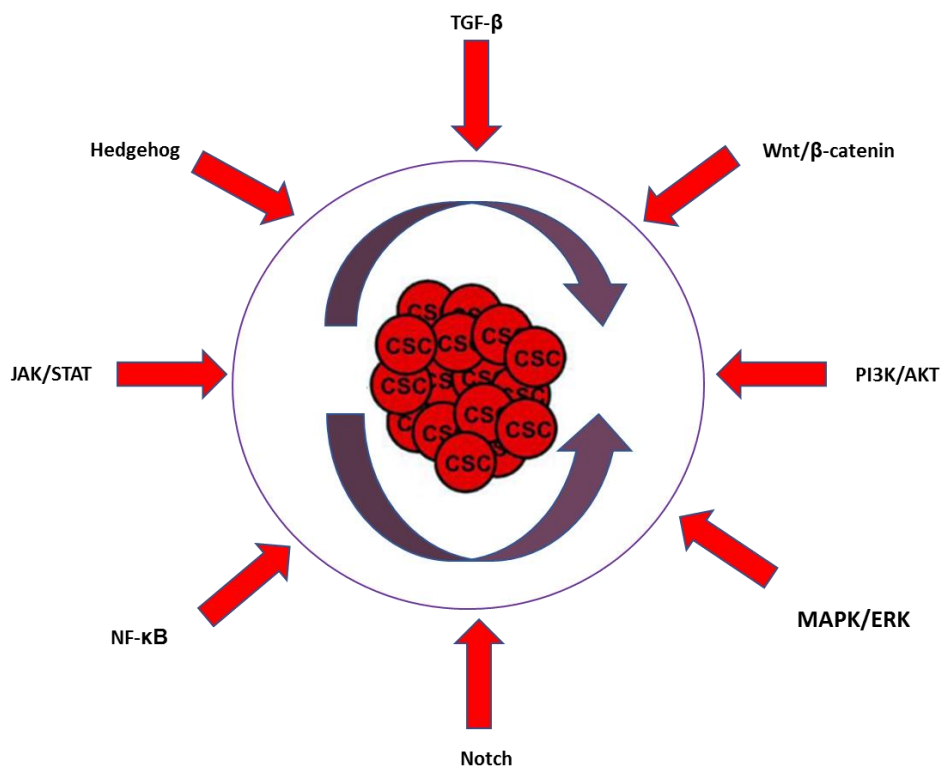


Figure 6. Signaling pathways involved in resistance of CSCs to therapy. Signal pathways and elements involved in the maintenance of the stemness of CSCs. Dysregulation of signal pathway network plays an important role in controlling the self-renewing and differentiation abilities of CSCs as well as normal stem cells including PI3K/AKT, JAK/STAT, Wnt/ β -catenin, hedgehog, Notch, and NF- κ B.

C. Three-Dimensional Models for Colorectal Cancer Stem Cells

1. Overview of Three-Dimensional Models

The identification of colorectal CSCs is not clear-cut. The need for models that identify, and isolate CSCs is of high importance for effective treatment of cancer recurrence. Recently, we have witnessed the development of different types of *in vitro* three-dimensional (3D) culture systems to recapitulate the *in vivo* cancer growth [47, 48]. *In vitro* 3D systems have bridged the gap between 2D systems and *in vivo* systems which were used for testing the efficacy of novel anticancer drugs [48]. 3D culture systems are being used for enrichment and isolation of CSCs, drug discovery, cancer cell study, and stem cell biology [49, 50].

3D culture systems mainly include organoids and multicellular spheres models. These 3D models closely resemble each other. Nonetheless, even though they share a common 3D conformation, each 3D model exhibits specific intrinsic properties.

2. Sphere Model

Sphere-formation assay is an *in vitro* method commonly used to identify CSCs based on their reported capacity to evaluate self-renewal and differentiation potentials at the single cell level. This *in vitro* model enables propagation of CSCs, molecular characterization of CSCs, as well as evaluating the antitumor potential of various conventional and novel chemotherapeutics to target this tumor-initiating population.

The sphere-forming assay was first presented as a functional approach for studying adult stem cells. Since then, it has been widely utilized to evaluate the stemness of CSC populations within tumors [51]. CSCs form 3D multicellular heterogenous spheres containing stem cells, progenitors, and differentiated cells, when

they are embedded in a 3D matrix called Matrigel with serum-free, non-adherent, and nutritionally deficient conditions [88]. Under these culture conditions, differentiated tumor cells do not form spheres and undergo apoptosis, while CSCs survive, proliferate, and form spheres upon propagations [51]. Only this rare sub-population, CSCs, will keep forming spheres that consistently display the similar phenotype equilibrium after appropriate propagation *in vitro* [52]. However, the progenitors differentiate, and the differentiated cells lose their self-renewal ability and in turn senesce.

Within the same spheroids, we can find cellular heterogeneity very similar to *in vivo* tissues and tumors, usually including proliferating (highly exposed to medium and oxygen), quiescent, apoptotic, hypoxic, and necrotic cells. However, tumorspheres do not fully recapitulate the 3D structure and microenvironment of an *in vivo* tumor. Tumorspheres or spheroid models, which can retain the stemness of CSCs, are excellent for CSC fraction enrichment but not for studying intrinsic properties of CSCs related to their 3D architecture [57]. These intrinsic properties of CSC can be more investigated by organoid models.

CSC isolation and expansion using sphere assay negligibly differ from one cancer type to another. Sphere cultures have been successfully used to enrich and propagate CSCs from different cancer cell lines, such as breast [58-60], prostate [61], pancreatic [62], brain [63], and CRC cell lines [39,64, 65]. Ponti has originally reported enrichment of CD44⁺/CD24⁻ cells with stem/progenitor cells properties within mammospheres, which were able to induce tumorigenesis [58]. Colonospheres have been successfully used to isolate and culture CSC from primary colon [65], but have been infrequently used to enrich CSCs from colorectal cancer cell lines [34, 53, 54].

3. Patient-Derived Organoid Model

Introducing Patient-derived organoid (PDO) culture systems to 3D models have revolutionized colorectal cancer. *In vitro* organoids are a 3D cell culture model in which organoids are derived from embryonic stem cells (ESCs), induced pluripotent stem cells (iPSCs) or tissue-resident stem/progenitor cells [55, 56]. In 2009, the stem cell field has witnessed a major methodical advancement by the successful development of the intestinal organoid culture system referred to as the R-spondin method. Sato et al. [57] produced indefinite expansion of 3D self-renewing intestinal organoids. This method used intestinal crypts sorted Lgr5⁺ intestinal epithelium cells embedded in Matrigel [57, 58]. These organoids embedded in Matrigel were supplemented with different growth factors establishing key endogenous niche signals: Wnt a Frizzled/LRP (lipoprotein receptor-related protein) ligand; Noggin (BMP inhibitor) for stem cell expansion; R-spondin (a WnT agonist) for maintaining stem cell populations; and EGF for promoting cell proliferation. After optimizing this method, the Clevers group derived epithelial organoid models from human colorectal cancers [9, 86, 89]. This culture system was subsequently adapted for not only generating human intestinal organoids, but also organoids derived from other organs [58-61]. This major technological breakthrough gives exciting promises for scientific discovery in developmental biology as well as in translational research [82, 83] (Figure 7). It provides a large range of both basic research and translational applications. A major advantage of this system is mainly represented by the ability to analyze stem cell behavior, novel markers, drug screening, gene editing, disease modelling , orthotopic transplantation, and predicting acquisition of drug resistance for developing personalized regimens [55].

With the presence of cellular heterogeneity, cell/cell interaction, and developing drug/chemo resistance, large-scale drug screening in 3D culture is reliable as a relevant model for CRC research, especially after the establishment of a living organoid biobank of organoids derived from colorectal cancer patients [62]. Intestinal epithelial organoids provide an opportunity for studying the efficacy of potential chemotherapeutics suitable for CRC patients prior to animal trials. By counting the number of organoids, their sizes, and phenotypes, we are provided by important data that guides the therapeutic efficacy of proposed chemotherapeutic drugs. Matano et al. have successfully generated genetically engineered organoids derived from normal human intestinal samples by using the CRISPR-Cas9 to establish driver mutations that are mainly observed in the development of CRC [63]. Using this model also helped in detecting the mutations that are involved in regulating metastasis and invasion [63].

Organoid Model

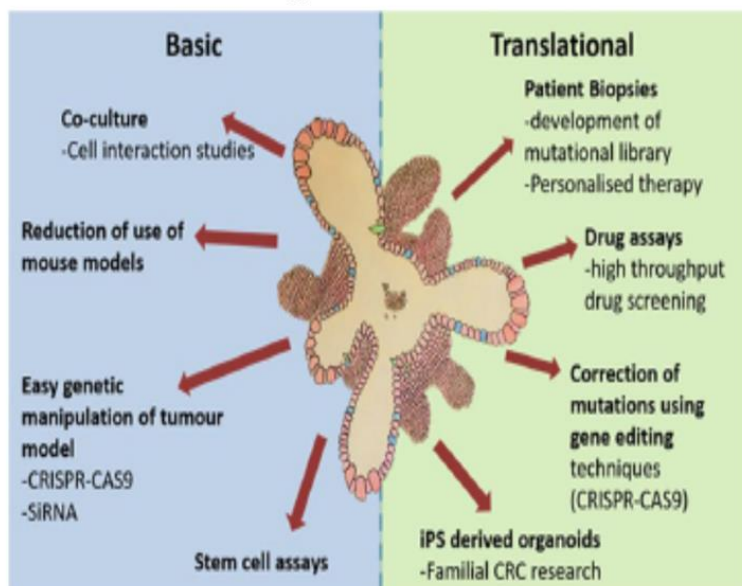


Figure 7. Organoid culture model for both basic and translational research.

Organoid culture provides a large range of both basic research including co-culture, stem cell assay and easy genetic manipulation of tumor models, and translational applications, such as drug assays, patient biopsies, correction of mutations using gene editing, and iPS derived organoids [Adopted and modified from [47]].

4. Advantages of Three-Dimensional Models Versus Two-Dimensional Models

The additional dimensionality of 3D cultures plays a critical role not only in determining the morphology and the spatial organization of the cells but also in inducing physical constraints. As opposed to 2D monolayer cultures, cells in 3D culture systems form spheroids or organoids in a matrix or in a suspension medium. The cells of spheroids and organoids have a morphology that is so close to its natural phenotype in the body due to the presence of cell–cell interactions and cell–ECM interactions. Biologically derived matrices used in 3D models, such as the most commonly used BD Matrigel™, are generated from the extracellular matrix (ECM) of biological sources [64-66]. These biologically derived matrices may better mimic the *in vivo* cell microenvironment. The behavior of cancer cells in biologically derived 3D matrices are closer to the *in vivo* cell behavior. These matrices affect and determine cell behavior, gene expression, and drug sensitivity, and activate various signaling pathways in cancer cells [64, 66]. Additionally, within the same spheroids, we can find cellular heterogeneity very similar to *in vivo* tissues and tumors, whereas cells cultured in 2D models are mostly proliferating cells [67, 68].

Cellular responses to drug treatments in 3D cultures have been shown to be more physiologically relevant to what happens *in vivo* compared to 2D cultures [69, 70]. 3D cultures are better predictors of *in vivo* drug responses. Several research groups have shown that cancer cells cultured in 3D systems make them gain resistance to some chemotherapeutics compared to 2D cultures [70-72]. Others have shown that depending on the cell and/or drug type, 3D culture systems either sensitize or desensitize cancer cells to anticancer therapeutics [73, 74]. These differences in drug sensitivity noted in 3D cultures are representing the way of how cancer cells *in vivo* respond to

chemotherapy [5]. For instance, paclitaxel has reduced the ovarian cancer cell survival and proliferation in 3D cultures by 40% or 60%, while it caused 80% reduction in cell viability in the 2D cell monolayer [71]. The emergence of drug resistance in 3D cultures primarily results from signals driven by the dynamic cellular interactions of neighboring cells with ECM input into the cellular decision-making process [75]. The increased drug resistance in 3D cultures can also be attributed to hypoxic conditions in the structure of 3D spheroids and the presence of stromal cells, which play a role in determining drug sensitivity. Such chemoresistance observed in 3D spheroids exists *in vivo* as well [76]. Drug sensitivity in 2D is misleading, whereas the use of animal models is not always possible due to ethical issues, in addition to the high cost and time-consuming factors [73, 77]. Also, the action of the drug is affected by its accessibility to cells and local pH. In 2D monolayer, drugs diffuse to cells almost evenly, however in 3D cultures drug diffusion to cells varies depending on the depth of cell surface [78]. Altogether, 3D culture models hold the promise for defining new targets that have not been observed and predicted in traditional 2D culture studies.

Table 1. Comparison of 2D versus 3D culture methods [Adapted and modified from [79]].

Type of culture	2D	3D
Time of culture formation	Within minutes to a few hours	From a few hours to a few days
Culture quality	High performance, reproducibility, long-term culture, easy to interpret, simplicity of culture	Worse performance and reproducibility, difficult to interpret, cultures more difficult to carry out
<i>In vivo</i> imitation	Do not mimic the natural structure of the tissue or tumour mass	<i>In vivo</i> tissues and organs are in 3D form
Cells interactions	Deprived of cell-cell and cell-extracellular environment interactions, no <i>in vivo</i> -like microenvironment and no “niches”	Proper interactions of cell-cell and cell-extracellular environment, environmental “niches” are created
Characteristics of cells	Changed morphology and way of divisions; loss of diverse phenotype and polarity	Preserved morphology and way of divisions, diverse phenotype and polarity
Access to essential compounds	Unlimited access to oxygen, nutrients, metabolites and signalling molecules (in contrast to <i>in vivo</i>)	Variable access to oxygen, nutrients, metabolites and signalling molecules (same as <i>in vivo</i>)
Molecular mechanisms	Changes in gene expression, mRNA splicing, topology and biochemistry of cells	Expression of genes, splicing, topology and biochemistry of cells as <i>in vivo</i>
Cost of maintaining a culture	Cheap, commercially available tests and the media	More expensive, more time-consuming, fewer commercially available tests

5. Limitations of 3D Models

Despite the many advantages and potential uses of 3D models, it still has a couple of limitations to be solved [48, 79, 80]

- First, lack of native microenvironment studies about the communication of stem cells with their niches.

- The limited presence (if not complete lack) of stromal components in their niches, including immune cells, restricts their use in demonstrating inflammatory responses to infection or drugs.

- Potential limitations to drug penetration due to the rigidity of ECM in drug-screening programs.

- The inability to mimic *in vivo* growth factor/signaling gradients in Matrigel matrix and resemble biomechanical forces that stem cells come across *in vivo*.

D. Diiminoquinone DIQ

1. Overview

A novel diiminoquinone compound (DIQ), synthesized by Professor Makhoul Haddadin (Chemistry Department, American University of Beirut (AUB)), exhibited anticancer effects against colorectal cancer stem-like cells [81]. We believe that the activity of DIQ is based on the similarities in structure between quinones and diiminoquinones (Figure 8), Thus, DIQ might exhibit anticancer activities in a manner analogous to quinone's mechanism of action.

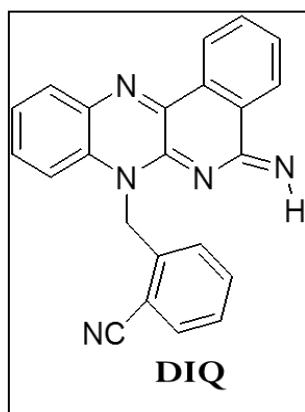


Figure 8. Chemical structure of DIQ.

Studies have shown that some quinones, which are often plant-derived secondary metabolites, are active agents against cancer [82, 83]. Furthermore, other quinones are active as anticancer compounds but such compounds did not become commercial. Two proposed mechanisms of action of quinones that were reported in

literature are either through an increase in the intracellular concentration of reactive oxygen species (ROS) including superoxide, hydrogen peroxide, and ultimately the hydroxyl radical or through acting as alkylating agents of crucial cellular proteins and/or DNA [84].

Quinones possess a cyclic structure with two keto functional groups [85]. In an aprotic medium, each keto group can be reduced in a one electron reduction step. The two successive steps produce semiquinone and quinonedianion (Q²⁻), respectively [86].

Several potent chemotherapeutic agents such as doxorubicin (adriamycin), emodin, mitomycin C, and mitoxantrone (shown in table 2) possess highly substituted stable p-quinone functionalities acting through the redox quinone-hydroquinone system [83, 87]. It is well known that doxorubicin is used as a component in a mixture of compounds used in the treatment of cancer [88]. The chemotherapeutic drugs adriamycin and mitomycin C act as anticancer active agents through the redox quinone-hydroquinone system [89]. In addition, p-quinonimines such as the 1, 2, 4-benzotriazinones have shown anticancer activities [90, 91]. The basic structure of doxorubicin is the anthraquinone moiety. It should be mentioned that a derivative of 1,4-diiminobenzoquinone (19, Y=Cl. X= H) has been reported to be the best, in ten compounds tested, against the ascitic form of sarcoma 180 in mice [112]. Some of the most well-known anticancer agents that belong to the quinone family are shown in Table 2.

2. Anticancer Activity of Quinones in Colorectal Cancer

Anthraquinones are a class of natural compounds that possess anticancer properties [92]. Emodin is an anthraquinone derived from multiple plant families, that has been used for centuries as herbal laxative, anti-inflammatory or antibiotic agent [92-95]. Studies have shown that Emodin promotes apoptosis, inhibits DNA synthesis, halts metastasis, and promotes free radical generation in breast, lung, and prostate cancers. It can also increase the efficacy of other anticancer agents, with minimal toxicity to normal cells. It was shown that Emodin treatment induces apoptosis in CRC by differentially modulating the expression of extrinsic and intrinsic apoptotic molecules, cell survival signaling, and the localization or activity of Bcl-2 family of proteins [96]. Emodin also reduces regulatory components involved in MAPK/JNK, PI3K/AKT, NF- κ B, and STAT pathways associated with apoptotic functions of Bcl-2 family proteins, in addition to decreasing the expression and function of mTOR [96].

In a recent study by Li et al [97], a series of new amide anthraquinone derivative compounds were synthesized, and the mechanism of action of anthraquinones was further examined in colon cancer. The compound 8a was shown to have the best anti-tumor activity against colon cancer cells, by inducing apoptosis via the ROS/JNK signaling pathways [97]. ROS-JNK signaling pathway caused increased ROS production and JNK phosphorylation in colon HCT116 cells, followed by a decrease in mitochondrial membrane potential and release of cytochrome c mediated by the actions of Bax and Bcl-2. These results then led to the cleavage of caspases 9 and 3, which ultimately result in apoptosis [97]

Studies have shown that thymoquinone (TQ), which has a basic quinone structure, induced apoptosis and halted metastasis in CRC [98-101]. TQ suppressed

mouse colon tumor cell invasion and reduced tumor growth in murine colon cancer models. TQ decreased the expression levels of CRC stem cell markers CD44 and EpCAM, and the proliferation marker Ki67 in colonospheres derived from CRC cell lines. TQ induced DNA damage and apoptotic CRC cell death, and inhibited NF- κ B and MEK signaling in mouse tumors.

Also, iminoquinone exerts anticancer effects through inhibition of cell proliferation, inducing cell cycle arrest, and inhibition of oncogene expression in prostate and breast cancer cell lines [102, 103].

Table 2. Anticancer agents that belong to the quinone family [Adapted from [83]]

Quinone	Chemical Structure	Biological Effect ^b	Quinone	Chemical Structure	Biological Effect
Ansamycins (geldanamycin)		Antibiotic, antitumor	β -Lapachone (pink trumpet tree)		Antitumor agent
Daunorubicin/ Doxorubicin	 Daunorubicin, R=H Doxorubicin, R=OH	Antitumor agent	Miltirone (danshen)		TCM
Deoxyxyboquinone		Antitumor agent	Mitomycin C		Antitumor agent
Diaziquinone		Antitumor agent	Mitoquinone		Parkinson's disease
Denbinobin (Shi-Hu, TCM)		Antitumor agent	Mitoxantrone		Antitumor agent
ES936		NQO1 inhibitor	Rhein (cassia acid, rhubarb)		Osteoarthritis
Emodin (rhubarb, buckthorn)		Antitumor agent	Streptonigrin		Antitumor agent
Idebenone		Alzheimer's disease	Ubiquinone (Coenzyme Q ₁₀)	 R=alkyl side chain	Co-factor
Juglone (Black walnuts)	 Juglone, R=H Plumbagin, R=CH ₃	Herbicide	Vitamin K	 R=alkyl side chain R=H, menadiolone	Vitamin

E. Imipridone DRD2 Antagonists

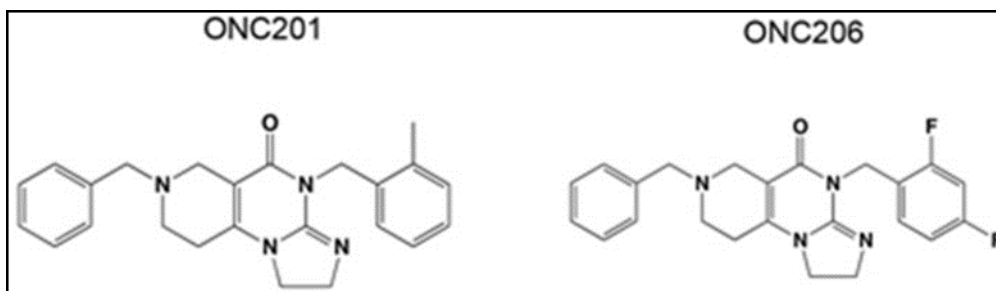


Figure 9. Chemical structure of ONC201 and ONC206.

1. *ONC201*

ONC201 belongs to the imipridone molecular family and was found to have selective competitive and non-competitive antagonist functions of dopamine receptor D2 (DRD2) [104, 105]. It is predicted that ONC201 targets DRD3 as well [104]. Dopamine receptors are upregulated and differentially expressed in several malignancies [106, 107]. The antagonism of DRD2 has resulted in anticancer effects in several tumor types [108-111] through a mechanism of action that is still under investigation. In addition, intracellular signaling can occur downstream of D2-like receptor signaling in a G protein-independent manner *via* β -arrestin, which performs functions related to receptor desensitization and internalization [112], which can further translate into decreased dopamine-mediated tumor growth. It was shown for instance that in glioblastoma cells, DRD2 knockdown mimicked downstream signaling by ONC201 involving both integrated stress response. In contrast, knockout of either DRD2 or DRD3 did not impact ONC201 sensitivity in breast cancer cells indicating a DRD2-independent mechanism of action. Furthermore, isogenic studies showed that ONC201-mediated cancer cell death was affected by transient changes in DRD2 expression, suggesting that it may affect ONC201 anticancer efficacy [113, 114].

In addition to DRD2/3 antagonism, evidence recently uncovered that direct activation of Caseinolytic protease P (ClpP) by ONC201 constitutes another anticancer mechanism of this drug [115]. ClpP is a serine protease located in the mitochondrial matrix that regulates several mitochondrial functions. Direct binding to ONC201 induces a conformational change that leads to hyperactivation of proteolytic activity of ClpP, which in turn leads to increased degradation of respiratory chain complex subunits. ClpP was found to play a role in the activation of the integrated stress response (ISR) [116] and downstream effects including protein synthesis inhibition and ultimately mitochondrial changes initiated by compounds such as ONC201 [115].

TRAIL is an endogenous protein that induces significant tumor-specific apoptosis by binding to death receptors DR4 or DR5 expressed in human tumor cells [117]. In response to ONC201, Foxo3a was found to be activated, where it translocated into the nucleus to transactivate the TRAIL gene by binding to its gene promoter [118]. In particular, pro-survival kinases AKT and ERK were shown to synergistically and indirectly be inactivated by ONC201, which resulted in decreased phosphorylation of their target sites on Foxo3a, effectively activating it [118, 119].

Gene expression profiling (GEP) studies undertaken in CRC and non-Hodgkin lymphoma cell lines showed an 11-gene ER stress response that was upregulated in many types of cells in response to ONC201 treatment [120, 121]. Many of these genes were then shown to be regulated by the ATFA/CHOP axis [122], which is known to promote apoptosis. In other terms, observations from these GEP studies strongly suggested that ATF4 is being activated in tumor cells treated with ONC201. Moreover, anticancer downstream signaling pathways of ONC201 mediated by activation of ISR

occurs by the phosphorylation of eukaryotic initiation factor 2 (eIF2 α) which results in selective increased translation of ATF4 and subsequent increase of CHOP [123] .

a. Anticancer Activity of ONC201 in Colorectal Cancer

ONC201 is in Phase II clinical trials for breast cancer, colorectal cancer, lung cancer, and serous endometrial cancer (SEC) [111]. In CRC, DRD2 is overexpressed in tumor samples [111]. ONC201 demonstrated cytotoxic and apoptotic effects in a dose- and frequency-dependent manner in CRC cell lines; *via* inactivation of AKT and ERK, as well as downstream induction of TRAIL and DR5 expression [124, 125]. ONC201 also induced TRAIL and subsequent cell death in a fresh CRC patient specimen that was not responsive to standard-of-care 5FU chemotherapy. *In vivo* studies using an orthotopic mouse model of p53^{-/-} metastatic CRC have shown that ONC201 has single agent antitumor efficacy, reducing both tumor burden and spread to metastatic sites without apparent toxicity [126].

Furthermore, ONC201 contributed to downregulate CSC markers such as ID1-3 and ALDH7A1, as well as decreasing self-renewal in CRC cell lines. Such effects were observed both *in vitro* and *in vivo* through the use of colonosphere formation assays and subcutaneous CRC xenografts in mice [126, 127]. It appears that resistance to ONC201 treatment in CRC arises through the overexpression or mutation of DRD5 or hyperactivation of mTOR [113, 127].

2. ONC206

ONC206 is an imipridone analogue of ONC201 but with higher potency [128]. ONC206 inhibited cellular proliferation through DRD2/5 and TRAIL/DR5 pathways, in

a dose-dependent manner, and was more potent than ONC201 in SEC cell lines [130]. ONC206 also induced apoptosis in SEC cells, which was demonstrated using ELISA assays, whereby there was increase in relative cleaved caspase-9 and caspase-3 activities in treated cells. In addition, ONC206 triggered ISR activation, manifested by production of ROS and reduction of mitochondrial membrane potential. Wound healing assays showed that ONC206 significantly inhibited cellular adhesion and migration. Pretreatment with the stress inhibitor N-acetylcysteine (NAC) significantly attenuated the efficacy of ONC206 on cell proliferation, ROS production and cellular invasion. This emphasizes the use of ISR activation as an important pathway in its anti-proliferative and anti-metastatic effects [129].

In the study of El-Soussi et al. [128] ONC206 showed more potent effects in targeting MYCN-Amplified Neuroblastoma cell lines than ONC201. ONC206 significantly induced apoptosis, slowed down migration and invasion potential, decreased cellular proliferation, viability, and tumorsphere formation potential in MYCN-amplified neuroblastoma cell lines. ONC206 decreased the protein expression of tumorigenic Sox-2, and Oct-4, and increased expression of cleaved PARP1/caspase-3 and γ -H2AX in the MYCN-amplified IMR-32 cell line [128].

In the study of Wagner et al. [141], ONC206 demonstrated cytotoxic and apoptotic effects in HCT116 cell lines.

With ONC206 exhibiting increased non-competitive DRD2 antagonism, nanomolar potency, distinct biodistribution, differentiated gene expression and disruption of DRD2 dimers relative to ONC201, it might be able to target tumors that are not targeted by ONC201 or that have acquired resistance to it [130].

F. Aim of the Study

The overall aim of this thesis is to investigate the anticancer activities of three novel colon cancer therapeutics, diiminoquinone DIQ, and the DRD2 antagonists ONC201 and ONC206, in 2D colon cancer cell lines, 3D colonospheres and in 3D patient-derived organoids. We hypothesized that 3D models can be used as an *in vitro* model to assess DIQ, ONC201 and ONC206 responses against human colorectal cancer. Altogether, this will hold great promise as it could lead to identifying new effective compounds for better management and treatment of patients with colon cancer. The specific aims of the project are:

- **Specific aim 1:** To investigate the toxicity of DIQ, ONC201, and ONC206 on non-tumorigenic colon cell lines and their ability to target cancer cells with stem-like properties.

- Sub-aim 1-A:* To assess the safety/toxicity of DIQ, ONC201, and ONC206 on non-tumorigenic cell lines in comparison to their anticancer activity against colon cancer cells.

- Sub-aim 1-B:* To investigate the potency of DIQ, ONC201, and ONC206 on sphere formation, sphere size, and self-renewal capacity of spheres derived from colon cancer cell lines grown in 3D setting for up to 5 generations.

- Sub-aim 1-C:* To determine the potential molecular targets of DIQ, ONC201, and ONC206 in 2D and 3D cultures.

- **Specific aim 2:** To establish and propagate 3D human colon organoids derived from fresh tissues from consented treatment-naïve patients undergoing radical

colectomy at American University of Beirut (AUBMC) and assess the effect of DIQ, ONC201, and ONC206 on them.

-Sub-aim 2-A: To assess the effect of DIQ, ONC201, ONC206, and the standard therapy for colorectal cancer 5-fluorouracil (5FU) on the growth of the different patient-derived colon cancer organoids by quantifying the number of organoids forming count (OFC) and calculating the average size (diameters).

Sub-aim 2-B: To examine the efficiency of DIQ, ONC201 and ONC206 on the growth of colorectal cancer cell-derived organoids.

CHAPTER II

METHODS

A. Cell Culture Conditions

Human colorectal cancer cell lines HCT116 and HT29 and non-tumorigenic fetal human fetal intestinal FHS74Int cell line, purchased from ATCC (ATCC, USA) were available in our laboratory. HCT116 and HT29 cell lines were cultured and maintained in RPMI 1640 (Sigma-Aldrich, Germany) and L-glutamine (Sigma-Aldrich). FHS74Int cells were grown in DMEM (Lonza, Belgium) supplemented with 10 µg/mL insulin and 1% sodium pyruvate. Cell culture media was supplemented with antibiotics [1% Penicillin-Streptomycin (P/S) (100 U/mL)], 10% heat-inactivated fetal bovine serum (FBS; Sigma-Aldrich, Germany), and 5 µg/mL Plasmocin™ Prophylactic (InvivoGen). Cells were maintained in an incubator at 37 °C in a humidified atmosphere of 5% CO₂ and 95% air and were routinely checked for mycoplasma contamination. All cells were mycoplasma free.

B. Drug Preparation and Treatment

The purified compound DIQ was synthesized by Professor Makhoul Haddadin (Department of Chemistry, American University of Beirut (AUB)) [81]. Stocks of the purified compound DIQ were prepared by dissolving 5 mg in 1 mL 100% dimethyl sulfoxide (DMSO) (Pan Biotech, Aidenbach, Germany). DIQ dilutions were stored at -20 °C. The drugs ONC201 and ONC206 were purchased from Oncoceutics and were both reconstituted in DMSO, as per manufacturer's instructions. The stock solutions

were then dissolved in cell culture medium such that the percentage of DMSO on cells was less than 0.1%.

C. MTT Cell Proliferation Assay

The anti-proliferative effects of DIQ, ONC201 and ONC206 were measured *in vitro* by using MTT ([3-(4, 5-dimethylthiazol-2-yl)-2, 5-diphenyltetrazolium bromide]) (Sigma-Aldrich) assay according to the manufacturer's instructions. HCT116, HT29 and FHS74Int cells were seeded in 96-well culture plates at a density of 10^4 cells per well and incubated overnight. Then, the subconfluent cells were treated in triplicates with different concentrations of DIQ (1, 4 and 10 μ M), ONC201 and ONC206 (1, 5 and 10 μ M) diluted in 100 μ L complete media for 24, 48 and 72 h. For each time point, 10 μ L of 5 mg/mL (in 1x PBS) MTT reagent was added to each well and incubated at 37 $^{\circ}$ C for 4 h. The reduced MTT dye was solubilized with absolute isopropanol (Sigma-Aldrich) (100 μ L/well) after which MTT optical density (OD) was measured at 595 nm by an ELISA reader (Multiskan Ex). The percent cell proliferation with respect to control was determined for each drug dose.

D. Trypan Blue Exclusion Assay

For the trypan blue dye exclusion method, HCT116, HT29 and FHS74Int cell lines were seeded in duplicates in 24-well culture plates at a density of 5×10^4 , 8×10^4 , 10^5 cells/300 μ L complete media per well, respectively. Cells were incubated overnight then treated in duplicates with various concentrations of DIQ (1, 4 and 10 μ M), ONC201 and ONC206 (1, 5 and 10 μ M) for 24, 48, and 72 h. The supernatant was collected and the attached live cells were harvested by trypsin EDTA. The cell pellet

was re-suspended in 300 μL media. Live cells were counted using a hemocytometer. The percentage cell viability was expressed as percentage growth relative to the control condition of each time point and are derived from the mean of triplicates wells. Each experiment was repeated-minimum three times.

E. Wound Healing Assay

For wound healing or scratch assay, CRC cells were seeded in 24-well plates and incubated until they reached 80–90% confluency. Cells were then treated with 10 $\mu\text{g}/\text{mL}$ mitomycin C (Sigma) to block cellular proliferation. A sterile 200 μL tip was used to scratch wounds of the same width on each monolayer. After washing the plates twice with phosphate buffered saline (PBS, Sigma-Aldrich) to remove the detached cells, the remaining cells were cultured in complete media with or without treatments at IC_{50} concentration. Images were subsequently taken using bright-field microscopy at 0 h and 72 h to compare the wound width. The wound width was measured and expressed as percentage of the relative wound width. The experiment was repeated three times with duplicate measurements in each experiment.

F. Transwell Invasion Assay

HCT116 and HT29 cell lines were seeded at a density of 0.3×10^5 and 0.5×10^5 cells respectively in serum-free medium in the top chamber of 24-well inserts (pore size, 8 μm ; Falcon) coated with 1:10 of Matrigel™ diluted in cold PBS (BD Bioscience, Franklin Lakes, NJ, USA). A medium supplemented with 10% FBS was used as a chemo-attractant in the lower chamber. Cells with or without treatments were allowed to migrate through the membrane coated with Matrigel™ at 37 °C in a 5% CO_2

incubator for 72 h. Cells which did not migrate and remained in the upper chamber were then gently scraped off with a cotton-tip applicator. Invading cells on the lower surface of the membrane were fixed and stained with Hematoxylin and Eosin (H&E). After staining, the total number of invading cells was counted using an inverted light microscope (10x objective) from six consecutive fields for each well.

G. Reactive Oxygen Species

The level of intracellular reactive oxygen species (ROS) in HCT116 and HT29 was determined using the fluorescent probe-DHE which detects ROS. For DHE staining, cells were seeded at a density of 5×10^4 cells on coverslips placed in 24-well cell culture plates and allowed to become 40-50% confluent. Following 48 h incubation with DIQ, or ONC206 treatments at the IC_{50} dose, CRC cells were fixed in 4% formaldehyde for 20 min. After fixation, CRC cells were washed twice with 1x PBS, then incubated with 20 μ M dihydroethidium (DHE) dye (Invitrogen, Carlsbad, CA). After 45 min staining, the DHE stain was removed, and the cells were washed with 1x PBS- and then incubated with mounting media with 4,6-diamidino-2-phenylindole (DAPI) dye. Fluorescence images were taken immediately under a Zeiss LSM710 laser confocal microscope (Carl Zeiss, Germany) equipped with Zen software to process the images.

H. Cell Cycle Analysis

Cells were seeded at 5×10^5 cells in 6-well cell culture plates and incubated overnight prior to drug treatment for 24 and 72 h. Cells were then harvested and washed in PBS then fixed in 70% ice-cold ethanol added dropwise to the cell pellet while

vortexing for 30 min on ice. To ensure that only DNA was stained, fixed cells were incubated for 30 min at 37 °C with 100 µL of a mixture of propidium iodide (PI) (Sigma, USA) and RNase [6 µL RNase, 30 µL PI (1 mg/mL)] in the dark in a flow tube (BD Flacon). A total of 10,000 gated events were acquired in order to assess the proportions of cells of different stages of the cell cycle. Cell cycle analysis was performed by flow cytometry using Guava EasyCyte8 Flow Cytometer- Millipore. GuavaSoft™ 2.7 Software.

I. Annexin V- PI Staining

HCT116 and HT29 cells were seeded at a density of 5×10^5 cells in 6-well cell culture plates and incubated overnight prior to drug treatment for 72 h. Cells were then harvested and washed in cold PBS. The pellet was resuspended in 100 µL binding buffer and stained with 5 µL annexin V-FITC and 5 µL PI in the dark for 30 min at room temperature. Then, 400 µL binding buffer was added and apoptotic cells were analyzed with Guava EasyCyte8 Flow Cytometer- Millipore.

J. Sphere Formation Assay

Self-renewal capacity is deemed to be one of the major defining hallmarks of stem/progenitor cells. Thus, to determine whether DIQ, ONC201 or ONC206 were able to target the self-renewing cancer stem cells (CSC) pool, we investigated sphere formation capability over 5 generations. Sphere formation assay was used as previously reported by our laboratory [131, 132]. Briefly, 1000 single cells were suspended in cold Matrigel™/serum-free medium (1:1) in a total volume of 10 µL. Cells were seeded uniformly in a circular manner around the bottom rim of the well of 96-well culture

plate and allowed to solidify in the incubator at 37 °C for 1 h. Subsequently, 100 µL of RPMI with 5% FBS treated with DIQ, ONC201 or ONC206 was added gently in the middle of each well. Each experimental condition was performed in duplicate. Spheres were replenished with warm media as in the original seeding every other day. Spheres were counted in the 96-well plate dishes after 8 to 12 days of sphere culture and bright field images of the spheres were obtained using Axiovert microscope from Zeiss at 10× magnification. Images were analyzed by Carl Zeiss Zen 2012 image software to determine sizes. Sphere-formation unit (SFU) was calculated for each generation (G) as follows: $SFU = \text{number of spheres formed} / \text{number of cells originally plated}$. Results were represented as percentage of the SFU of each condition.

K. Sphere Propagation Assay

To enrich the stem-like population of cells, the media was aspirated from the well. Spheres were collected using cold media, incubated in 300 µL of Trypsin/EDTA at 37 °C for 1-3 min and then passed through 27-gauge syringes three times. Single cells resulting from the dissociation of spheres were re-plated and treated at the same density of 1000 cells/well in 96-well culture plates as previously described. We believe that at least 5 generations of colonospheres were required to enrich the subpopulation of progenitor/stem-like colon cancer cells.

L. 3D Imaging of Colonospheres

Spheres at G1 were collected with cold RPMI media and centrifuged to washout all MatrigelTM debris. After centrifugation, spheres were fixed in-situ in 4% paraformaldehyde (PFA) at room temperature for 20 min. The PFA was aspirated

gently, and spheres were permeabilized with 0.5% Triton X-100 for 30 min at room temperature. After carefully aspirating the permeabilization solution, spheres were blocked using the sphere blocking buffer (0.1% BSA, 0.2% Triton X-100, 0.05% Tween-20, and 10% normal goat serum in PBS) for 2 h at room temperature. Spheres were washed in PBS then incubated overnight with different primary antibodies for assessment of treatment and characterization including Ki67, CD44, γ -H2AX, CK19 and CK8 (refer to table 5 for details on antibodies used). After gentle washing with PBS containing 0.1% Tween-20, spheres were incubated with Alexa-488 and/or 568 conjugated IgG (Invitrogen, CA) for 2 h at room temperature. Spheres were mounted with the anti-fade Fluoro-gel II with DAPI (Abcam, Cambridge, UK). Confocal fluorescent images were acquired and analyzed using the Carl Zeiss LSM 710 laser scanning confocal microscope.

M. Western Blot Analysis

For 2D western blot (WB) results, cells were plated in 12-well plates, treated with DIQ, ONC201 or ONC206 and then collected. For 3D WB results, HCT116 and HT29 cells were plated in 24-well plates (3×10^5 cells/well) with or without treatment to form spheres. At day 8-10 of culture, spheres were collected with cold RPMI media then washed with PBS to remove any residual media. Proteins were then extracted from collected cells and spheres with RIPA lysis buffer (sc-24948, Santa Cruz, CA, USA). Protein extracts were quantified using the DC Bio-Rad Protein Assay (Bio-Rad Laboratories, Hercules, California, USA) according to the manufacturer's protocol. Equal amounts of protein lysate were mixed with 5% β -mercaptoethanol and 2X Laemmli Sample Buffer (Bio-Rad, CA, USA), electrophoresed in 12% sodium dodecyl

sulfate (SDS)-polyacrylamide gel electrophoresis (PAGE), and then transferred to 0.45 µm nitrocellulose membrane (Bio-Rad, CA, USA) for 2 h. Membranes were blocked for 1 h with 5% skim milk in tris-buffered saline with 0.1% tween 20 (TBST), then blotted with primary antibodies (antibodies used are listed in Table 6) overnight at 4 °C. The next day, membranes were washed three times with TBST and blotted with corresponding secondary antibodies for 1 h at room temperature. Hybridization with GAPDH-HRP (6C5) coupled antibody was performed for 1 h at room temperature as housekeeping gene. Membranes were developed and target proteins were detected using the ECL system (Bio-Rad, CA, USA). Images were generated and quantified using ChemiDoc™ Imaging Systems (Bio-Rad, CA, USA).

N. Ethical Consideration

The study with all its experimental protocols was conducted under the Institutional Review Board (IRB) approvals of AUB-and American University of Beirut Medical Center (AUBMC) to obtain patient information and human colorectal tissue samples from consented patients. All protocols were performed in accordance with The Code of Ethics of the World Medical Association (Declaration of Helsinki) and in agreement with all ethical considerations of the IRB for experiments involving human subjects. Oral/Written informed consent was obtained from all patients and confidentiality was maintained. If a consented patient was undergoing any colon cancer surgery, a primary or metastatic tissue sample was collected only if it did not compromise the sample for diagnosis or staging.

O. Tissue Processing and Organoid Culture

Colon and prostate tumor tissues from patients were rinsed with PBS, manually minced using sterile scalpels. The majority of minced fragments was employed for organoid culturing; remaining fragments were transferred directly to 4% PFA for histological examination. Colon minced fragments for organoid culturing were digested in advanced adDMEM/F12 (Gibco) supplemented with 1x P/S, collagenase IV (Sigma-Aldrich), and amphotericin B (Sigma-Aldrich) at 37 °C for 1 h according to the protocol described by Boehnke et al [133]. Prostate minced fragments for organoid culturing were digested with the same mixture at 37 °C overnight according to the protocol used in the laboratory of Dr. Abou-Kheir [134]. During incubation, the tissue fragments were repeatedly suspended with a 100 µL micro-pipette. To exclude undigested tissue fragments, the suspension was filtered through a 100 µm cell strainer (Corning). The flowthrough was subjected to consecutive filtrations when needed. Isolated cells were seeded in 24-well plates with Matrigel™ at a cell density of 2×10^4 single cells/well. 20 µL drops were plated into the middle of the well. The plate was placed upside down in the 37 °C incubator for 15 min to allow the Matrigel™ to solidify. Finally, 300 µL of pre-warmed human colon growth medium plus Y-27632 was added into each well. Cells were cultured with adDMEM/F12 supplemented with various factors added to maintain tumor's biological traits and growth activity. Medium with or without treatment was changed every 2-3 days. Cultures were passaged when the aggregates reached 800 µm diameter. Colon Organoids were counted at day 8-12 of each passage under Axiovert inverted microscope- whereas prostate organoids were counted at day 19-21. Images of organoids were taken, then analyzed by Carl Zeiss Zen 2012 image software to determine size. The organoid formation count (OFC) was calculated at each

generation by counting the number of organoids formed, starting with the same number of input cells in all conditions.

Table 3. List of components and their respective concentrations used in human colorectal organoids culture medium. Adopted and modified from Boehnke et al. [133].

Component	Stock Concentration	Final Concentration
N2	100X	1X
B27	50X	1X
NAC	500mM	1mM
EGF	500µg/mL	50ng/mL
Noggin	100 µg/mL	50 ng/mL
FGF2	50µg/mL in PBS + 0.1% BSA	20ng/mL

Table 4. List of components and their respective concentrations used in human prostate organoids culture medium. Adopted and modified from Cheaito et al. [134].

Component	Stock concentration	Final concentration
B27	50X	1X
Nicotinamide	1M	10 mM
NAC	500 mM	1.25 mM
A83	5 mM	500 nM
Noggin	100 µg/mL	50 ng/mL
FGF10	0.1 mg/mL	10 ng/mL
RI	10 mM	10 µM

P. Passaging of the Newly Established Organoids

Organoids were collected when they reached the appropriate size and confluency for passaging (8-12 days after plating). Ice-cold medium was used to dissolve MatrigelTM and collect organoids. Organoids were then centrifuged at 200 g for 5 min at 4 °C. After that, the pellet was resuspended in 1 mL ice-cold addMEM/F12 to dissolve residual Matrigel. After counting the cells in the pellet, the cells were

resuspended in 90% cold Matrigel™ and seeded as a 5 µL drop in 96-well plate. Cells were cultured with adDMEM/F12 additional with various factors and medium was changed every 2-3 days with or without treatments. Cultures were passaged when the aggregates reached 800 µm diameter. The previous steps were repeated for several generations.

Q. Cell Line-Derived Organoids

Briefly, 5000 HCT116 and HT29 single cells were suspended in cold Matrigel™/serum-free medium (9:1) in a total volume of 5 µL and added as drops in the middle of individual wells of 96-well culture plates. Plated colon cells were allowed to solidify in the incubator at 37 °C for 30 min. Subsequently, 200 µL/well of advanced DMEM/F12 media with several factors, with or without DIQ, ONC201 or ONC206 treatments were added. Each experimental condition was performed in duplicate. Organoids were replenished with warm media as in the original seeding every other day. Organoids were counted in the 96-well plate dishes after 8 to 12 days of organoid culture and bright field images of the organoids were obtained using Axiovert microscope from Zeiss at 10× magnification.

R. Immunofluorescence and Morphological Analysis of Organoids

Indirect immunofluorescence analysis was used to characterize the colon epithelial lineage CK19 and stem cell marker CD44 expressed by the 3D organoids. To preserve the 3D architecture, immunofluorescence analysis was performed in suspension. Collected organoids using cold medium were fixed in-situ in 4% PFA at room temperature for 20 min. The PFA was aspirated gently, and organoids were

permeabilized with 0.5% Triton X-100 for 30 min at room temperature. After carefully aspirating the permeabilization solution, organoids were blocked using the blocking buffer (0.1% BSA, 0.2% Triton X-100, 0.05% Tween-20, and 10% normal goat serum in PBS) for 1 h at room temperature. Organoids were incubated overnight with the primary antibodies, CK19 and CD44, at 4 °C. After gentle washing with PBS containing 0.1% Tween-20, organoids were incubated with Alexa-488 and/or 568 conjugated IgG for 2 h at room temperature. Organoids were mounted with the anti-fade Fluoro-gel II with Dapi. Confocal microscopic analyses were performed using Zeiss LSM 710 confocal microscope and images were acquired and analyzed using the ZEN 2012 image software.

Paraffin embedding, microtome sectioning and standard hematoxylin and eosin (H&E) staining were all performed by the Histology Laboratory at the Diana Tamari Sabbagh building; all steps were performed at room temperature.

S. Animal Experiments

Animal experiments were performed according to approved protocols by the Institutional Animal Care and Use Committee of the American University of Beirut (AUB, IACUC). Mice were housed under optimum conditions of temperature and light set in specific pathogen-free animal housing. Mice were kept in plastic cages covered with sawdust and had unrestricted access to a commercial mouse diet (24% protein, 4.5% fat, 4% fiber) and water. Animals were sacrificed by cervical dislocation following deep anesthesia with isoflurane. For tumor induction in mice, a group of 6-8 week old NOD/SCID male mice were inoculated subcutaneously into the flanks with 100 HCT116-derived spheres in a total volume of 50 µL growth media and Matrigel™

(1:1). Upon the detection of a palpable tumor post cells/spheres injection, mice were divided to 2 groups. The first group was treated with saline (control group), and the second group was treated with DIQ (20 mg/Kg). Mice were treated three times/week until tumor burden necessitates that we sacrificed the animals. Tumor size was measured every other day using Mitutoyo caliper throughout the study. Mice were daily monitored for signs of morbidity. Body weight recordings were carried out biweekly.

T. Microscope Imaging

Cells were visualized and imaged by Axiovert inverted microscope from Zeiss at 5, 10, and 20× magnification. Confocal images were taken on Confocal Microscope Zeiss LSM710 at 40× oil immersion magnification.

U. Statistical Analysis

All statistical tests were performed including student's t-test, One-way or two-way ANOVA tests using GraphPad Prism 7 (version 7.0, GraphPad Software Inc., La Jolla, CA, USA). Statistical significance was reported at p-values of < 0.05. * P<0.05; ** P<0.01; *** P<0.001. Experimental values are means ± standard error of the mean (SEM).

Table 5. List of primary and secondary antibodies used in immunofluorescent staining

Antibody name	Species	Dilution	Catalog number	Company
Primary antibodies				
CK8	Mouse	1:200	904801	Biologend
CK19	Rabbit	1:200	ab15463	Abcam
CD44	Mouse	1:100	sc-7297	Santa Cruz
Ki67	Mouse	1:50	sc-23900	Santa Cruz
p- Histone H2AX	Rabbit	1:200	# 9718S	Cell signaling
Secondary antibodies				
Alexa fluoro 488	Goat anti-mouse	1:200	A-28175	Invitrogen
Alexa fluoro 568	Goat anti-rabbit	1:200	A-11011	Invitrogen
Phalloidin		1:200	R415	Invitrogen

Table 6. List of primary and secondary antibodies used in western blot experiments

Antibody name	Species	Dilution	Catalog number	Company
Primary antibodies				
p53	Rabbit	1:50	sc-6243	Santa Cruz
p21	Rabbit	1:1000	sc-2947	Cell signaling
CD133	Rabbit	1:500	# 64326S	Cell signaling
β -catenin	Mouse	1:200	sc-7963	Santa Cruz
PCNA	Mouse	1:50	sc-25280	Santa Cruz
p-ERK	Mouse	1:300	sc-7383	Santa Cruz
ERK	Rabbit	1:300	sc-93	Santa cruz
p-AKT	Rabbit	1:1000	#4060	Cell signaling
AKT	Rabbit	1:1000	#4691	Cell signaling
GAPDH-HRP (6C5)	Mouse	1:20,000	#MAB5476	Abnova
Secondary antibodies				
Goat anti-mouse	Goat	1:1000	sc-516102	Santa Cruz
Mouse anti-rabbit	Mouse	1:1000	sc-2357	Santa Cruz

Table 7. Colorectal cancer patients' clinical and histopathologic characteristics

	Patient 1	Patient 2	Patient 3	Patient 4	Patient 5
Gender	N/A	Female	Male	Female	Female
Age	N/A	86 (deceased)	62	55	61
BMI	N/A	28.3	29.7	25	21
Smoking	N/A	No	Yes	No	Yes
Chemotherapy preop	N/A	No	No	No	No
Radiation therapy preop	N/A	No	No	No	No
Location of tumor	N/A	Left (descending) colon	Rectum	Sigmoid colon	Descending colon/ sigmoid colon
Type	Adenocarci noma	Adenocarcin oma	Mucinous adenocarcinoma	Adenocarcinoma	Adenocarcinoma
T stage	N/A	pT3	pT2	pT2	pT3
N stage	N/A	pN0	pN0	pN0	pN0
M stage	N/A	N/A	N/A	N/A	N/A
Size	N/A	7 cm	6 cm	4.5 cm	2 cm
Grade	N/A	2: Moderately differentiated	Not applicable: mucinous tumor	2: Moderately differentiated	2: Moderately differentiated

CHAPTER III

RESULTS

A. Effect of DIQ, ONC201 and ONC206 Compounds on the Cell Proliferation of Human Non-Tumorigenic and Colorectal Cancer Cell Lines in 2D in vitro Models

To assess the effect of DIQ, ONC201 and ONC206 compounds on the proliferation of human CRC cell lines cultured in 2D monolayers, we employed the MTT assay. Two human CRC cell lines, HCT116 and HT29, were treated with different concentrations of DIQ (1, 4, and 10 μM), ONC201 and ONC206 (1, 5, and 10 μM) for 24, 48 and 72 h. The MTT results revealed that the three novel therapeutics significantly inhibited the proliferation of HCT116 and HT29 human CRC cells in a time- and dose-dependent manner (Figures 10 and 11). Interestingly, a concentration of each DIQ and ONC206 compounds as low as 4 and 1 μM respectively were able to inhibit cell proliferation by approximately more than 30% at 24 h in HCT116 and more than 50% cell reduction was observed at 48 and 72 h in both cell lines. The mean IC_{50} values of DIQ, ONC201 and ONC206 were $\sim 4 \mu\text{M}$, $\sim 5 \mu\text{M}$, and $\sim 1 \mu\text{M}$ respectively in both cell lines (Figures 10 and 11).

As shown in Figures 9 and 10, ONC206 exhibited dose-dependent anti-proliferative effects on tested cell lines at significantly lower doses than that of ONC201. The maximum percentage of reduction in proliferation of HCT116 and HT29 cells upon 1 μM ONC201 treatment at 72 h was almost 10% and 12% compared to 70% and 62% upon the same concentration of ONC206 treatment respectively. These

experiments revealed that the micromolar activity of ONC206 was more potent as compared to that of ONC201 in both cell lines (Figures 10 and 11).

The effect of DIQ, ONC201 and ONC206 on the viability of the human CRC cell lines was further confirmed by trypan blue method (Figures 12 and 13). There was consistency between the MTT results and trypan blue exclusion assay. Following 72 h, the inhibitory effects of DIQ, ONC201 and ONC206 were accompanied with considerable changes in cell morphology and confluency. Treated cell lines were less clumped, unlike control cells which had large nuclei and were more clumped (Figure 14).

It is worth noting that the toxicity of all treatments at their corresponding IC_{50} concentrations was investigated in FHS74Int cells derived from non-tumorigenic human fetal intestinal tissue by MTT and Trypan blue exclusion assays. Interestingly, all treatments had relatively limited toxicity to the human non-tumorigenic intestinal FHS74Int cells when applied over 72 h period (Figures 15 and 16).

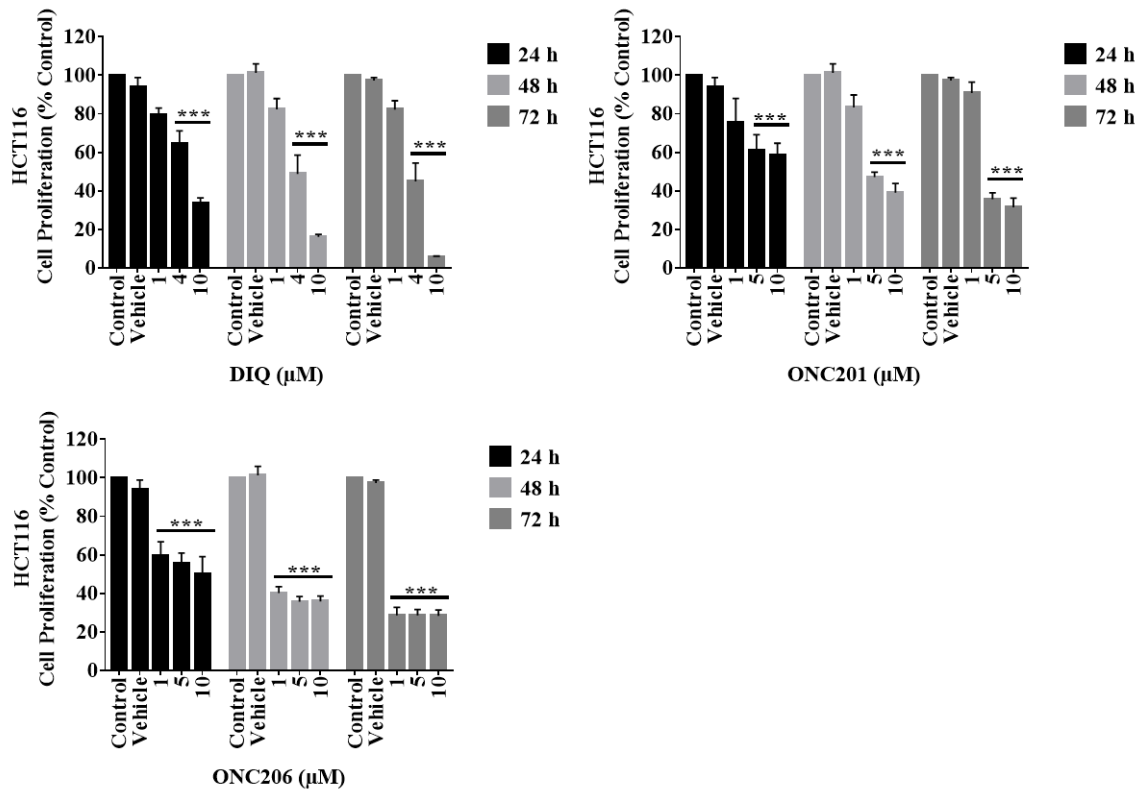


Figure 10. DIQ, ONC201 and ONC206 reduce the proliferation of HCT116 CRC cell lines in a time and dose-dependent manner. The anticancer effect of different concentrations of DIQ, ONC201 and ONC206 on the proliferation of HCT116 cells using MTT assay was determined in triplicates at 24, 48 and 72 h. Results are expressed as percentage of proliferation of the treated group compared to control at every time point. Data represents an average of three independent experiments and is reported as mean \pm SEM (* P<0.05; ** P<0.01; *** P<0.001).

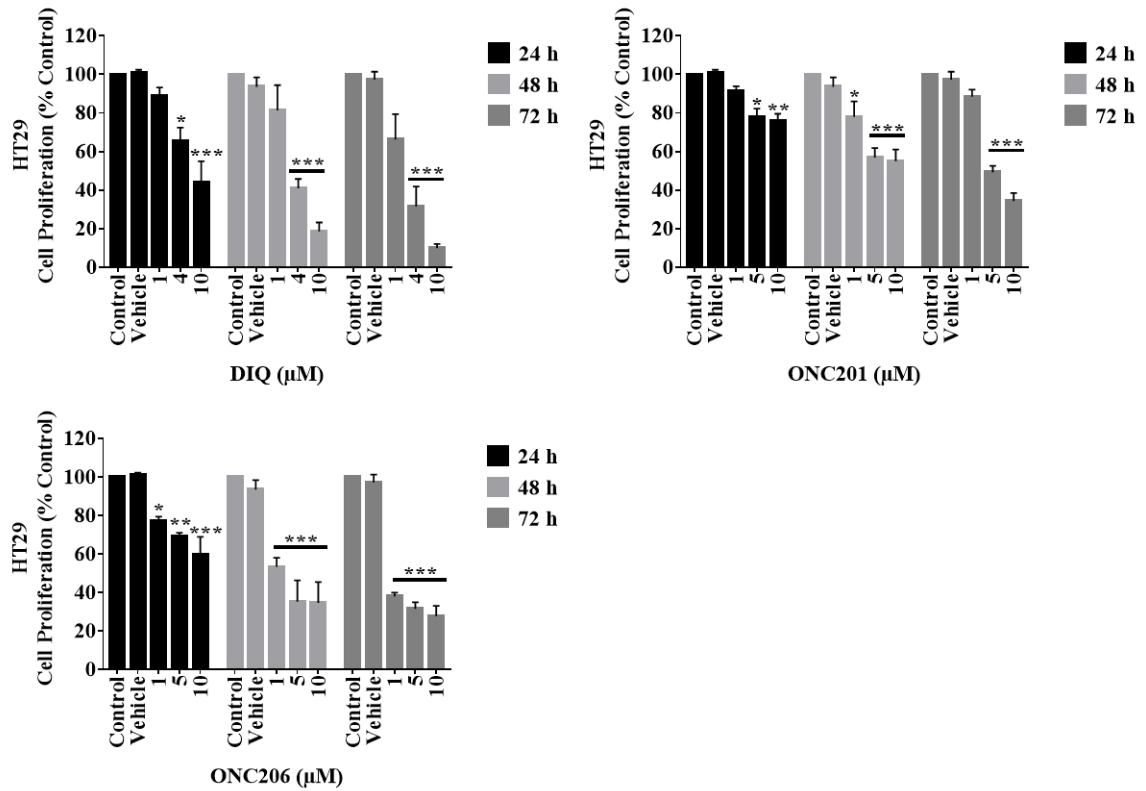


Figure 11. DIQ, ONC201 and ONC206 reduce the proliferation of HT29 CRC cell lines in a time and dose-dependent manner. The anticancer effect of different concentrations of DIQ, ONC201 and ONC206 on the proliferation of HT29 cells using MTT assay was determined in triplicates at 24, 48 and 72 h. Results are expressed as percentage of proliferation of the treated group compared to control at every time point. Data represents an average of three independent experiments and is reported as mean \pm SEM (* P<0.05; ** P<0.01; *** P<0.001).

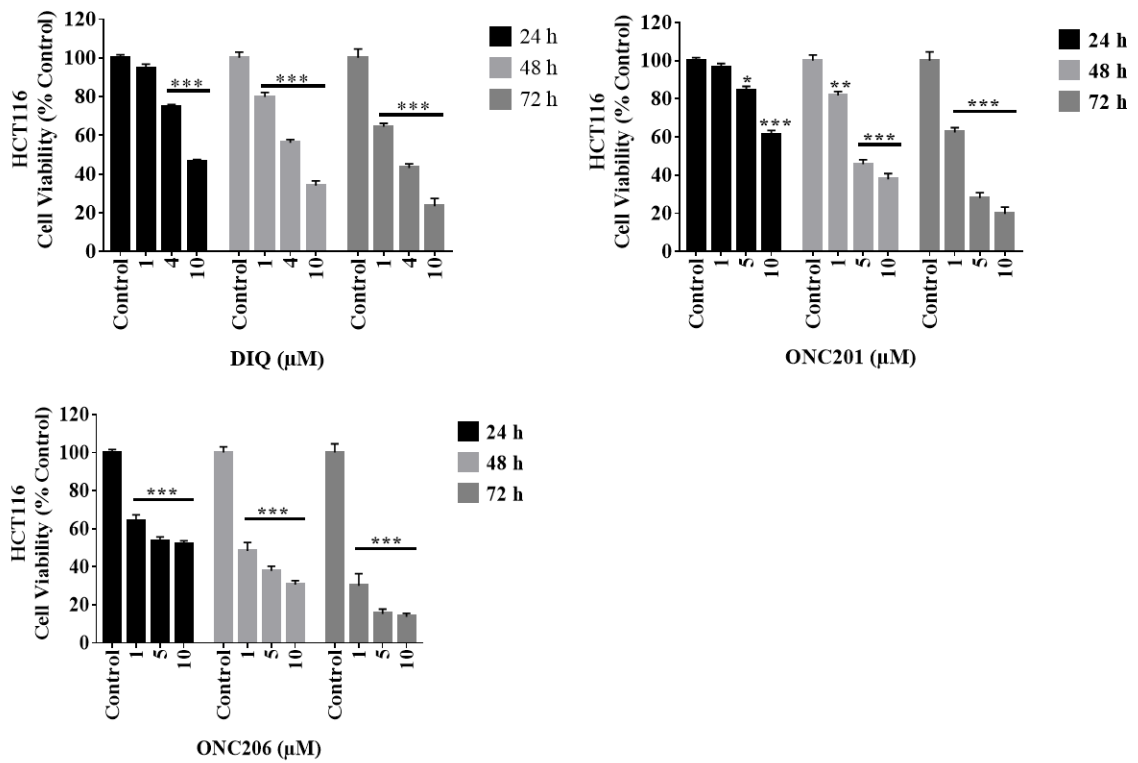


Figure 12. DIQ, ONC201 and ONC206 reduce the viability of HCT116 CRC cell lines in a time and dose-dependent manner. The anticancer effect of different concentrations of DIQ, ONC201 and ONC206 on the viability of HCT116 cells using trypan blue exclusion assay was determined in duplicates at 24, 48 and 72 h. Results are expressed as percentage of proliferation of the treated group compared to control at every time point. Data represents an average of three independent experiments and is reported as mean \pm SEM (* P<0.05; ** P<0.01; *** P<0.001).

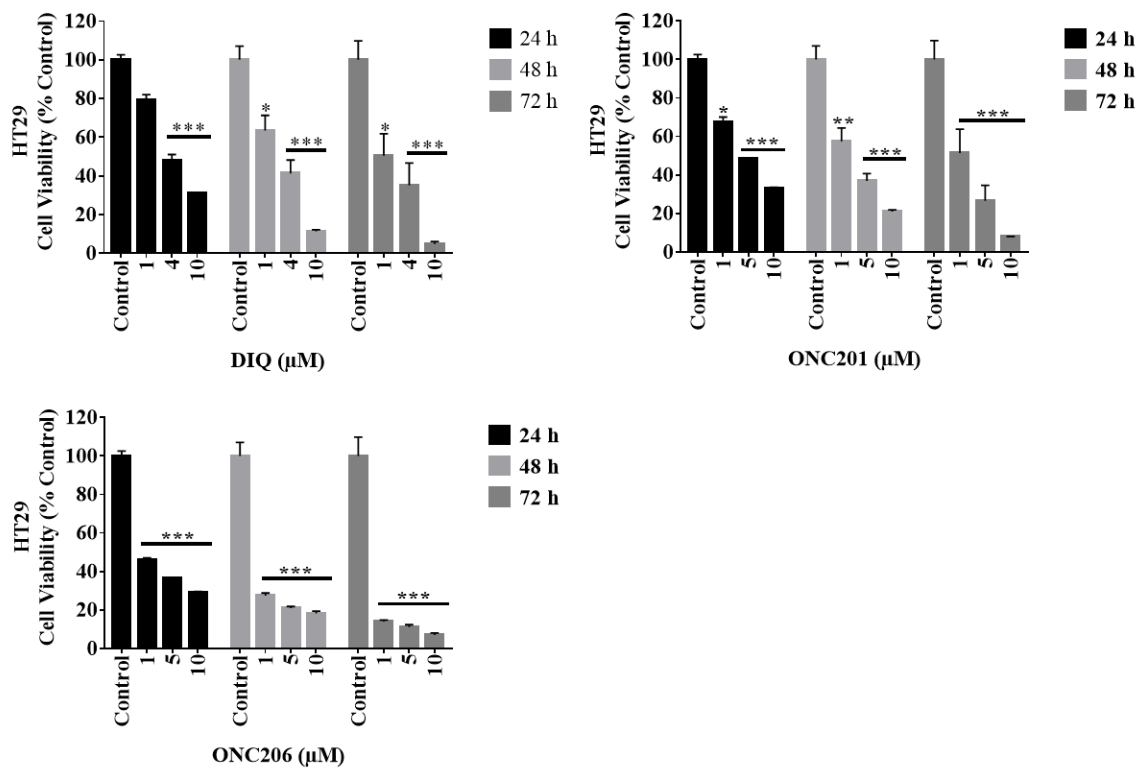


Figure 13. DIQ, ONC201 and ONC206 reduce the viability of HT29 CRC cell lines in a time and dose-dependent manner. The anticancer effect of different concentrations of DIQ, ONC201 and ONC206 on the viability of HT29 cells using trypan blue exclusion assay was determined in duplicates at 24, 48 and 72 h. Results are expressed as percentage of proliferation of the treated group compared to control at every time point. Data represents an average of three independent experiments and is reported as mean \pm SEM (* P<0.05; ** P<0.01; *** P<0.001).

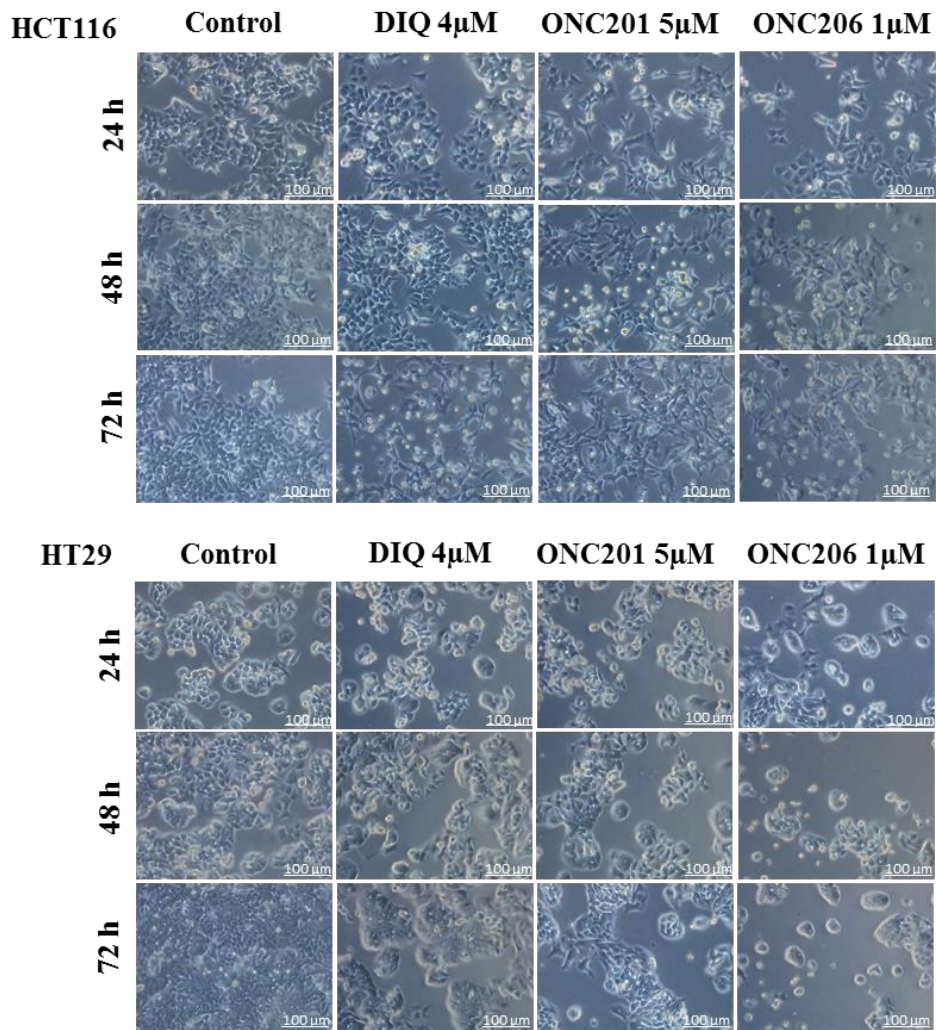


Figure 14. The inhibitory effects of DIQ, ONC201 and ONC206 were accompanied with considerable changes in cell morphology and confluency. Representative images of HCT116 and HT29 cells upon DIQ, ONC201 or ONC206 treatment up to 72 h at 20 \times magnification (scale bar = 100 μ m).

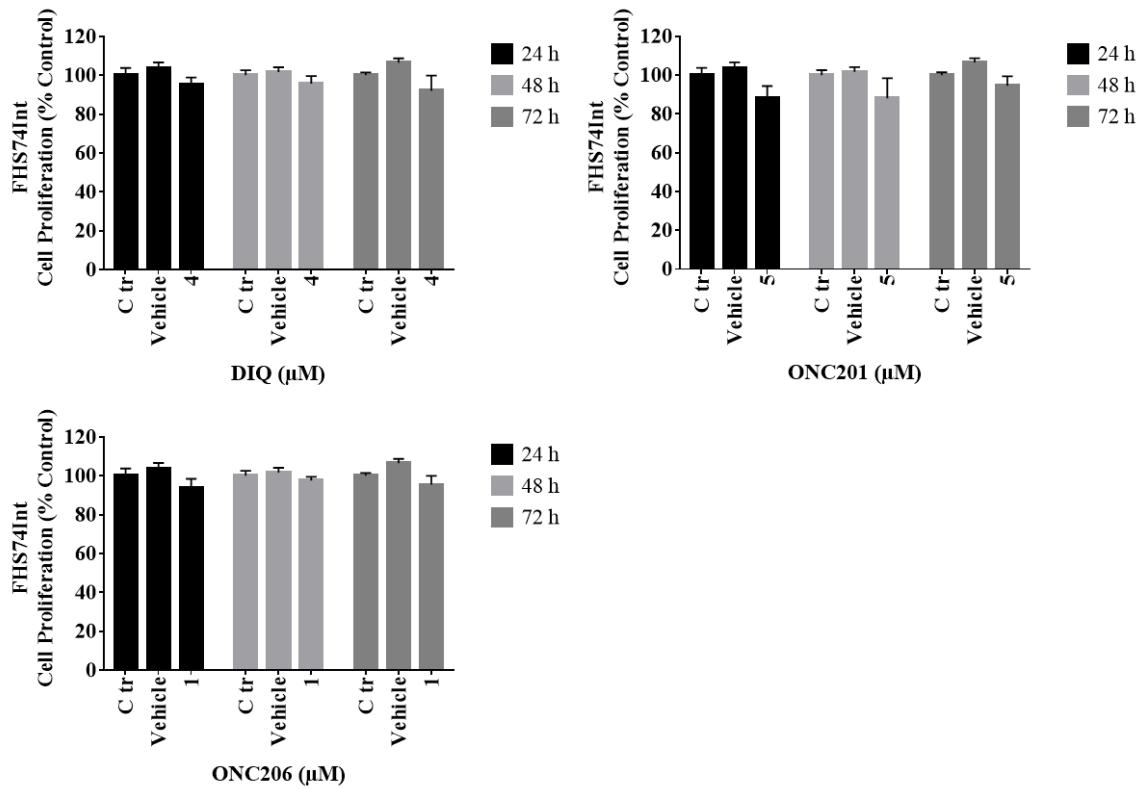


Figure 15. DIQ, ONC201 and ONC206 have relatively limited toxicity on the proliferation of FHS74Int cell line. The anticancer effect of DIQ (4 μM), ONC201 (5 μM) and ONC206 (1 μM) on the proliferation of FHS74Int cells was determined at 24, 48 and 72 h using MTT. Results are expressed as percentage of proliferation or viability of the treated group compared to control at every time point. Data represents an average of three independent experiments and is reported as mean ± SEM (* P<0.05; ** P<0.01; *** P<0.001).

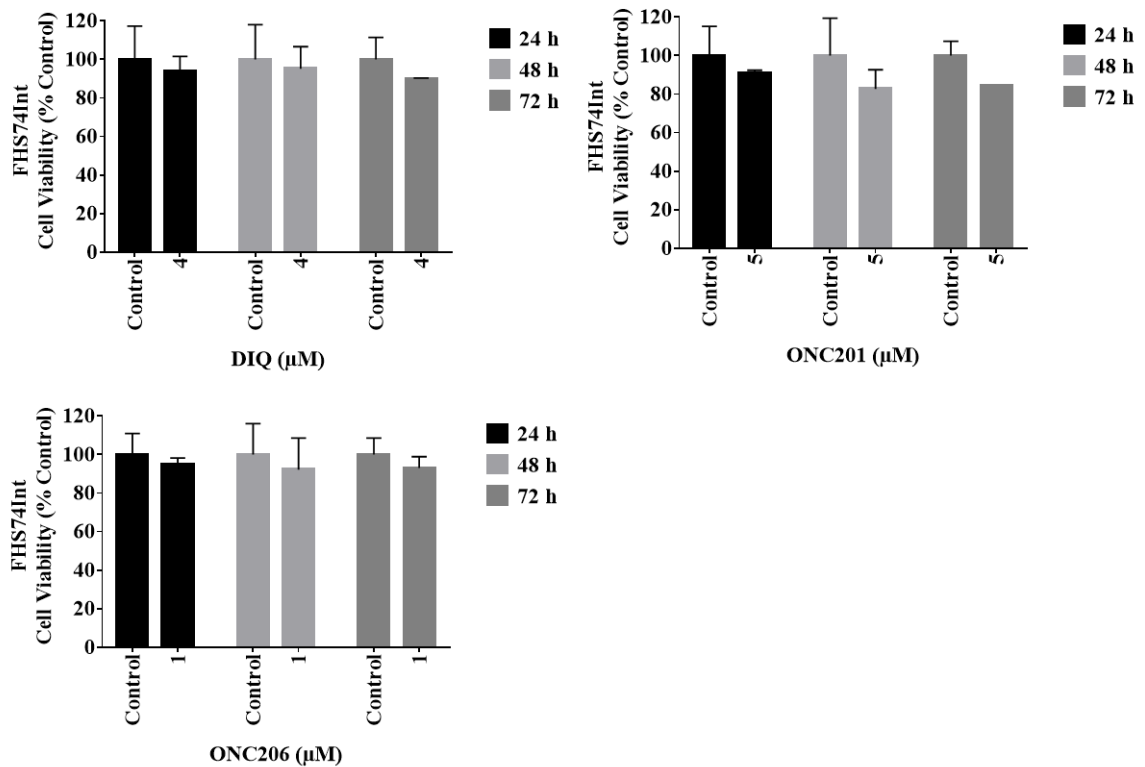


Figure 16. DIQ, ONC201 and ONC206 have relatively limited toxicity on the viability of FHS74Int cell line. The anticancer effect of DIQ (4 μM), ONC201 (5 μM) and ONC206 (1 μM) on the viability of FHS74Int cells was determined at 24, 48 and 72 h using Trypan blue exclusion assays. Results are expressed as percentage of proliferation or viability of the treated group compared to control at every time point. Data represents an average of three independent experiments and is reported as mean ± SEM (* P<0.05; ** P<0.01; *** P<0.001).

B. Effect of DIQ, ONC201 and ONC206 on Migration and Invasion Ability of Colorectal Cancer Cells

As activating invasion and metastasis are hallmarks of cancer progression, wound healing and transwell invasion assays were employed to evaluate the effects of DIQ, ONC201 and ONC206 on human CRC cell migration and invasion. All treatments at their corresponding IC₅₀ concentrations significantly suppressed and slowed down cell migration ability of both cell lines at 72 h compared to the vehicle-treated control cells as determined by the wound healing assay (Figures 17 and 18). The treatments

failed to close the wound by more than 70% in both cell lines compared with control conditions, which were able to almost complete wound closure (Figures 17 and 18).

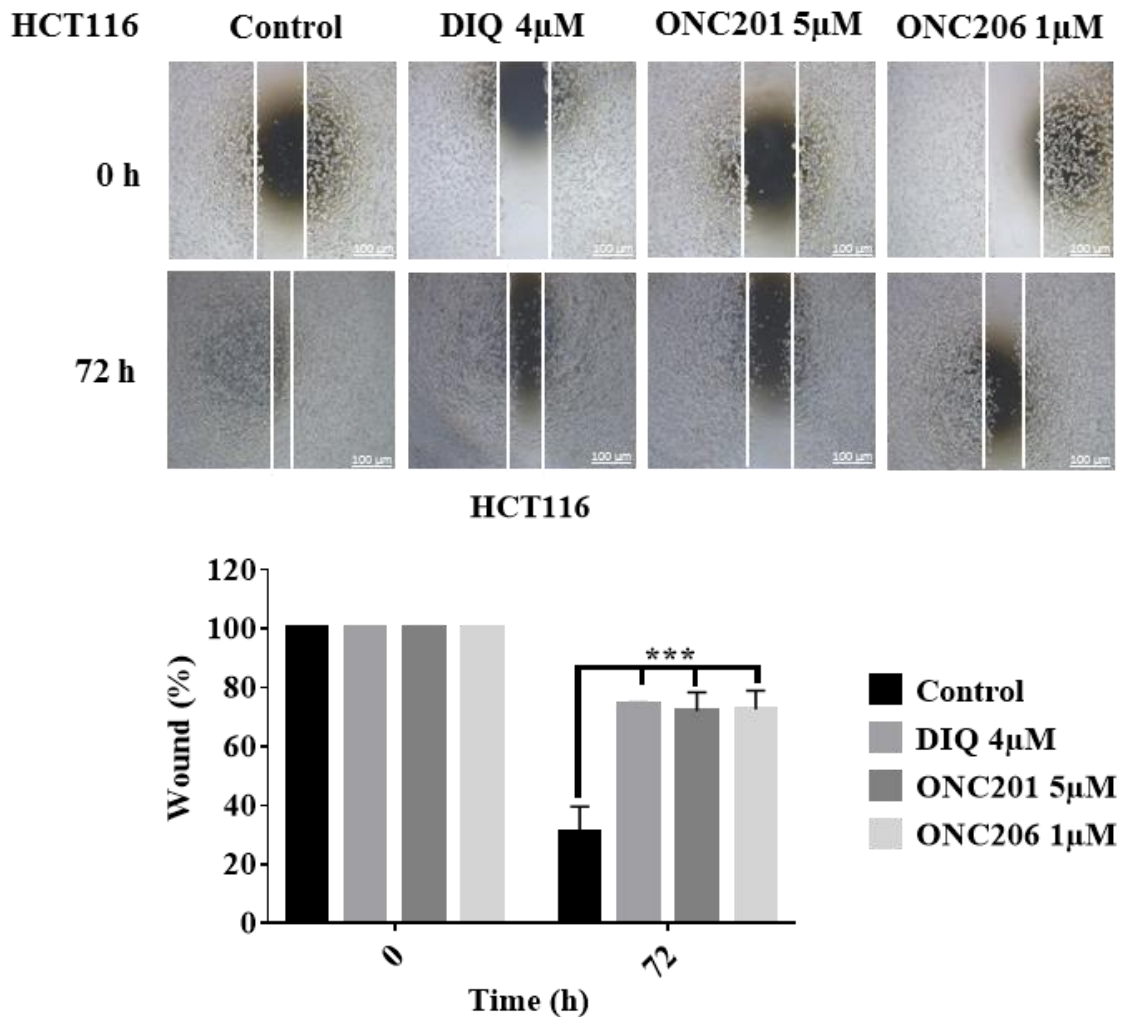


Figure 17. DIQ, ONC201, and ONC206 reduce the migration of HCT116 colorectal cancer cells. HCT116 cells were seeded in 24-well plate. A scratch was made on confluent cells using a 200 µL tip and images were taken at 0, 24, 48 and 72 h with or without the indicated treatment concentration. Representative images of wound healing assay at 5× magnification (scale bar = 100 µm). Quantification of the distance of the wound closure was assessed over time. Results are expressed as a percentage of each group compared to its condition at 0 h. Data represent an average of three independent experiments. The data are reported as mean ± SEM (* P<0.05; ** P<0.01; *** P<0.001).

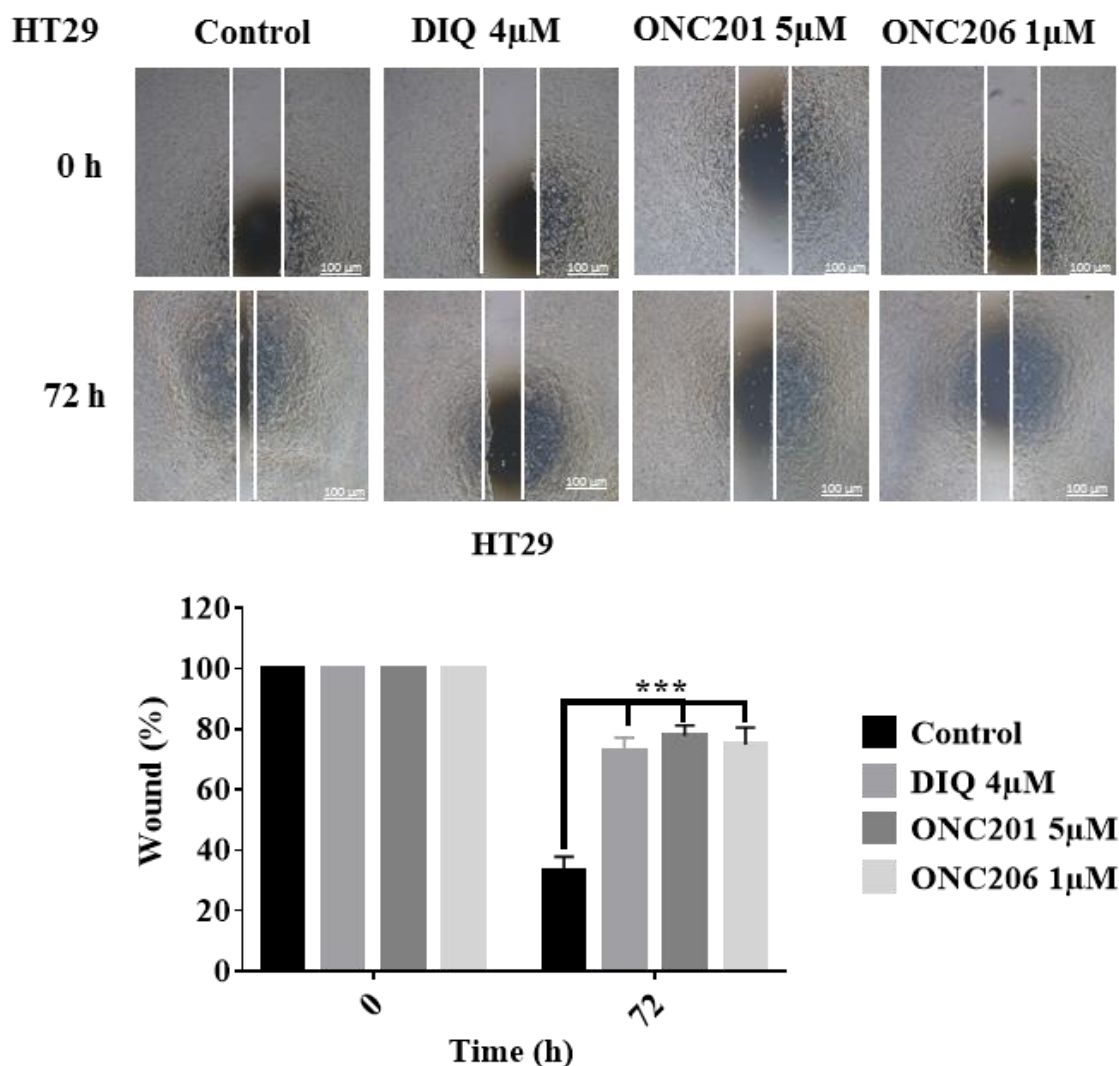


Figure 18. DIQ, ONC201, and ONC206 reduce the migration of HT29 colorectal cancer cells. HT29 cells were seeded in 24-well plate. A scratch was made on confluent cells using a 200 µL tip and images were taken at 0, 24, 48 and 72 h with or without the indicated treatment concentration. Representative images of wound healing assay at 5× magnification (scale bar = 100 µm). Quantification of the distance of the wound closure was assessed over time. Results are expressed as a percentage of each group compared to its condition at 0 h. Data represent an average of three independent experiments. The data are reported as mean ± SEM (* P<0.05; ** P<0.01; *** P<0.001).

In addition, DIQ and ONC206 showed significant inhibitory potential on CRC cell invasion. The number of HCT116 and HT29 invasive cells were remarkably decreased in response to FBS in treated conditions reaching a value of less than two-folds compared to the control condition at 72 h (Figure 19). Collectively, these results

suggest that DIQ and ONC206 have anti-migratory and invasive effects on CRC cell lines.

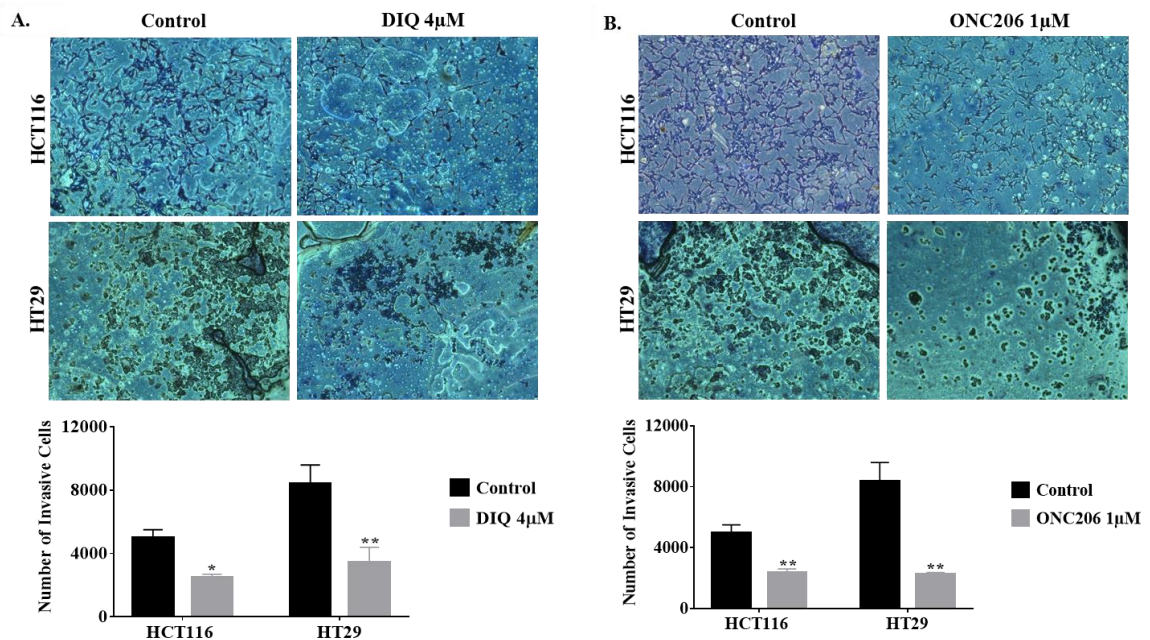


Figure 19. DIQ and ONC206 reduce the invasion of HCT116 and HT29 colorectal cancer cells. HCT116 and HT29 cells were seeded onto the MatrigelTM-coated membrane in the top chamber of the transwell and were either treated or not with the indicated treatment concentration of DIQ (A) or ONC206 (B) in the presence of FBS in the lower chamber. Cells that invaded to the lower chamber after 72 h were fixed with methanol, stained with H&E, counted and represented as number of invading cells compared to the control. Data represent an average of three independent experiments. The data are reported as mean \pm SEM (* $P < 0.05$; ** $P < 0.01$; *** $P < 0.001$).

C. Effect of DIQ, ONC201 and ONC206 on Cell Cycle and Apoptosis in Colorectal Cancer Cells

To evaluate the underlying mechanism of growth inhibition by DIQ, ONC201 and ONC206 in CRC, the cell cycle distribution analysis of HCT116 and HT29 cells treated with the IC_{50} concentrations of each treatment for 72 h was performed using flow cytometry. As shown in Figure 20, DIQ treatment in HCT116 cells caused G1 arrest with concomitant decreases in the S and G2/M fractions mainly after 72 h. No

changes in the cell cycle were noticed after treating both cell lines with DIQ for 24 h. DIQ effect on the HCT116 cell cycle was pronounced at 72 h. The proportion of HCT116 cells in G1 phase was increased from 45.6% in control cells to 60.2% in cells treated with DIQ for 72 h, while the proportion of cells in G2/M phase decreased from 35.2 to 21.5% (Figure 20). However, in HT29 cells, DIQ treatment induced S phase (38.35%) cell cycle arrest after 72 h treatment and depleted cells at G1 and G2/M phases. Interestingly, upon treatment with 4 μ M DIQ, the percentage of HCT116 and HT29 cells in the sub-G1 phase significantly increased reaching 3.5- and 5-folds at 72 h, respectively; suggesting that the reduction in cell viability in response to DIQ could be due to cell death (Figure 20).

ONC201 and ONC206 significantly induced sub-G1 apoptotic cells and S arrest in HCT116 and HT29 cells. As illustrated in Figures 21 and 22, treatment with 5 μ M ONC201 and 1 μ M ONC206 for 72 h caused significant increase in the S phase with concomitant increase in G1 phase and decrease in G2/M fractions in CRC cells. S arrest phase increased from 17% in control cells to 31.2% in the ONC201-treated HCT116 cells and from 30 to 37% in the HT29 cells. The S phase cell population significantly increased from 17 to 30% with ONC206 in the HCT116 and from 30 to 35% in the HT29 cells.

To further confirm whether growth inhibition was related to apoptosis, Annexin V and PI staining was performed. As shown in Figures 20, 21 and 22, after treating CRC cells with DIQ, ONC201 or ONC206 at the indicated concentrations for 72 h, the total apoptotic cell populations were significantly increased in both cell lines.

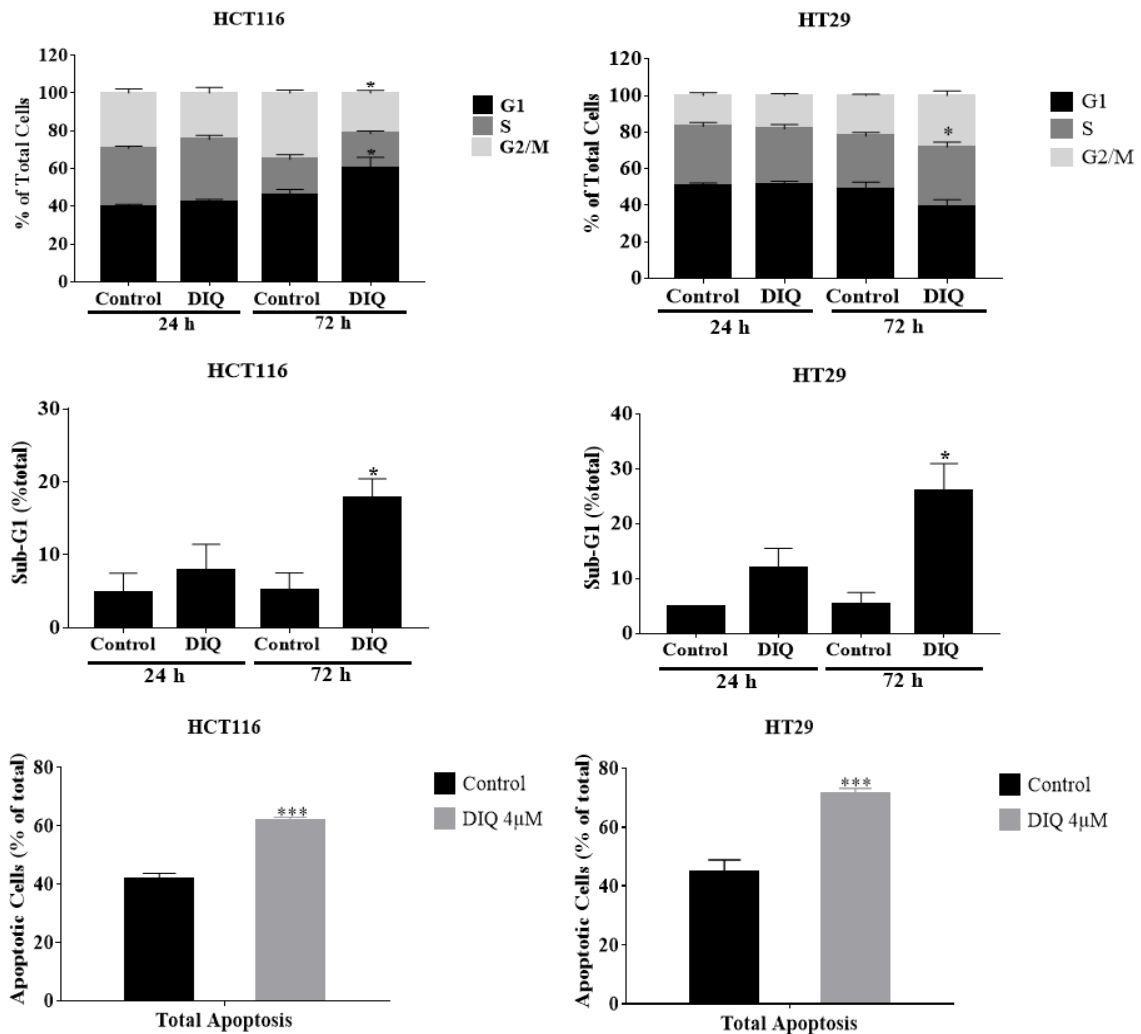


Figure 20. DIQ induces an accumulation of HCT116 and HT29 cancer cells in the sub-G1 region and apoptosis. The distribution of phases of the cell cycle upon DIQ treatment at 24 and 72 h in HCT116 and HT29 cells using propidium iodide-based flow cytometric analysis of DNA content were shown. HCT116 and HT29 cells were stained with PI and FITC-conjugated Annexin V, and analyzed by Guava EasyCyte8 Flow Cytometer for the detection of apoptosis. Data represent the average of three independent experiments and are reported as mean \pm SEM (* $P < 0.05$; ** $P < 0.01$ treatment compared to control).

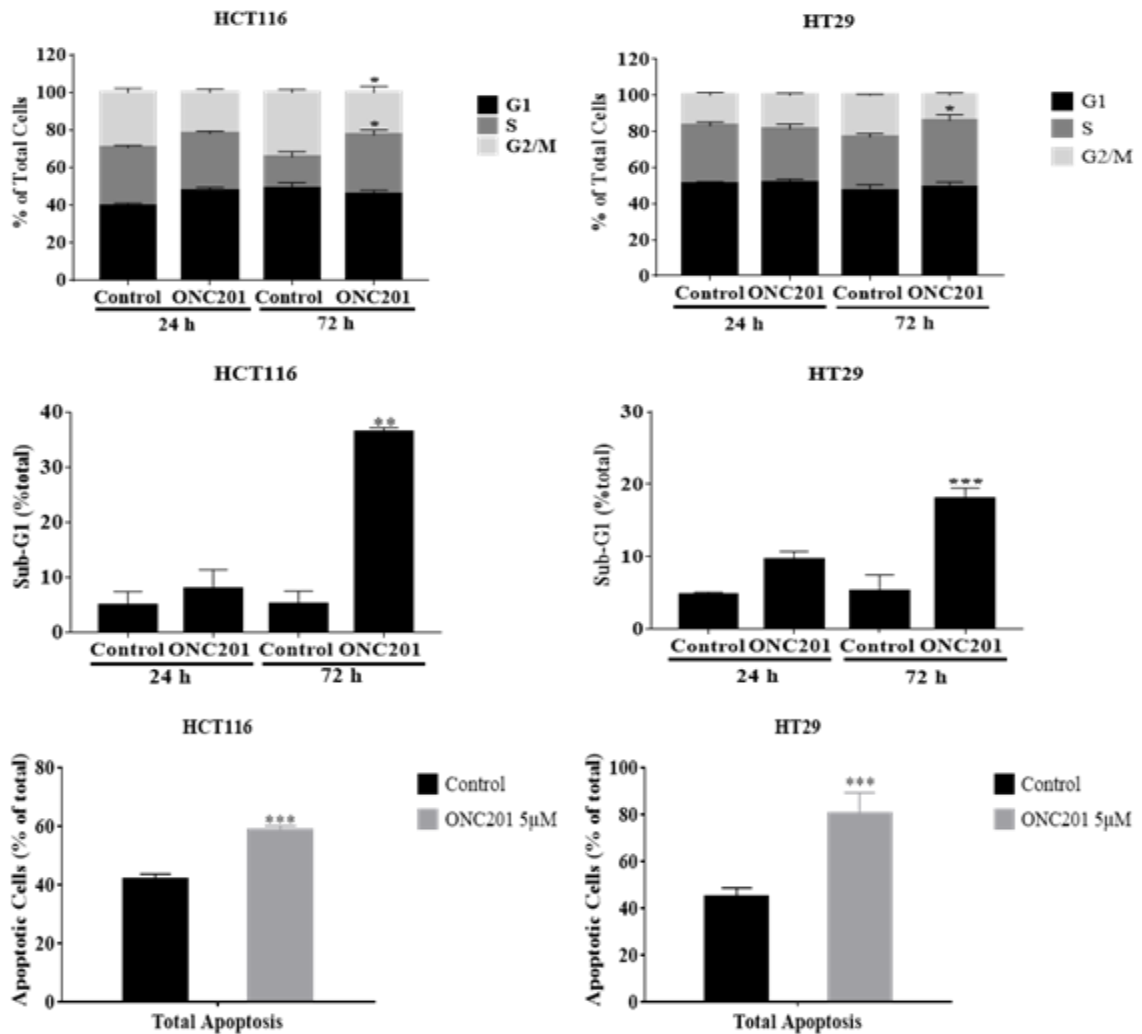


Figure 21. ONC201 induces an accumulation of HCT116 and HT29 cancer cells in the sub-G1 region and apoptosis. The distribution of phases of the cell cycle upon ONC201 treatment at 24 and 72 h in HCT116 and HT29 cells using propidium iodide-based flow cytometric analysis of DNA content were shown. HCT116 and HT29 cells were stained with PI and FITC-conjugated Annexin V, and analyzed by Guava EasyCyte8 Flow Cytometer for the detection of apoptosis. Data represent the average of three independent experiments and are reported as mean \pm SEM (* $P < 0.05$; (** $P < 0.01$) treatment compared to control).

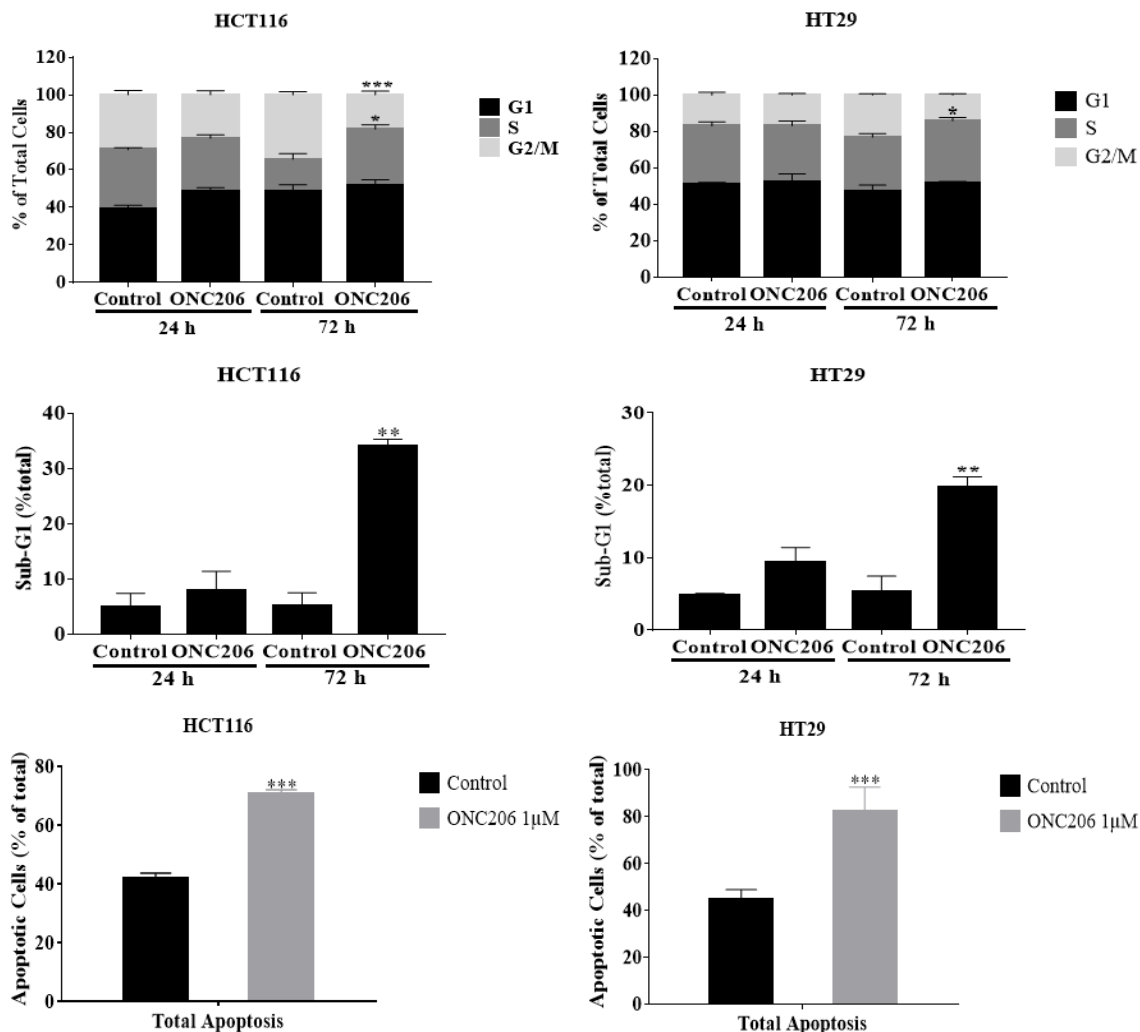


Figure 22. ONC206 induces an accumulation of HCT116 and HT29 cancer cells in the sub-G1 region and apoptosis. The distribution of phases of the cell cycle upon ONC206 treatment at 24 and 72 h in HCT116 and HT29 cells using propidium iodide-based flow cytometric analysis of DNA content were shown. HCT116 and HT29 cells were stained with PI and FITC-conjugated Annexin V, and analyzed by Guava EasyCyte8 Flow Cytometer for the detection of apoptosis. Data represent the average of three independent experiments and are reported as mean \pm SEM (* $P < 0.05$; (** $P < 0.01$) treatment compared to control).

D. Effect of DIQ, ONC201 and ONC206 on the Production of Reactive Oxygen

Species (ROS) in Colorectal Cancer Cells

Recently, targeting cancer via ROS-based mechanisms has been reported as a radical therapeutic approach as increased ROS level could be detrimental for stem cells, might inhibit cancer metastasis, and mediate apoptosis via mitochondrial DNA damage

[26]. To investigate the effect of DIQ and ONC206 on cellular stress and the involvement of oxidative stress in their anti-proliferative effect in CRC, ROS production was examined by DHE stain intensity. DHE is a fluorescent dye that can easily permeate cell membranes and has been widely used to quantify cellular $O_2^{\bullet-}$ and H_2O_2 by producing red fluorescent products. Our results showed that a significant increase of the DHE staining intensity was detected in treated cells at 48 h as compared to the control (Figure 23). Thus, DIQ and ONC206 treatment induced ROS production in both CRC cell lines.

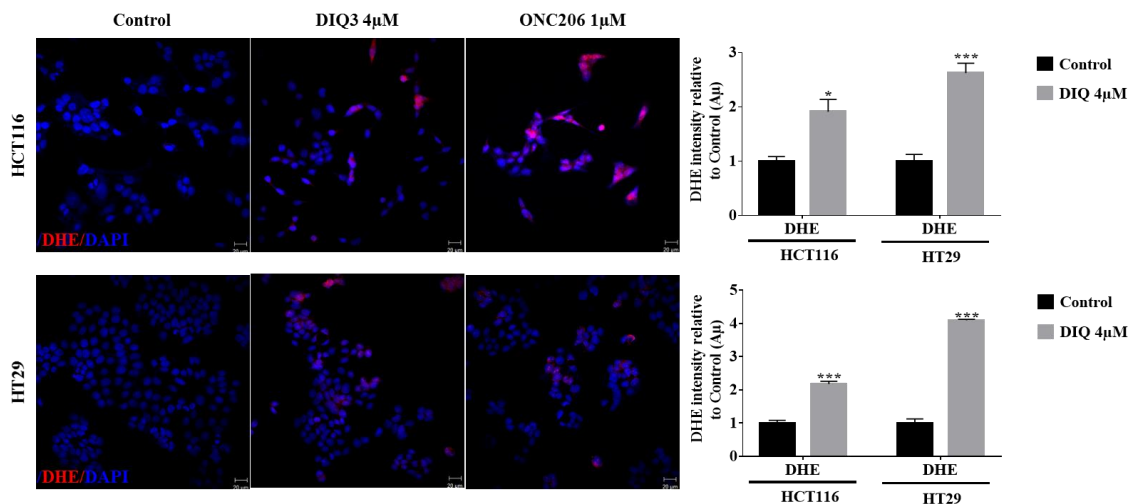


Figure 23. ROS production in HCT116 and HT29 cells as detected by dihydroethidium (DHE) staining. Panel shows representative images of CRC cells exposed to different treatments stained with dihydroethidium (DHE) for ROS content (red color). Cell nuclei were stained with DAPI (blue). A summary of the quantification of the red fluorescence intensity is represented. Data represent an average of three independent experiments and are reported as mean \pm SEM (* $P < 0.05$; ** $P < 0.01$; *** $P < 0.001$). Scale bar 20 μ m.

E. DIQ, ONC201 and ONC206 Effects on the Expression of the Survival, Proliferation, and Stem Cell Markers in Colorectal Cancer Cells

To determine the association between the observed cell cycle arrest and the increased ROS in HCT116 and HT29, western immunoblot analyses were performed on

total cell extracts prepared from 2D-treated cells to detect possible changes in the expression of cell cycle and proliferation markers. As shown in Figure 24, the expression levels of the proteins p53 and p21, which are cell cycle regulators of G1 phase, were upregulated by 1.3 and 1.5 folds in HCT116 upon DIQ treatment respectively as compared to control conditions. Whereas, p53 was downregulated in HT29 treated cells but showed a significant upregulation of p21 expression by 1.8 folds, suggesting that the inhibitory mechanism of DIQ is different in HCT116 and HT29 cells. ONC206 downregulated the expression levels of the proteins p53 and p21 in both CRC cell lines by more than 50% as compared to control conditions (Figure 25).

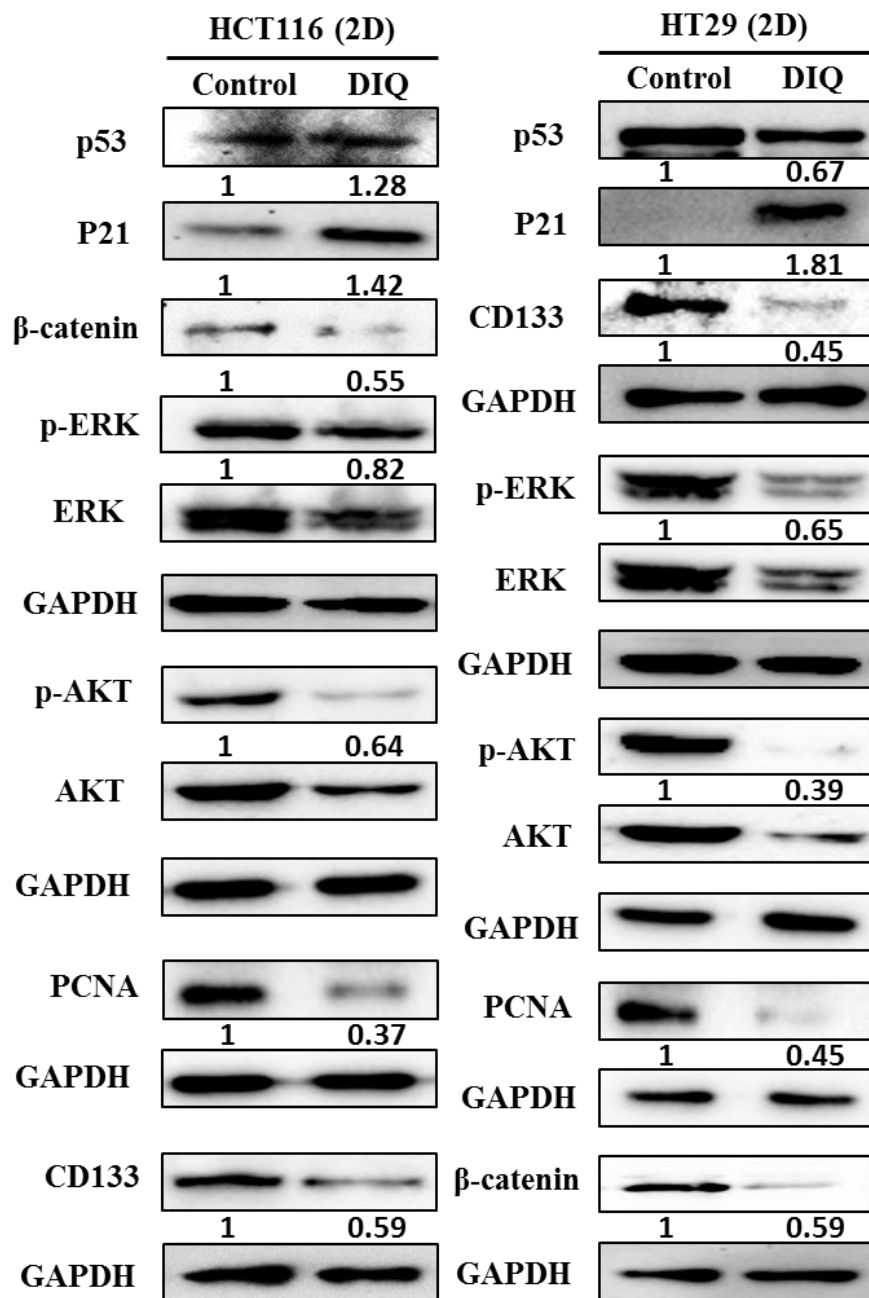


Figure 24. DIQ alters the expression of the survival, proliferation, and stem cell markers in 2D colorectal cells. Lysates of CRC cells treated with 4 μ M DIQ were immunoblotted against p53, p21, β -catenin, p-ERK, ERK, p-AKT, AKT, PCNA. Bands were detected by enhanced chemiluminescence (ECL) and quantified using ChemiDoc MP Imaging System. Data represents an average of three independent experiments.

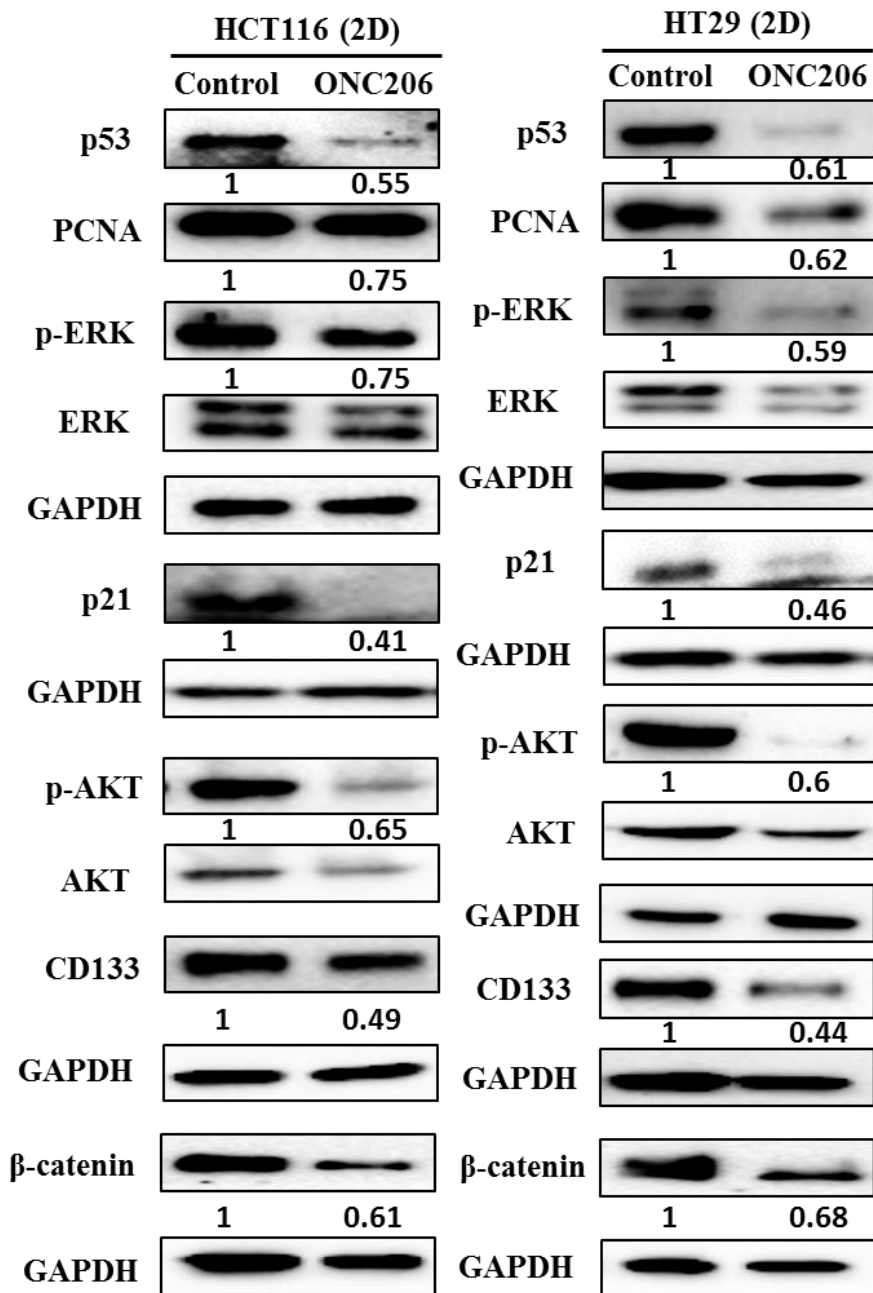


Figure 25. ONC206 alters the expression of the survival, proliferation, and stem cell markers in 2D colorectal cells. Lysates of CRC cells treated with 1 μ M ONC206 were immunoblotted against p53, p21, β -catenin, p-ERK, ERK, p-AKT, AKT, PCNA. Bands were detected by enhanced chemiluminescence (ECL) and quantified using ChemiDoc MP Imaging System. Data represents an average of three independent experiments.

F. Establishing DIQ, ONC201 and ONC206 Effects on an Enriched Population of Human Colorectal Cancer Stem Cells in 3D

1. Effect of DIQ, ONC201 and ONC206 on HCT116 and HT29 Sphere Counts and Sizes

We investigated colonosphere formation of HCT116 and HT29 cells, a salient feature of cancer stem cells. To better visualize their sphere forming capabilities in 3D cultures, HCT116 and HT29 cells were cultured as single cells in Matrigel™ for 8-12 days in the presence of DIQ, ONC201 and ONC206. The spheres were then visualized under an inverted light microscope and bright-field images were taken (Figures 26, 27, 28, 29, 30 and 31). Cells that were able to form spheres in the first generation (G1) were collected and propagated by dissociating spheres into single cells and re-seeding the same number of cells (1000 cells/well). The assay was performed until the fifth generation (G5). Our data showed that both HCT116 and HT29 cells formed spheres suggesting the presence of a unique population with stem cell-like properties. Notably, a clear dose-dependent attenuation of the sphere-forming unit (SFU) at G1 for both cell lines was observed when treated with different concentrations of DIQ (0.5, 1 μ M), ONC201 (0.5, 1, 2, 3 μ M), or ONC206 (0.5, 1 μ M) (Figures 26, 27, 28, 29, 30 and 31). The SFU was always significantly and remarkably lower in drug-treated cells compared to that of the control condition by more than 50%.

Consecutive propagations of formed spheres at each generation with successive treatment with DIQ, ONC201 and ONC206 were performed up to 5 generations. Interestingly, our results showed additional inhibition of the SFU upon DIQ treatment when the cells were propagated from G1 up to G5 spheres (Figures 26 and 27). 1 μ M of DIQ treatment decreased SFU of HCT116 cells by more than 10 times compared to the

control (13.3%) at G5 reaching approximately 1%. Moreover, as shown in Figure 27, HT29 cells were more sensitive to DIQ and there was an eradication of spheres at G4 (SFU=0%) compared to the control (14.28%). ONC201 and its analogue ONC206 significantly decreased the sphere formation ability in CRC cell lines up to G5 (Figures 28, 29, 30 and 31). ONC206 treatment as low as 0.5 μ M was more effective than the same concentration of ONC201 treatment at G1 in both cell lines. Upon propagation, ONC206 was more potent than ONC201 in decreasing SFU at a dose that is 10 times lower. It is noteworthy mentioning that this low 0.1 μ M ONC206 concentration used in the 3D culture spheres assay is 10-folds less than the concentration adapted in all 2D assays.

In addition to assessing the effect of DIQ, ONC201 and ONC206 on self-renewal capacity, we investigated their effects on sphere size over 5 generations. All treatments significantly decreased the sizes of the spheres compared to untreated control conditions. Further decrease in sphere sizes was recognized over the 5 generations in both cell lines depicting pronounced additive effect of the treatments on the formed spheres upon propagation (Figures 26, 27, 28, 29, 30 and 31). Thus, DIQ, ONC201 and ONC206 have led to the formation of a lower number and smaller spheres.

Interestingly, none of these treatments showed any significant effect on the size and SFU of FHS74Int-derived spheres over 5 generations (Figure 32). Taken together, these findings suggest that DIQ, ONC201 and ONC206 specifically target the colorectal CSC.

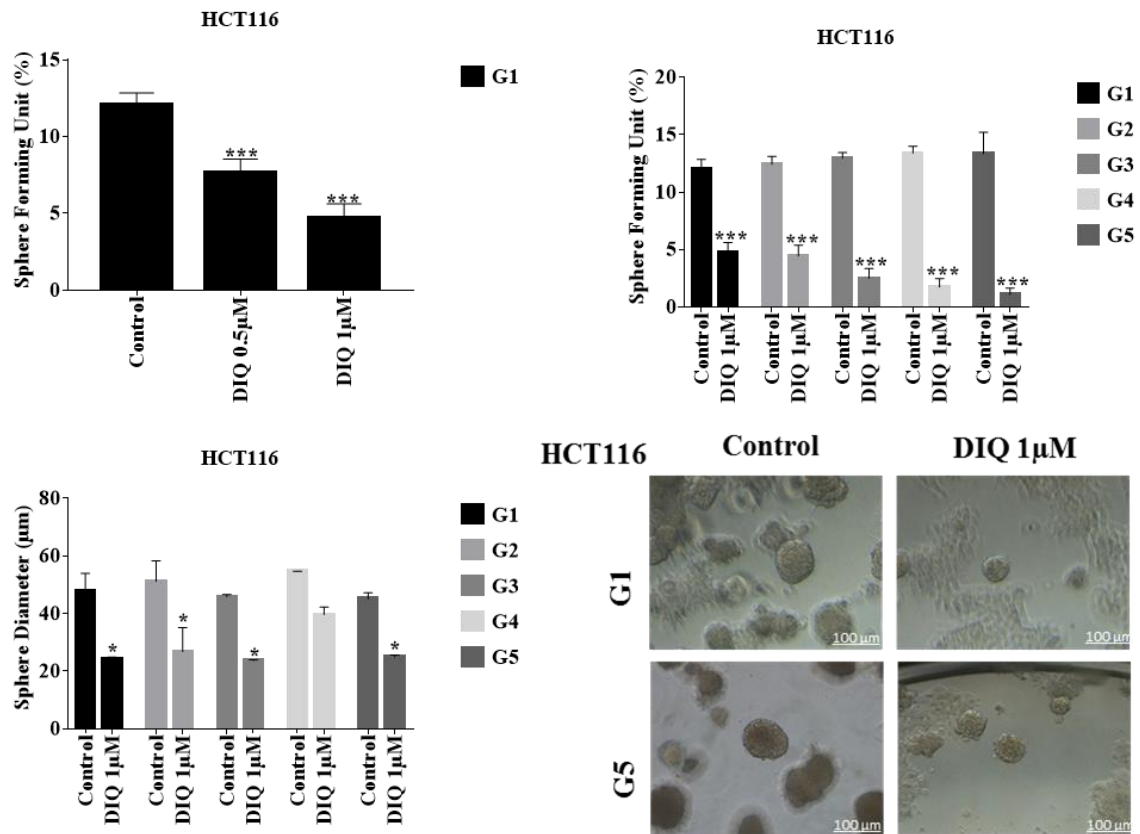


Figure 26. DIQ reduces the sphere-forming and self-renewal ability of HCT116 colorectal cancer stem/progenitor cells. HCT116 cells were seeded at a density of 1,000 single cells/well in Matrigel™ for 8 days with and without 0.5 and 1 µM DIQ treatment at G1. Spheres with or without 1 µM DIQ were propagated for five generations (G1-G5) in duplicates for each condition. Media or treatment was replenished every 2 days. Spheres were counted at day 8-12 of sphere culture. Results are expressed as SFU which is calculated according to the following formula: $SFU = (\text{number of spheres counted} / \text{number of input cells}) \times 100$. Quantification of the average size of G1 to G5 colon cancer spheres with or without treatment conditions. Spheres sizes were measured by Carl Zeiss Zen 2012 image software. Data represent an average diameter (µm) of 50 measured spheres. Representative bright field images of HCT116 colorectal spheres in Matrigel™ taken by the Axiovert inverted microscope are shown. Data represents an average of three independent experiments and are reported as mean ± SEM (* P<0.05; ** P<0.01; *** P<0.001). Scale bar 100 µm.

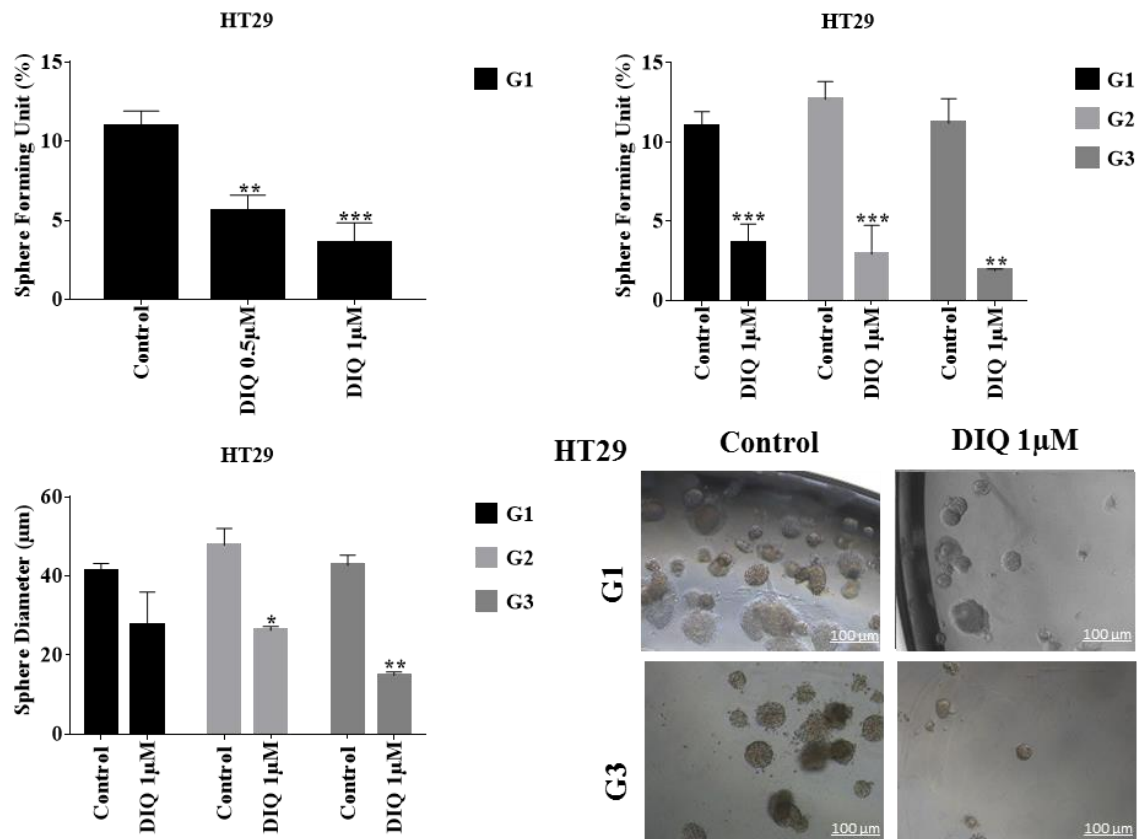


Figure 27. DIQ reduces the sphere-forming and self-renewal ability of HT29 colorectal cancer stem/progenitor cells. HT29 cells were seeded at a density of 1,000 single cells/well in Matrigel™ for 8 days with and without 0.5 and 1 μM DIQ treatment at G1. Spheres with or without 1 μM DIQ were propagated for five generations (G1-G5) in duplicates for each condition. Media or treatment was replenished every 2 days. Spheres were counted at day 8-12 of sphere culture. Results are expressed as SFU which is calculated according to the following formula: $SFU = (\text{number of spheres counted} / \text{number of input cells}) \times 100$. Quantification of the average size of G1 to G5 colon cancer spheres with or without treatment conditions. Spheres sizes were measured by Carl Zeiss Zen 2012 image software. Data represent an average diameter (μm) of 50 measured spheres. Representative bright field images of HT29 colorectal spheres in Matrigel™ taken by the Axiovert inverted microscope are shown. Data represents an average of three independent experiments and are reported as mean ± SEM (* P<0.05; ** P<0.01; *** P<0.001). Scale bar 100 μm.

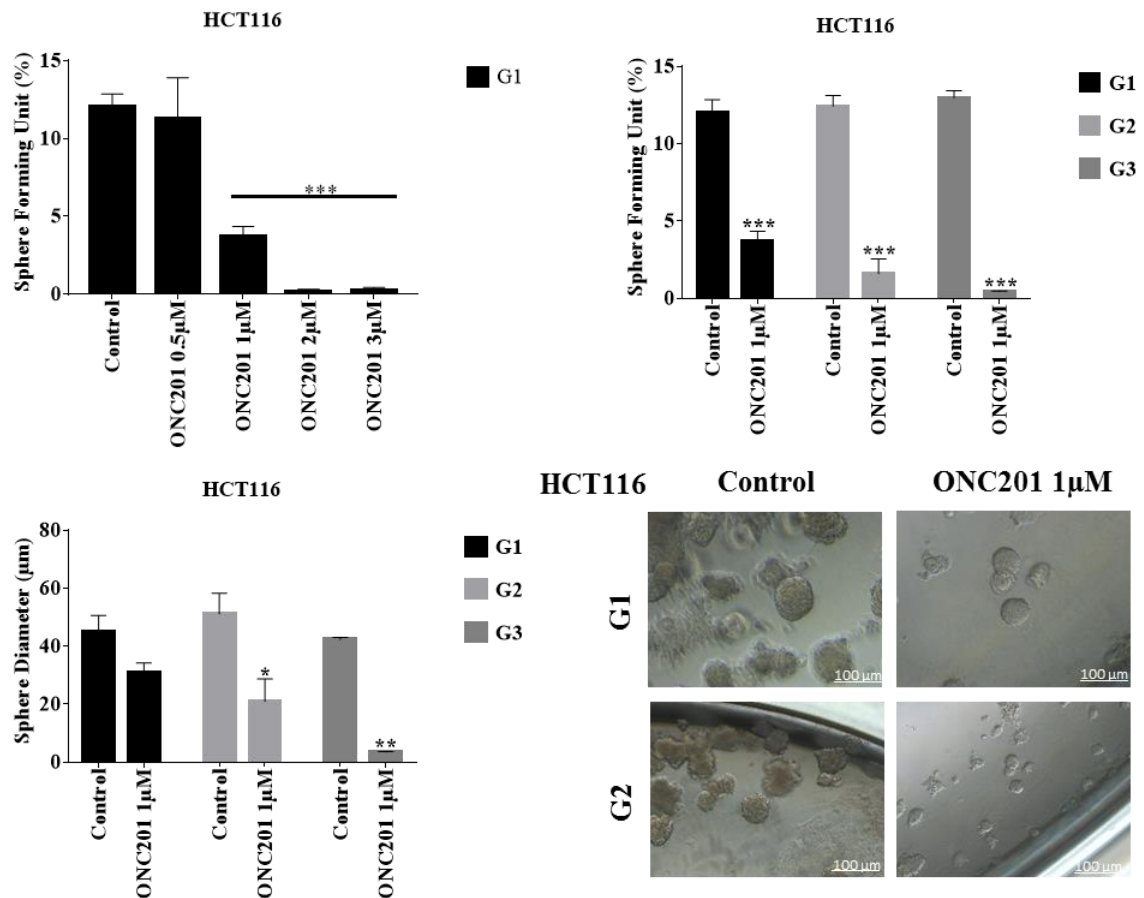


Figure 28. ONC201 reduces the sphere-forming and self-renewal ability of HCT116 colorectal cancer stem/progenitor cells. HCT116 cells were seeded at a density of 1,000 single cells/well in Matrigel™ for 8 days with and without 0.5-3 μM ONC201 treatment at G1. Spheres with or without 1 μM ONC201 were propagated for five generations (G1-G5) in duplicates for each condition. Media or treatment was replenished every 2 days. Spheres were counted at day 8-12 of sphere culture. Results are expressed as SFU which is calculated according to the following formula: $SFU = (\text{number of spheres counted} / \text{number of input cells}) \times 100$. Quantification of the average size of G1 to G5 colon cancer spheres with or without treatment conditions. Spheres sizes were measured by Carl Zeiss Zen 2012 image software. Data represent an average diameter (μm) of 50 measured spheres. Representative bright field images of HCT116 colorectal spheres in Matrigel™ taken by the Axiovert inverted microscope are shown. Data represents an average of three independent experiments and are reported as mean ± SEM (* P<0.05; ** P<0.01; *** P<0.001). Scale bar 100 μm.

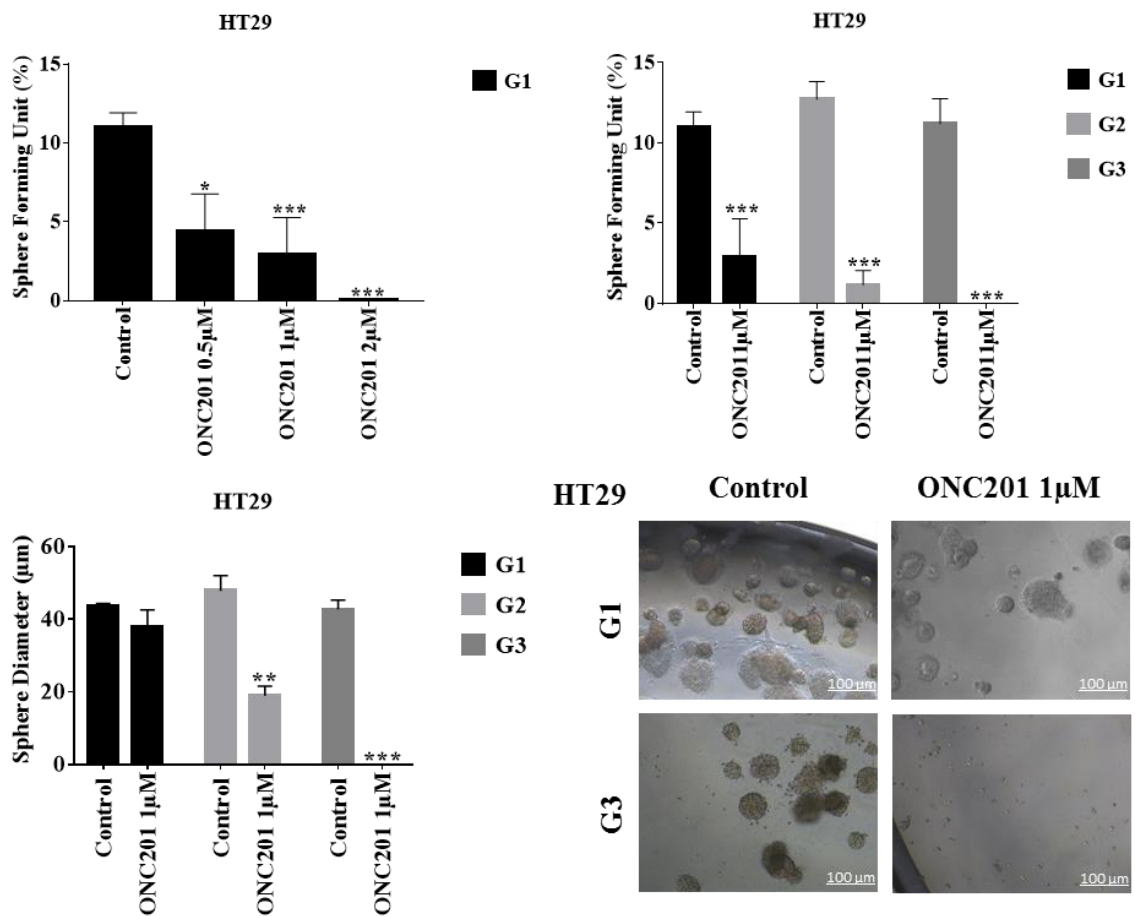


Figure 29. ONC201 reduces the sphere-forming and self-renewal ability of HT29 colorectal cancer stem/progenitor cells. HT29 cells were seeded at a density of 1,000 single cells/well in Matrigel™ for 8 days with and without 0.5-3 µM ONC201 treatment at G1. Spheres with or without 1 µM ONC201 were propagated for five generations (G1-G5) in duplicates for each condition. Media or treatment was replenished every 2 days. Spheres were counted at day 8-12 of sphere culture. Results are expressed as SFU which is calculated according to the following formula: $SFU = (\text{number of spheres counted} / \text{number of input cells}) \times 100$. Quantification of the average size of G1 to G5 colon cancer spheres with or without treatment conditions. Spheres sizes were measured by Carl Zeiss Zen 2012 image software. Data represent an average diameter (µm) of 50 measured spheres. Representative bright field images of HT29 colorectal spheres in Matrigel™ taken by the Axiovert inverted microscope are shown. Data represents an average of three independent experiments and are reported as mean ± SEM (* P<0.05; ** P<0.01; *** P<0.001). Scale bar 100 µm.

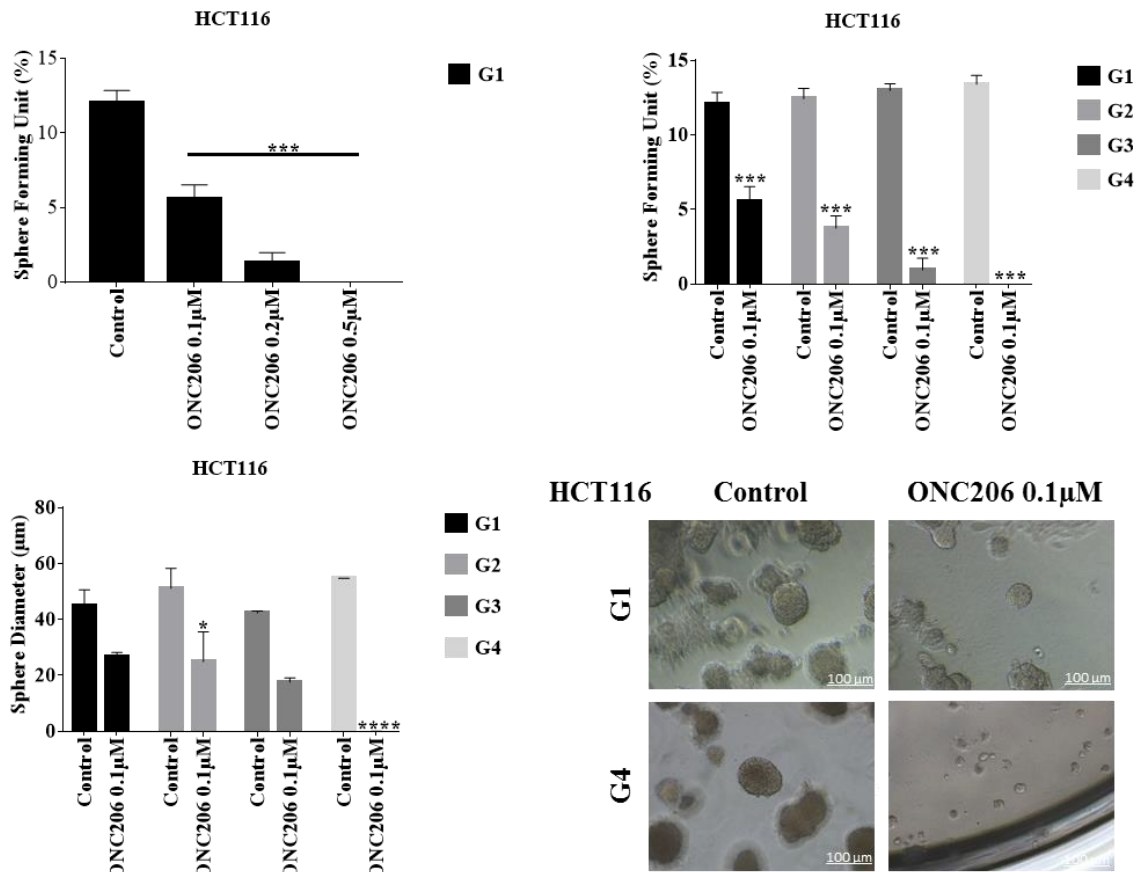


Figure 30. ONC206 reduces the sphere-forming and self-renewal ability of HCT116 colorectal cancer stem/progenitor cells. HCT116 cells were seeded at a density of 1,000 single cells/well in Matrigel™ for 8 days with and without 0.1-0.5 μM ONC206 treatment at G1. Spheres with or without 0.1 μM ONC206 were propagated for five generations (G1-G5) in duplicates for each condition. Media or treatment was replenished every 2 days. Spheres were counted at day 8-12 of sphere culture. Results are expressed as SFU which is calculated according to the following formula: $SFU = (\text{number of spheres counted} / \text{number of input cells}) \times 100$. Quantification of the average size of G1 to G5 colon cancer spheres with or without treatment conditions. Spheres sizes were measured by Carl Zeiss Zen 2012 image software. Data represent an average diameter (μm) of 50 measured spheres. Representative bright field images of HCT116 colorectal spheres in Matrigel™ taken by the Axiovert inverted microscope are shown. Data represents an average of three independent experiments and are reported as mean ± SEM (* P<0.05; ** P<0.01; *** P<0.001). Scale bar 100 μm.

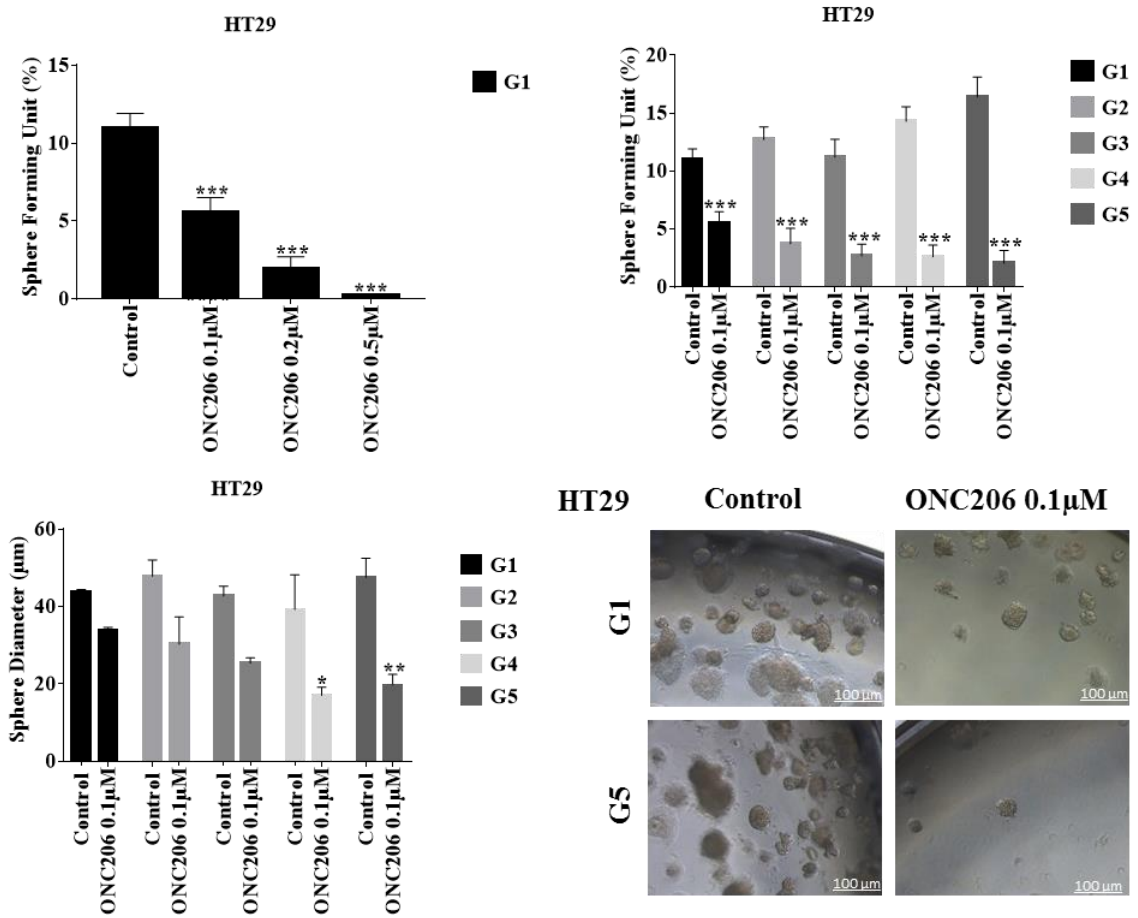


Figure 31. ONC206 reduces the sphere-forming and self-renewal ability of HT29 colorectal cancer stem/progenitor cells. HT29 cells were seeded at a density of 1,000 single cells/well in Matrigel™ for 8 days with and without 0.1-0.5 μM ONC206 treatment at G1. Spheres with or without 0.1 μM ONC206 were propagated for five generations (G1-G5) in duplicates for each condition. Media or treatment was replenished every 2 days. Spheres were counted at day 8-12 of sphere culture. Results are expressed as SFU which is calculated according to the following formula: $SFU = (\text{number of spheres counted} / \text{number of input cells}) \times 100$. Quantification of the average size of G1 to G5 colon cancer spheres with or without treatment conditions. Spheres sizes were measured by Carl Zeiss Zen 2012 image software. Data represent an average diameter (μm) of 50 measured spheres. Representative bright field images of HT29 colorectal spheres in Matrigel™ taken by the Axiovert inverted microscope are shown. Data represents an average of three independent experiments and are reported as mean ± SEM (* P<0.05; ** P<0.01; *** P<0.001). Scale bar 100 μm.

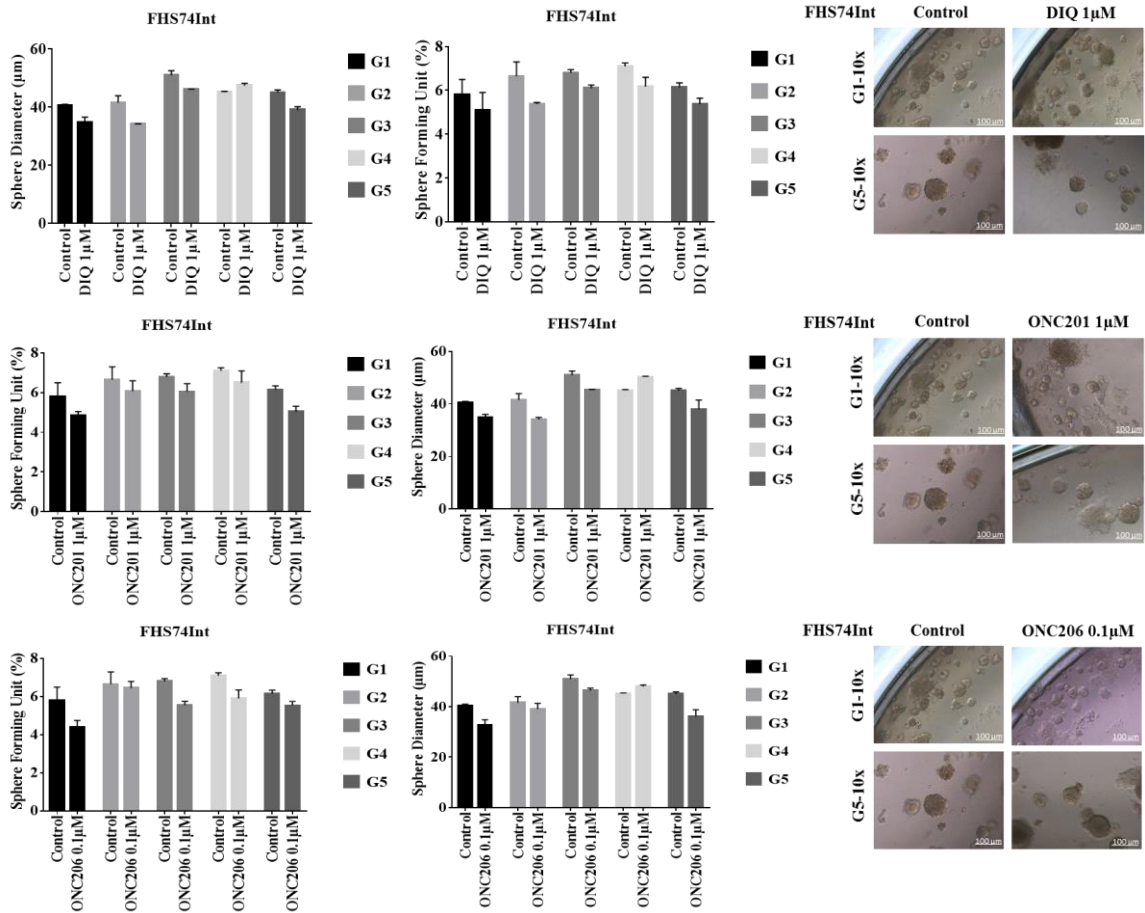


Figure 32. DIQ, ONC201 and ONC206 are not targeting non-tumorigenic FHS74Int cells. FHS74Int cells were seeded at a density of 2,000 single cells/well in Matrigel™ for 8 days with and without 1µM DIQ, 1µM ONC201, and 0.1µM ONC206 treatments at G1. Spheres were propagated for five generations (G1-G5) in duplicates for each condition. Media or treatment was replenished every 2 days. Spheres were counted at day 8-12 of sphere culture. Results are expressed as SFU, which is calculated according to the following formula: $SFU = (\text{number of spheres counted} / \text{number of input cells}) \times 100$. Quantification of the average size of G1 to G5 colon cancer spheres with or without treatment conditions using Carl Zeiss Zen 2012 image software. Data represent an average diameter (µm) of 50 measured spheres. Representative bright field images of FHS74Int spheres in Matrigel™ taken by the Axiovert inverted microscope are shown. Data represents an average of three independent experiments and is reported as mean ± SEM (*P < 0.05, **P < 0.01, ***P < 0.001). Scale bar 100 µm.

2. DIQ and ONC206 Effect on Proliferation, Epithelial and Stem Cell Markers Expression in 3D Colonospheres

To further assess the effect of the novel therapeutics DIQ and ONC206 on the enriched CSCs population, spheres collected at G1 were subjected to

immunofluorescence analysis of the expression of the proliferation marker Ki67, cytokeratin epithelial markers, CK8 and CK19, and the stem cell marker CD44. Our data revealed that Ki67, CK8 and CK19 expression were significantly reduced in treated spheres derived from HCT116 and HT29 cell lines (Figures 33, 34, 35 and 36). This suggests that the mechanism of reduction of colon sphere formation in CSCs could be due to inhibition of proliferation. The downregulation of CK19 marker in both HCT116 and HT29 spheres at G1 could be an indicator of an inhibition of the EMT process. Immunofluorescence staining showed high expression of CD44 in control spheres at G1 indicating enriched stemness in these cells. Treatment with DIQ or ONC206 showed a significant reduction of CD44 expression in HCT116 and HT29 colonospheres as compared to the control, which is in tune with the downregulation of the CRC stem marker CD133 data (Figures 37 and 38). Finally, DIQ and ONC206 effect on DNA damage was studied by assessing the expression of γ -H2AX. Our results revealed that the expression of γ -H2AX was markedly increased in treated spheres in both cell types (Figures 34 and 36).

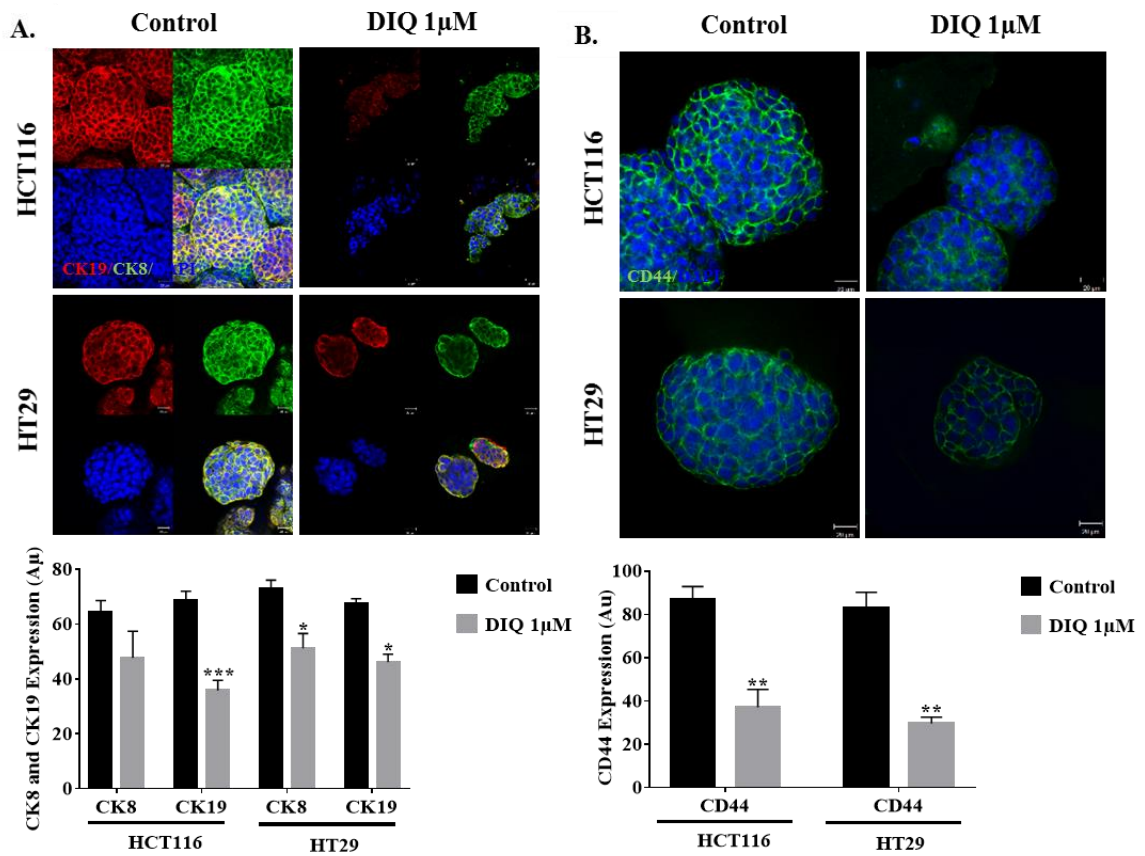


Figure 33. DIQ reduces the expression of the cytokeratin epithelial markers, CK8 and CK19, and the stem cell marker CD44 in 3D colonospheres. Representative immunofluorescence imaging of control and DIQ-treated HCT116 and HT29 spheres collected at G1. Spheres stained for A: CK8 (green) and CK19 (red), B: CD44 were obtained using confocal microscopy. The nuclei were stained with anti-fade reagent Fluorogel II with DAPI. The quantification of the intensity of CK8, CK19, CD44 stain in control and DIQ treated spheres was performed using Carl Zeiss Zen 2012 image software. Stain intensity was normalized to size. Scale bar 20 μ m.

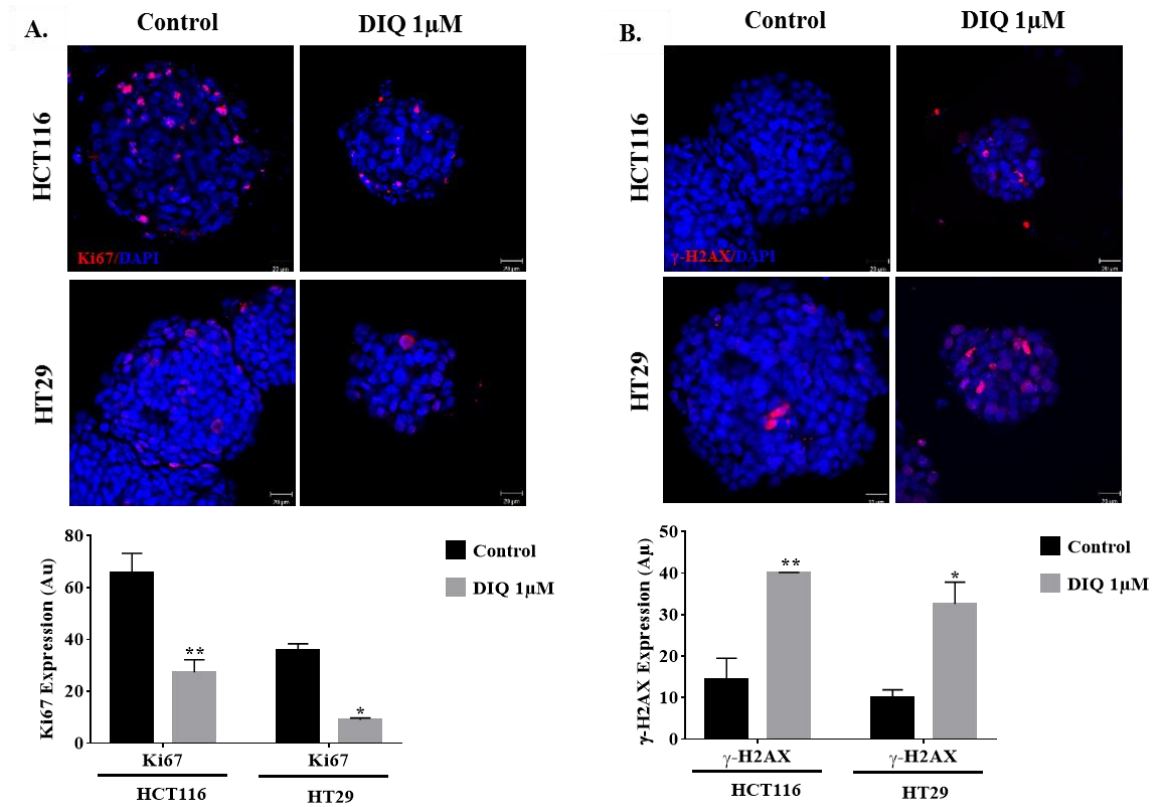


Figure 34. DIQ reduces the expression of the proliferation marker Ki67 and increases the expression of the DNA damage marker γ -H2AX in 3D colonospheres. Representative immunofluorescence imaging of control and DIQ-treated HCT116 and HT29 spheres collected at G1. Spheres stained for A: Ki67, B: γ -H2AX were obtained using confocal microscopy. The nuclei were stained with anti-fade reagent Fluorogel II with DAPI. The quantification of the intensity of Ki67 and γ -H2AX, were stain in control and DIQ treated spheres was performed using Carl Zeiss Zen 2012 image software. Stain intensity was normalized to size. Scale bar 20 μ m.

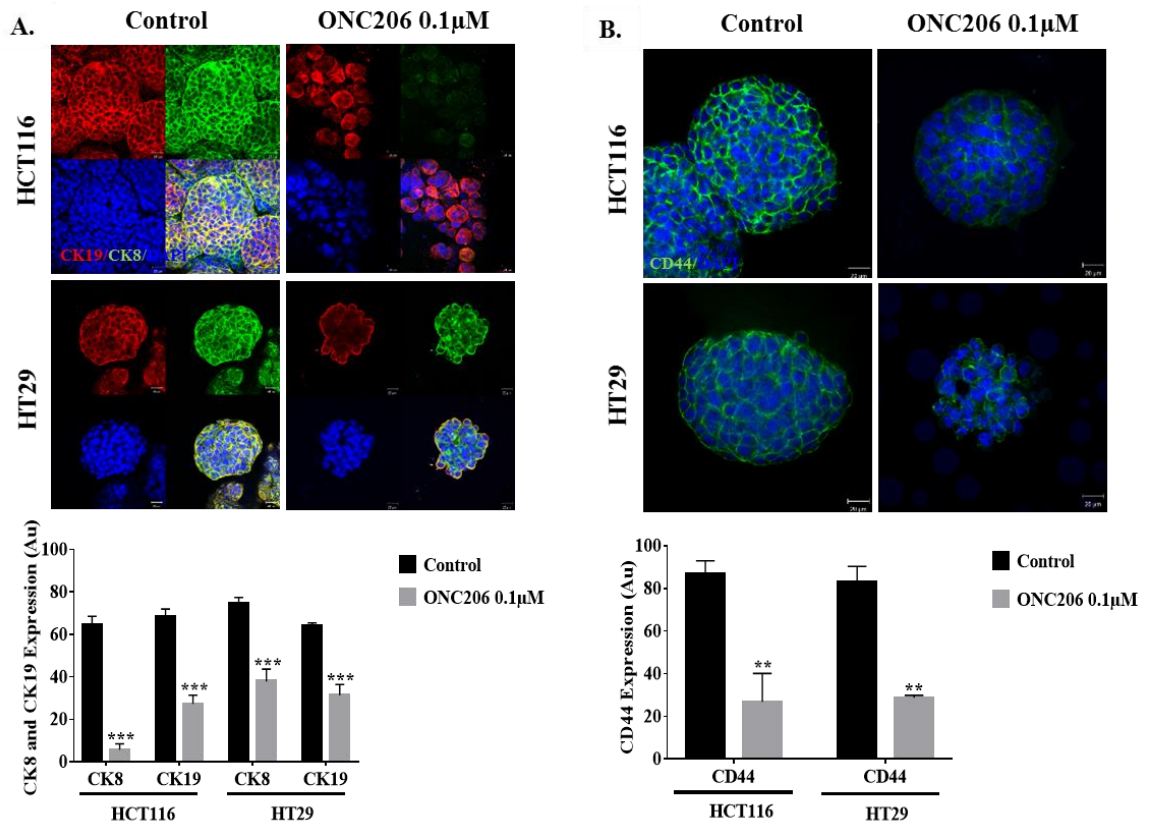


Figure 35. ONC206 reduces the expression of the cytokeratin epithelial markers, CK8 and CK19, and the stem cell marker CD44 in 3D colonospheres.

Representative immunofluorescence imaging of control and ONC206-treated HCT116 and HT29 spheres collected at G1. Spheres stained for A: CK8 (green) and CK19 (red), B: CD44 were obtained using confocal microscopy. The nuclei were stained with anti-fade reagent Fluorogel II with DAPI. The quantification of the intensity of CK8, CK19, CD44 stain in control and ONC206 treated spheres was performed using Carl Zeiss Zen 2012 image software. Stain intensity was normalized to size. Scale bar 20 μm.

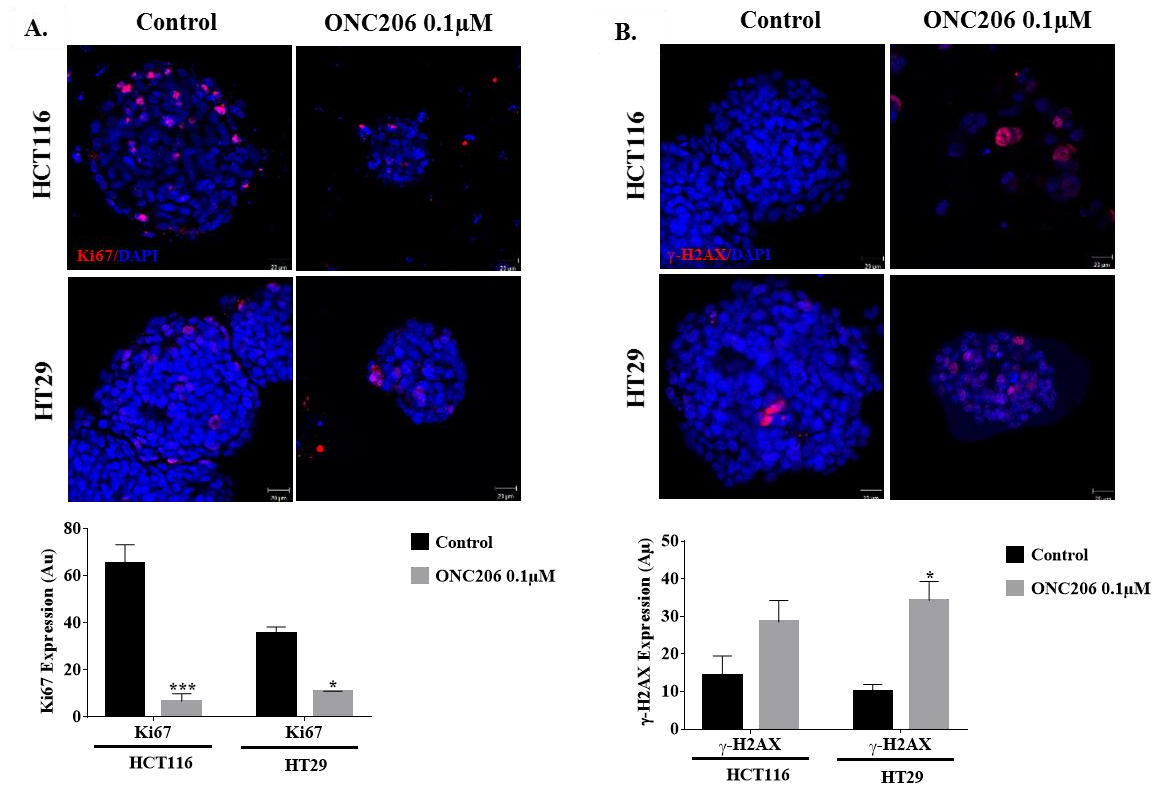


Figure 36. ONC206 reduces the expression of the proliferation marker Ki67 and increases the expression of the DNA damage marker γ -H2AX in 3D colonospheres. Representative immunofluorescence imaging of control and ONC206-treated HCT116 and HT29 spheres collected at G1. Spheres stained for A: Ki67, B: γ -H2AX were obtained using confocal microscopy. The nuclei were stained with anti-fade reagent Fluorogel II with DAPI. The quantification of the intensity of Ki67 and γ -H2AX, were stain in control and ONC206 treated spheres was performed using Carl Zeiss Zen 2012 image software. Stain intensity was normalized to size. Scale bar 20 μ m.

To further assess the effect of DIQ and ONC206 on the enriched CSCs population, we were interested in determining the effect of these treatments on the expression of proliferation markers, stem cell markers, and Wnt signaling molecules of cancer stem cells using western blot. Consistent with the western blot analyses of 2D CRC cells, the expression of the proliferation markers p-AKT and p-ERK were remarkably downregulated by DIQ and ONC206 treatment in both HCT116 and HT29-derived spheres confirming DIQ and ONC206's inhibitory effects on the proliferation of 3D CSCs colonospheres (Figures 37 and 38). Western blot analysis revealed a decrease in the levels of the proliferation marker PCNA protein post treatment consistent with the

data that DIQ and ONC206 decreased the size of HCT116 and HT29-derived spheres. For the Wnt signaling studies, we investigated treatment effects on β -catenin, which plays an important role in CRC stemness properties. Western blot analysis showed a down regulation of β -catenin expression in treated compared to untreated spheres. Analysis of p53 and p21 protein expression in HCT116 spheres upon DIQ treatment showed up-regulation of these proteins by 1.32 and 1.99 folds respectively further confirming apoptosis induction. p21 expression was upregulated in HT29 cells by 1.29 folds as compared to non-treated spheres, whereas the expression of p53 was not affected by DIQ treatment in HT29 spheres (Figure 37). The expression of p53 and p21 did not change upon ONC206 treatment in both CRC cell lines, in contrast to what happened in 2D culture (Figure 38).

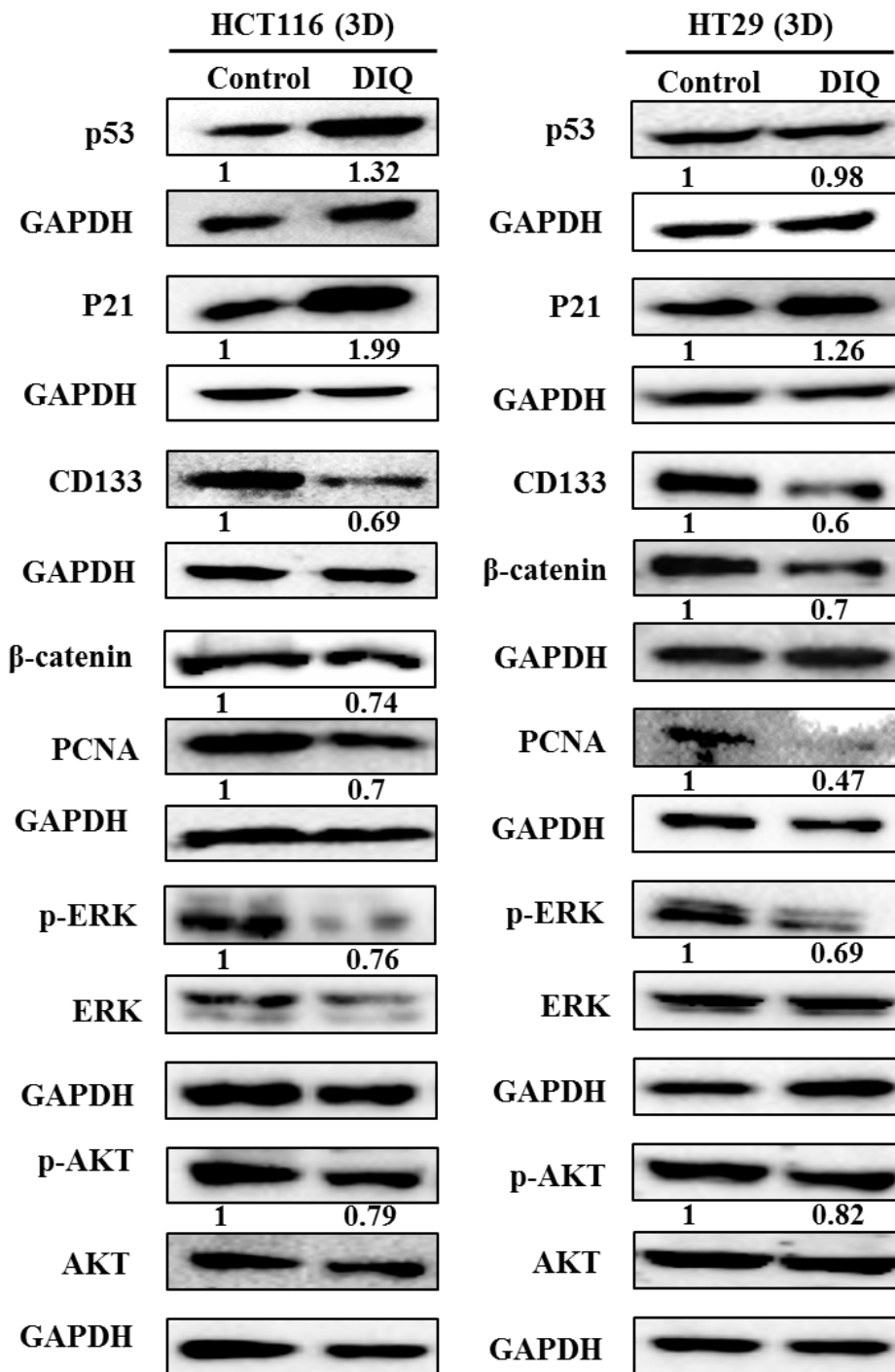


Figure 37. DIQ induces apoptosis and inhibit proliferation in colorectal cancer stem/progenitor cells. Analysis of p53, p21, CD133, β-catenin, PCNA, p-ERK, ERK, p-AKT, and AKT protein expression in HCT116 and HT29 G1 spheres upon treatment is shown. GAPDH served as an internal control. Bands were detected by enhanced chemiluminescence (ECL) using ChemiDoc MP Imaging System. Fold expression changes normalized to GAPDH, and to total ERK and total AKT in case of p-ERK and p-AKT expression respectively, are given. Data represents an average of three independent experiments.

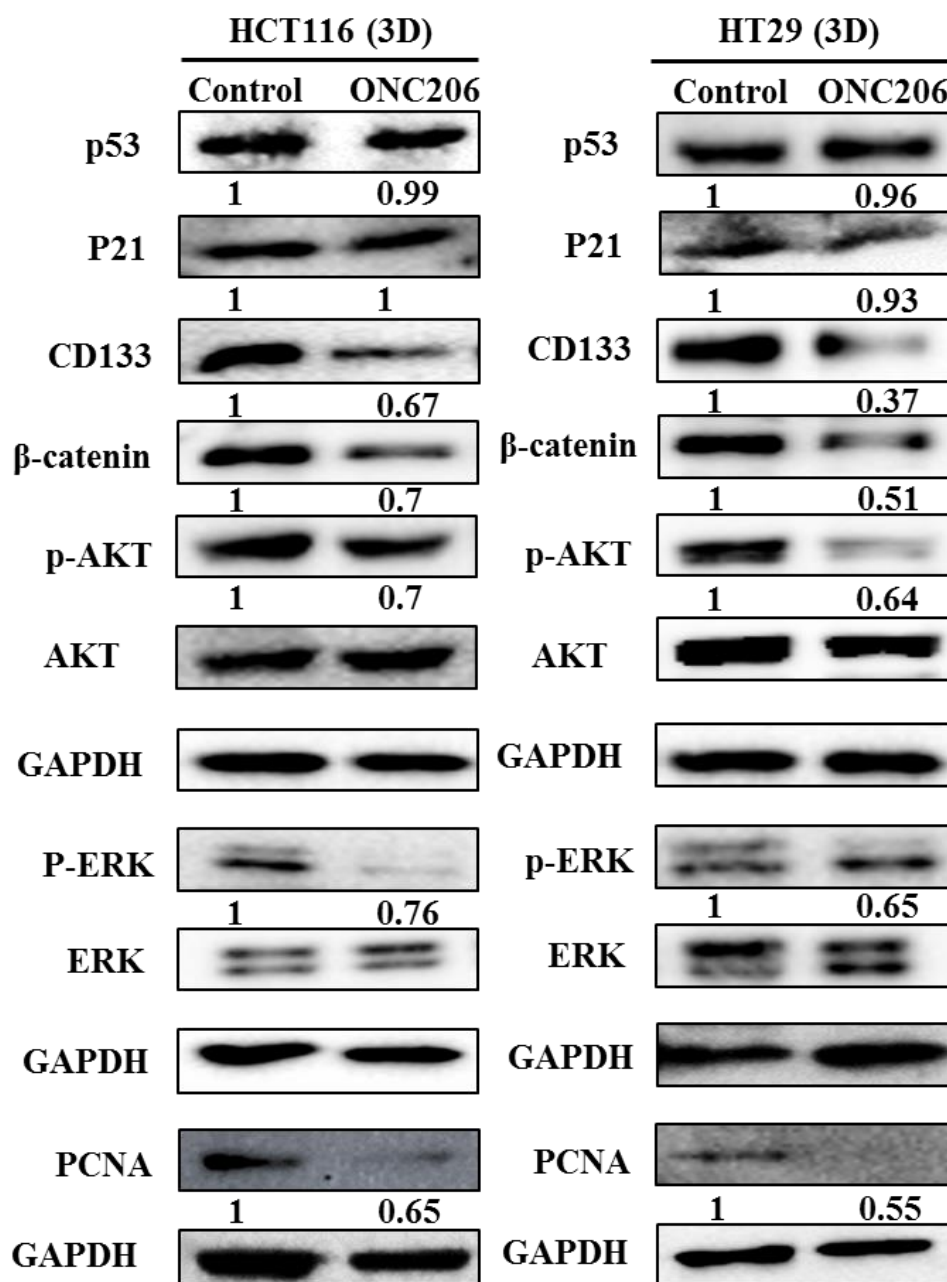


Figure 38. ONC206 induces apoptosis and inhibit proliferation in colorectal cancer stem/progenitor cells. Analysis of p53, p21, CD133, β -catenin, PCNA, p-ERK, ERK, p-AKT, and AKT protein expression in HCT116 and HT29 G1 spheres upon treatment is shown. GAPDH served as an internal control. Bands were detected by enhanced chemiluminescence (ECL) using ChemiDoc MP Imaging System. Fold expression changes normalized to GAPDH, and to total ERK and total AKT in case of p-ERK and p-AKT expression respectively, are given. Data represents an average of three independent experiments.

3. DIQ has Anti-Tumor Potential in NOD-SCID Mice Injected with HCT116 Spheres

To investigate the anti-tumor effect of DIQ on targeting CSC population of cells *in vivo*, we injected subcutaneously two groups of mice each with 100 spheres derived from HCT116 cells. NOD-SCID mice developed tumors in 2 weeks. Mice were treated with 20 mg/Kg DIQ three times per week for 21 days. DIQ treatment did not cause any change in the body weight or death of mice, indicating no toxicity.

DIQ significantly inhibited tumor growth in the treated group when compared to the control group particularly at day 21 (Figure 39). Interestingly, the average tumor volume was 403.2 mm³ in DIQ treated mice at sacrifice while it was 2158.5 mm³ in control group (Figure 39).

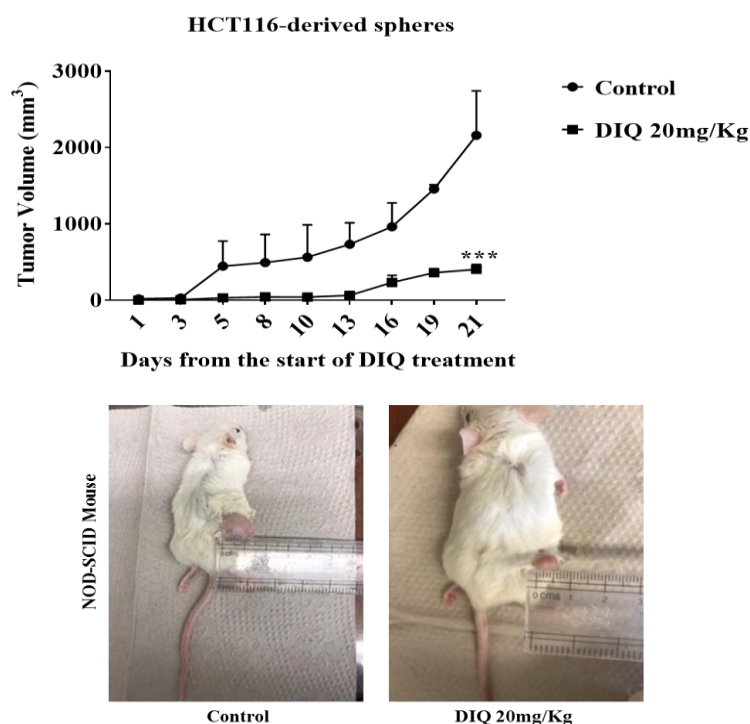


Figure 39. DIQ reduces tumor growth in NOD-SCID mice. NOD-SCID mice (5 mice/group) were injected with 100 HCT116 G1 spheres. Tumor growth was monitored by measuring the tumor volume during 21 days of treatment (3 times per week) with either 20 mg/kg DIQ or physiologic saline. Representative images of control and TQ-treated mice at day 21. Data represent an average of two independent experiments and is reported as mean \pm SEM (***) $P < 0.001$.

G. Assessment of the Effect of DIQ, ONC201 and ONC206 Treatments on the Established Colon Cancer Patient Derived Organoids

1. Organoids as Models for DIQ, ONC201 and ONC206 Assessment

Patient-derived organoids technology has made a great impact on drug discovery programs, toxicity screens, and predicting acquisition of drug resistance for developing and designing personalized regimes. In this study, we generated patient-derived organoids from colon where we used them to test the anticancer effect of a novel compounds DIQ, ONC201, and ONC206 against CRC. We established a 3D organoid system from fresh tissue samples obtained from different stages of five random colon cancer consented patients. As described in the methods section, a total of 20,000 single cells derived from freshly digested tissues were plated per 20 μ L droplets of 90% MatrigelTM in 24-well plates. Cells were plated depending on the total cell count that was successfully derived from the tissue specimens. Despite the expected challenges in modeling colon cancer, we succeeded in establishing colon organoids from patients undergoing radical colectomy. Organoids formed at G1 were dissociated, propagated to G2, and the effect of DIQ, ONC201 and ONC206 on the organoids formed was assessed. The growth of organoids was determined by the total number (OFC) and size (diameters) of the organoids formed. The response of colon cancer patient-derived organoids to DIQ, ONC201 and ONC206 was compared to that of 5FU, which is the standard first-line treatment option for CRC. This response was evaluated on 5 random treatment-naïve patients with different clinical data (Table 7). We succeeded in establishing colon organoids and propagating them. The two different doses of DIQ (0.5 and 1 μ M), ONC201 (1 and 2 μ M), and ONC206 (0.1, 0.5 and 1 μ M) displayed a highly significant inhibition in the OFC and the size of tumor

organoids derived from the five studied patients when they were compared to the control group in a dose-dependent manner (Figures 41,42,44, 45 and 46).

In Patient 1 (Figures 40 and 41), organoids were successfully propagated up to G6 as shown in Figure 40. Interestingly, an increase in the number of tumor organoids formed was observed with each propagation, thus indicating enrichment of stem cells and enhancement of the establishment of colon organoids. Characterization of the established patient 1-derived organoids was performed by studying the expression of the CRC epithelial lineage markers CK19 and CK8 and the stem cell marker CD44. Using immunofluorescence staining, the tumor organoids showed a positive expression of CK19, CK8 and CD44 confirming the presence of stem-like/progenitor CRC cells within the bulk of our patient-derived organoids.

In Patients 2 exhibiting similar grade (grade 2) moderately differentiated sigmoid colon adenocarcinoma and of stage pT3, DIQ treatment at concentrations as low as 0.5 μ M displayed a decrease in the growth of the organoids (Figure 42).

As shown in Figure 44, a dose-dependent reduction in the OFC and size of the treated organoids with DIQ, ONC201 and ONC206 was noticed in patient 3 with rectal mucinous adenocarcinoma (pT2 stage). Characterization of the patient 3-derived organoids and corresponding tissue was assessed by investigating the expression of CK19 and CD44 markers using immunofluorescence staining. These organoids mimicked the heterogeneity of corresponding tumor tissue. Strong expression of CK19 and CD44 was noted in organoids, thus consistent with the corresponding tumor tissue (Figure 43). The co-expression of CK19 and CD44 was decreased upon all treatments (Figure 43).

Organoids formation was eradicated upon DIQ (0.5 and 1 μ M), ONC201 (2 μ M), and ONC206 (0.1 and 0.5 μ M) treatment in Patient 4 diagnosed with moderately differentiated (grade 2) pT2 sigmoid colon adenocarcinoma (Figure 45).

In Patient 5 of grade 2 moderately differentiated sigmoid colon adenocarcinoma and of stage pT3, DIQ treatment at concentrations as low as 0.5 μ M displayed an eradication of organoids (Figure 46). Both ONC201 and ONC206 significantly decreased the growth of the organoids at concentrations as low as 1 μ M and 0.1 μ M respectively.

ONC206 was more potent than ONC201 in decreasing the OFC and the size of the organoids at a dose that is 2, 10 and 10 times lower in patients 3, 4 and 5 respectively.

Interestingly, DIQ effect on the OFC and the size of the organoids was more potent than 5FU particularly in patients 2, 4 and 5 (Figure 42, 45 and 46). ONC201 and ONC206 effects on the OFC and the size of the organoids was more potent than 5FU in patient 4, and as potent as 5FU in patient 5 (Figure 45 and 46).

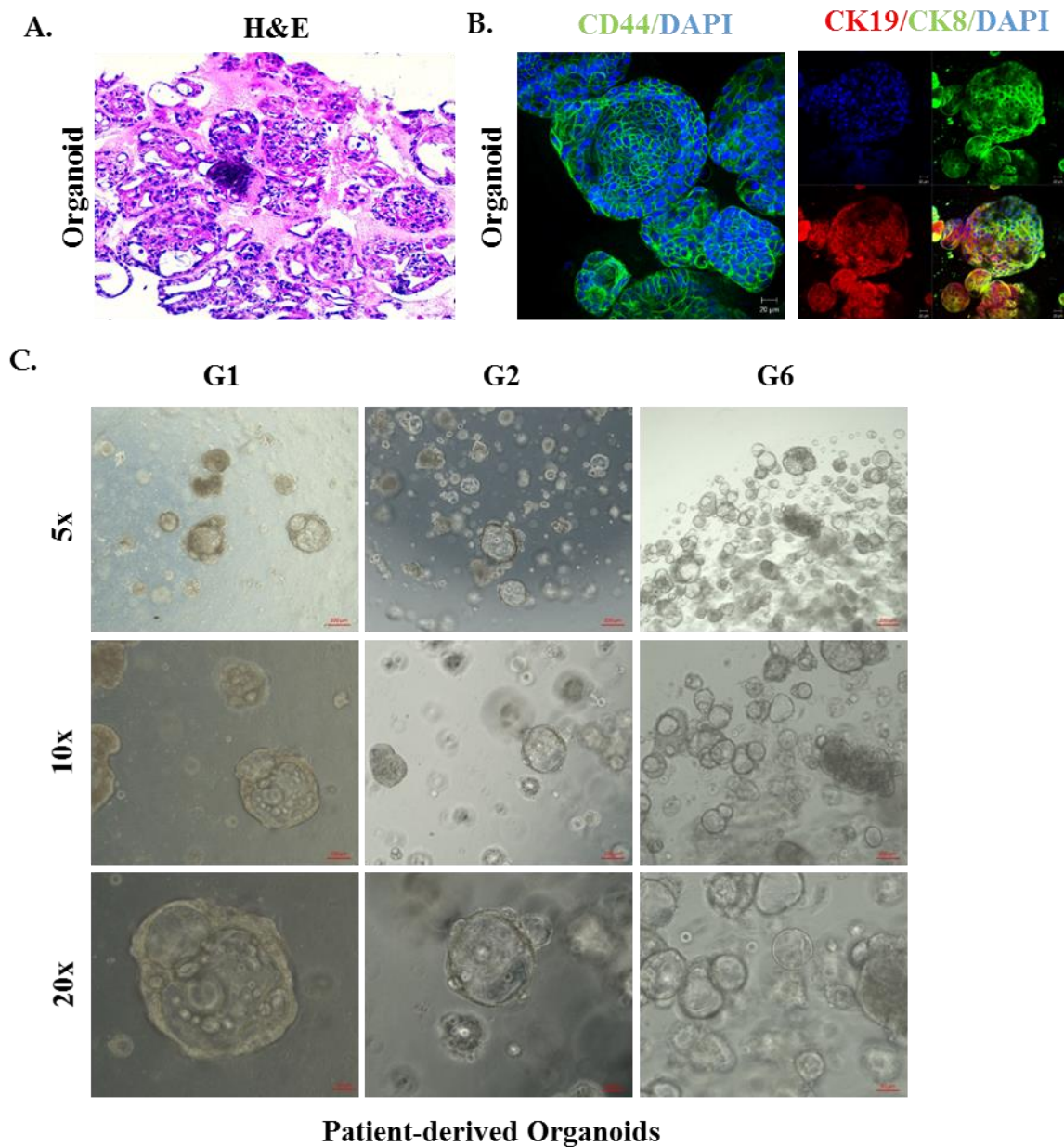


Figure 40. Establishment and characterization of patient-derived organoids from colon cancer patient 1. A: Representative image of organoids derived from patient 1 stained with H&E. B: Immunofluorescent images of organoids stained with colon lineage epithelial markers CK19 and CK8 and stem cell marker CD44. The nuclei were stained with anti-fade Fluorogel II with DAPI. Representative confocal microscopy images were acquired using a Zeiss LSM 710 laser scanning confocal microscope. Scale bar 100 μ m. C: Representative bright-field images of organoids at G1, G2, and G6. Fresh tumor tissues were enzymatically digested, and single cells were plated in 90% Growth Factor reduced Matrigel. G1 organoids were successfully propagated up to G6. Images were visualized by Axiovert inverted microscope at 5, 10, and 20 \times magnification. Scale bar 100 μ m.

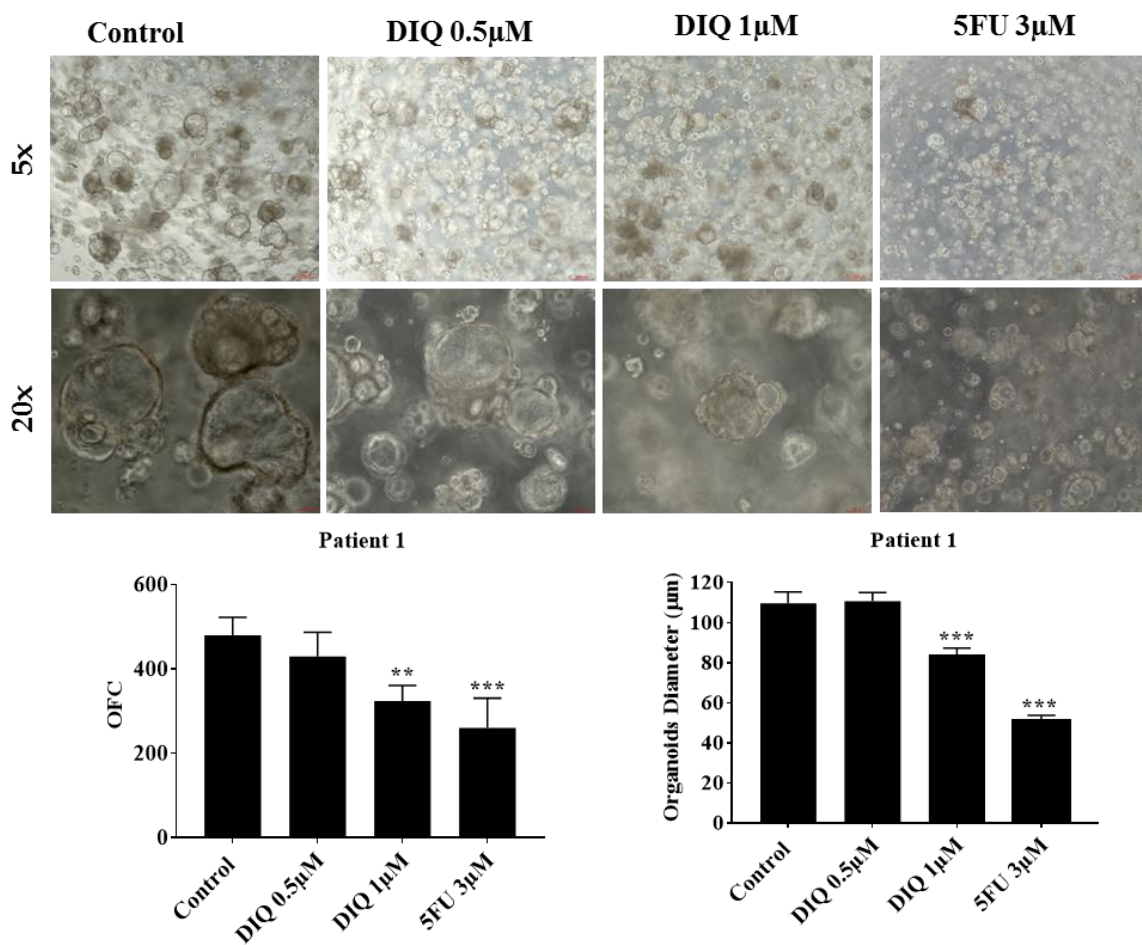


Figure 41. DIQ reduces the growth of the patient-derived organoids from colon cancer patient 1. Representative bright-field images of G2 patient 1 organoids treated with DIQ (0.5 and 1µM) or 5FU (3µM). OFC and size were calculated, and mean values were reported as mean ± SEM (*P < 0.05, **P < 0.01, ***P < 0.001). Images were visualized by Axiovert inverted microscope at 5 and 20× magnification. Scale bar 100 µm.

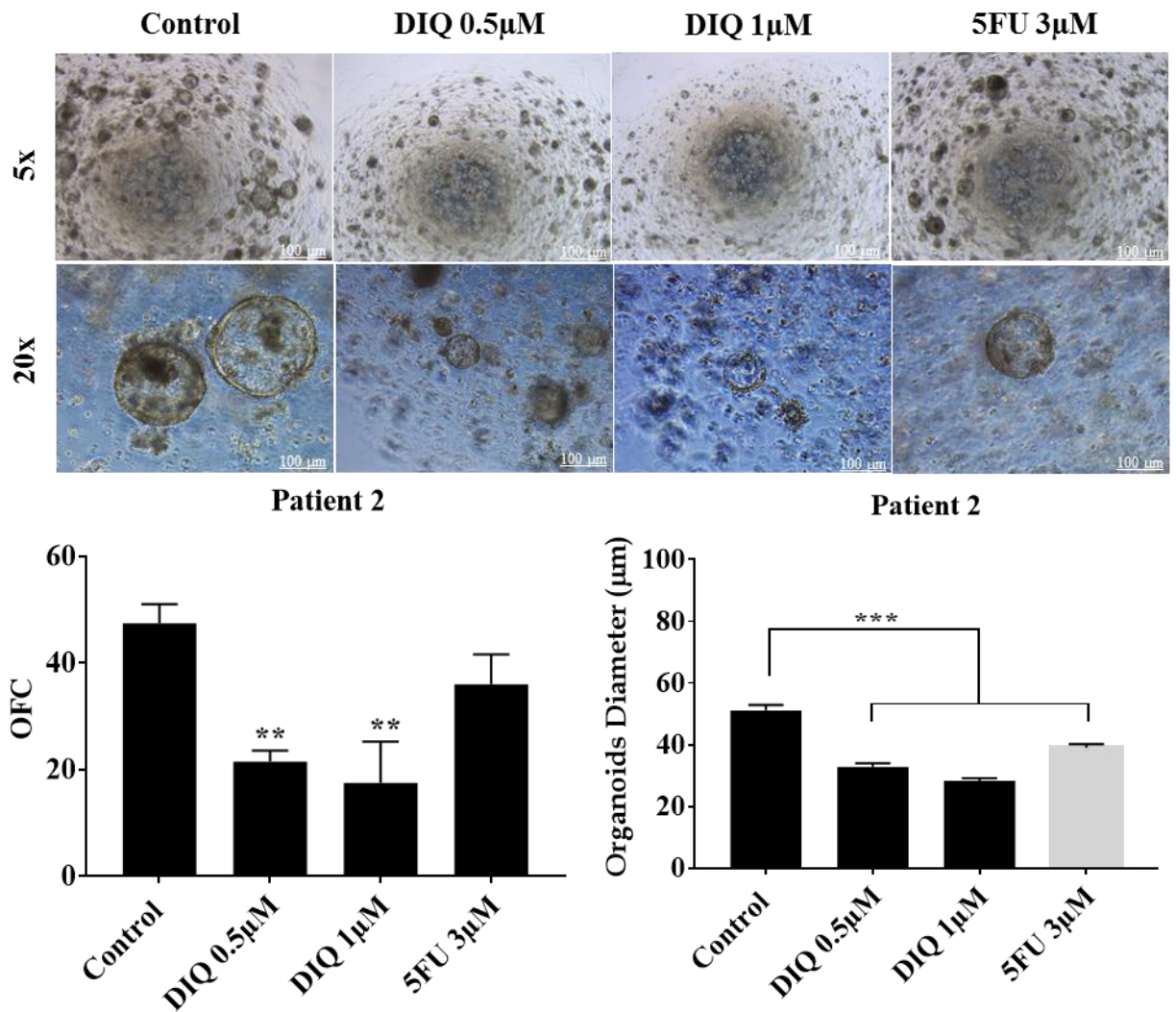


Figure 42. DIQ reduces the growth of the patient-derived organoids from colon cancer patient 2. Representative bright field images of G1 organoids derived from patient 2 [grade 2; stage T3] grown with or without DIQ or 5FU. OFC was calculated in duplicate wells per condition. The quantification of the average diameter was calculated. The data of OFC and size are presented in two separate graphs. OFC was calculated in duplicate wells per condition. The quantification of the average diameter was calculated. The average mean of OFC and size are presented in two separate graphs. All mean values were reported as mean \pm SEM (* $P < 0.05$, ** $P < 0.01$, *** $P < 0.001$). Scale bar 100 μm .

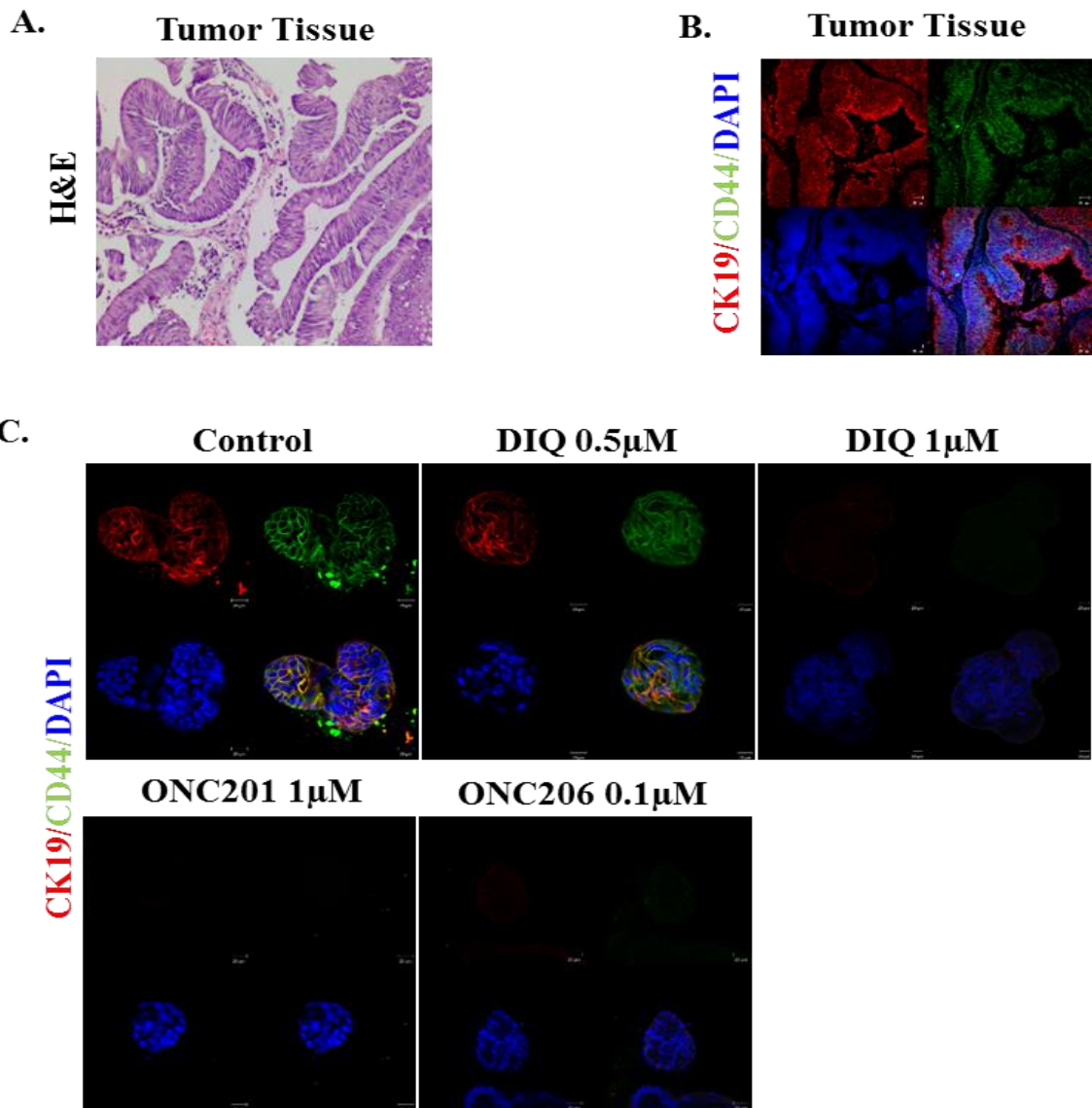


Figure 43. Establishment and characterization of patient-derived organoids from colon cancer patient 3. A: Immunohistochemistry images of tissue derived from patient 3 stained with H&E. B: Immunofluorescent images of tissue stained with colon lineage epithelial markers CK19 and stem cell marker CD44. The nuclei were stained with anti-fade Fluorogel II with DAPI. Representative confocal microscopy images were acquired using a Zeiss LSM 710 laser scanning confocal microscope. Scale bar 20 µm. C: Representative confocal microscopy images of organoids derived from colon cancer patient 3 at G2 in the presence and absence of DIQ, ONC201 and ONC206 treatments stained with colon lineage epithelial markers CK19 and stem cell marker CD44 were acquired using a Zeiss LSM 710 laser scanning confocal microscope. The nuclei were stained with anti-fade Fluorogel II with DAPI. Scale bar 20 µm.

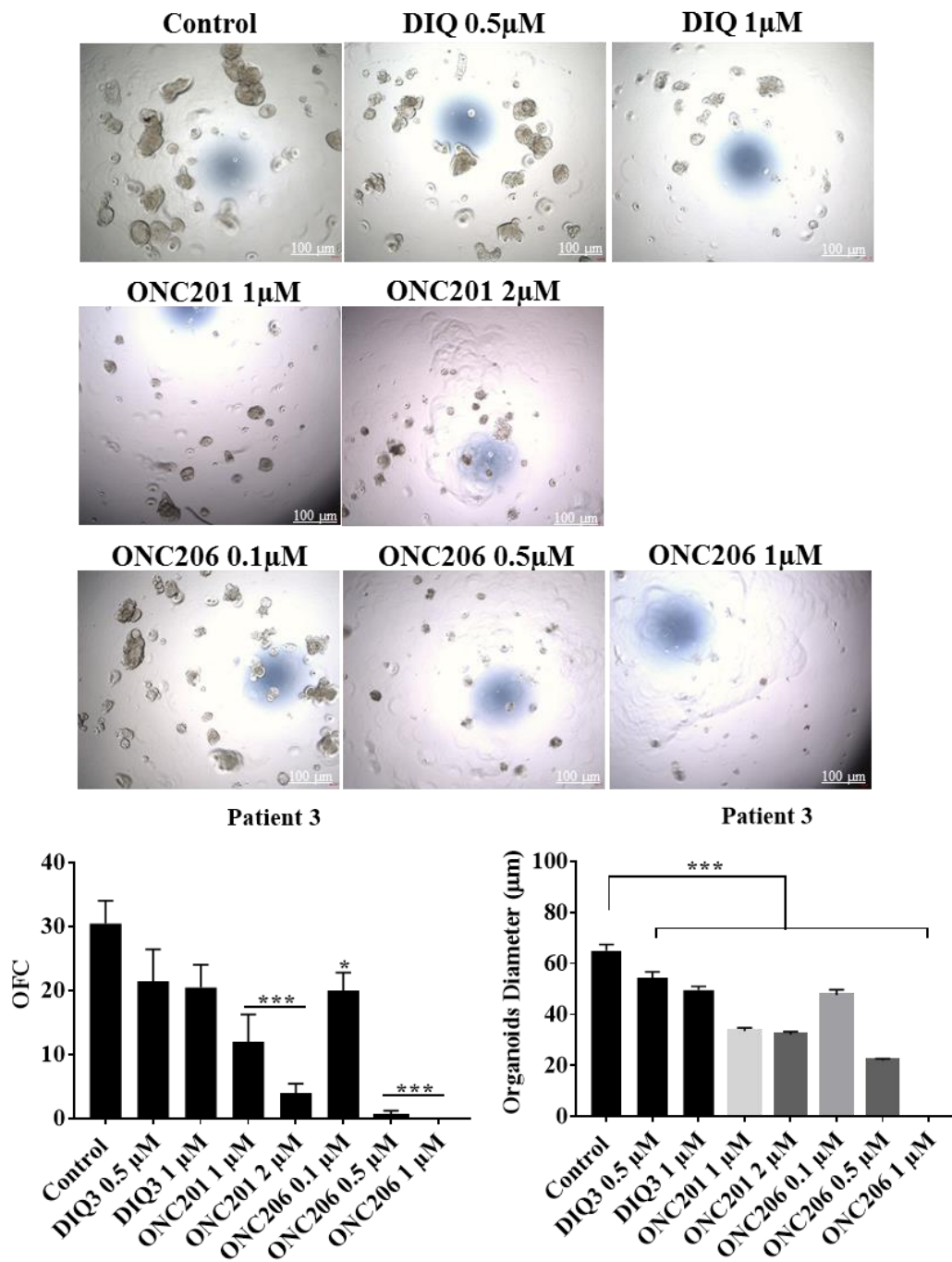


Figure 44. DIQ, ONC201 and ONC206 reduce the growth of patient-derived organoids from colon cancer patient 3. Representative bright-field images of organoids derived from colon cancer patient 3 at G2 in the presence and absence of treatments. Images were visualized by Axiovert inverted microscope at 5× magnification. OFC and size of G2 organoids were calculated, and mean values were reported as mean ± SEM (*P < 0.05, **P < 0.01, ***P < 0.001). Scale bar 100 μm.

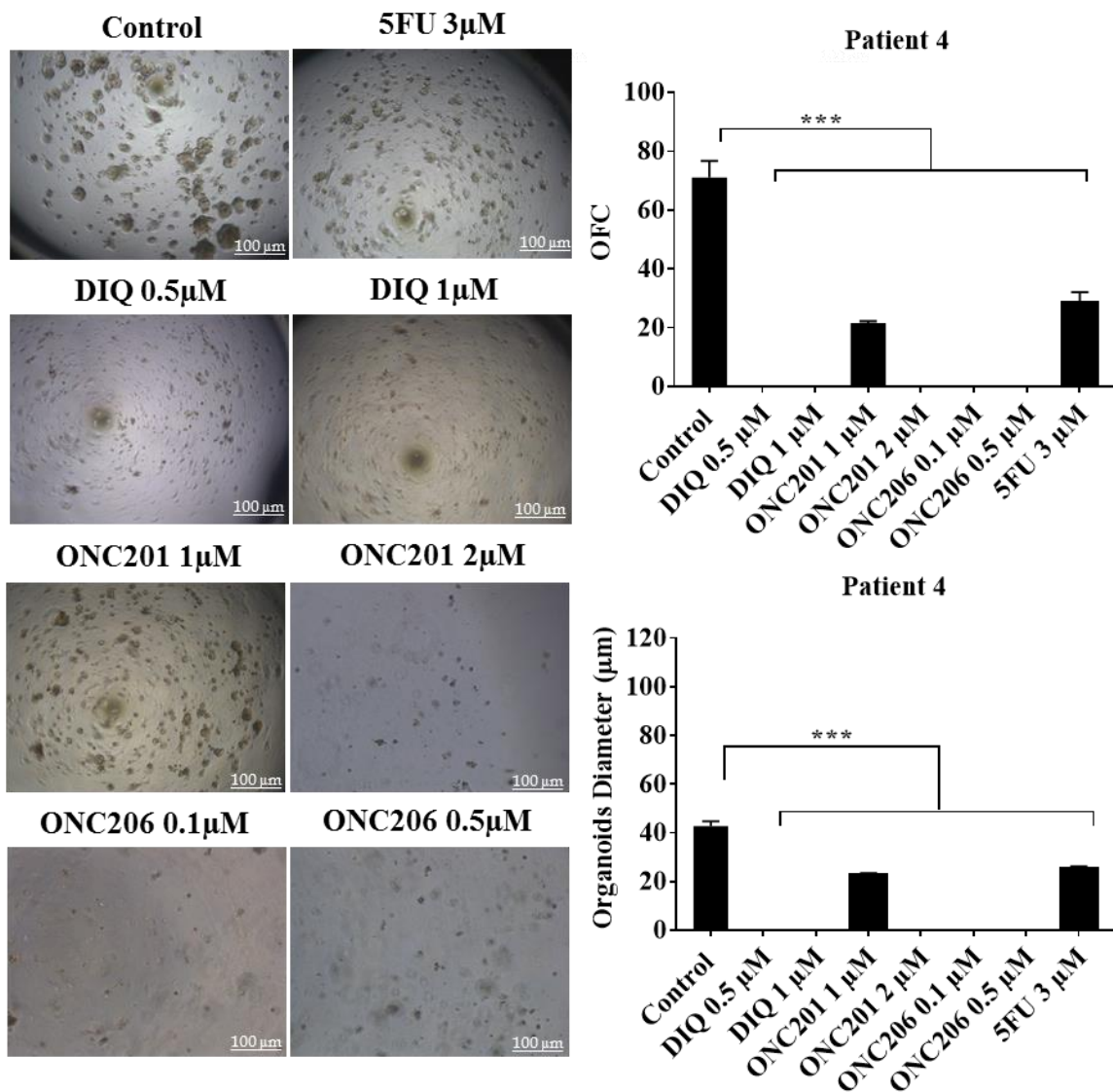


Figure 45. DIQ, ONC201 and ONC206 reduce the growth of the patient-derived organoids from colon cancer patient 4. Representative bright field images of G4 organoids derived from patient 4 [grade 2; stage T2] grown with or without DIQ, ONC201, ONC206 or 5FU. OFC was calculated in duplicate wells per condition. The quantification of the average diameter size was calculated. The average mean of OFC and size are presented in two separate graphs. All mean values were reported as mean \pm SEM (*P < 0.05, **P < 0.01, ***P < 0.001).

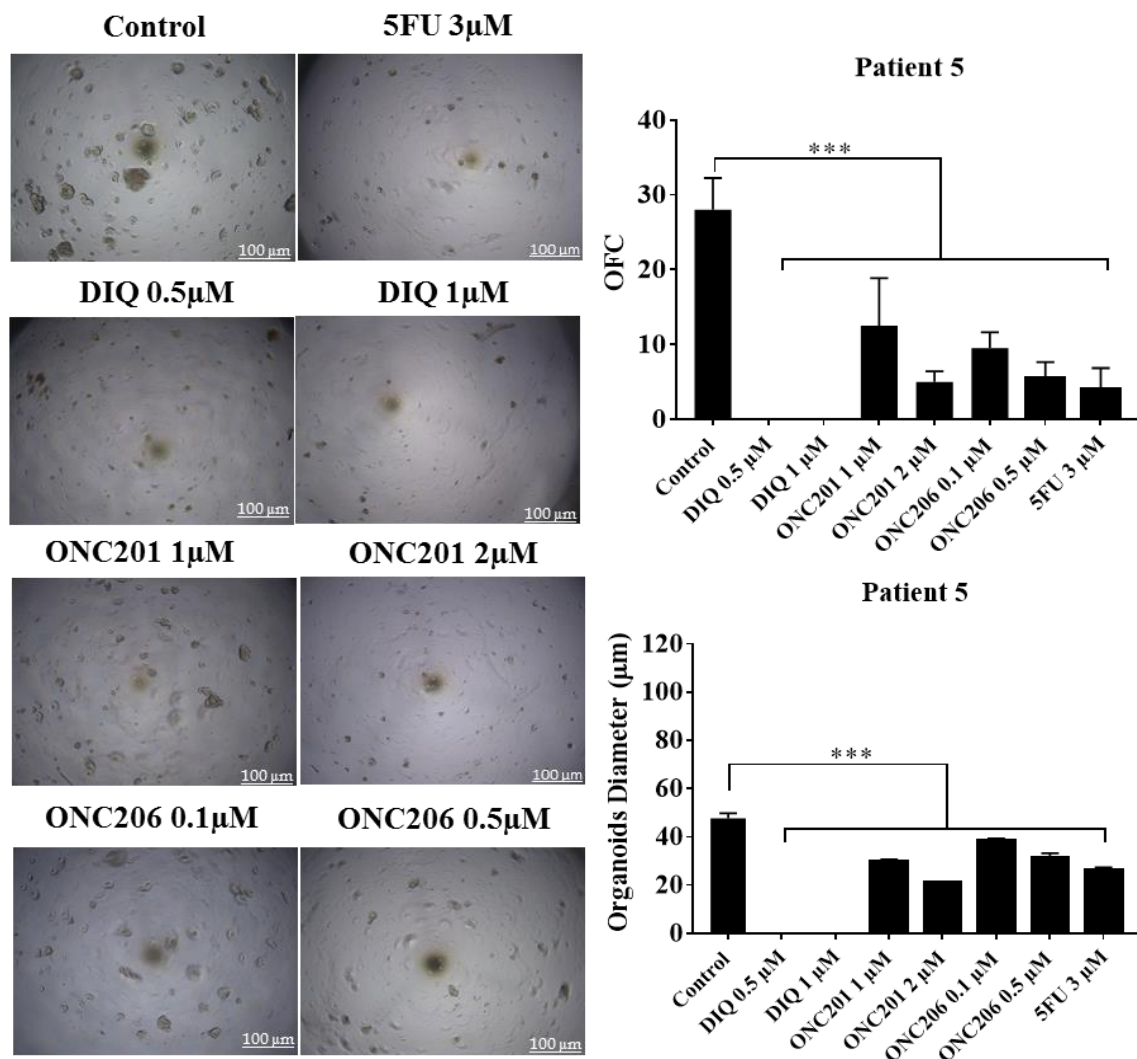


Figure 46. DIQ, ONC201 and ONC206 reduce the growth of the patient-derived organoids from colon cancer patient 5. Representative bright field images of G2 organoids derived from patient 5 [grade 2; stage T3] grown with or without DIQ, ONC201, ONC206 or 5FU treatment. OFC was calculated in duplicate wells per condition. The quantification of the average diameter was calculated. The average mean of OFC and size are presented in two separate graphs. All mean values were reported as mean ± SEM (*P < 0.05, **P < 0.01, ***P < 0.001).

2. DIQ, ONC201 and ONC206 Assessment on Cell-Derived Organoids from

Colorectal Cancer Cell Lines

The effect of DIQ, ONC201 and ONC206 on the growth of the organoids was further confirmed by assessing the effect of these treatments on cell-derived organoids from CRC cells. The results of response of HCT116 and HT29 cell-derived organoids to

DIQ, ONC201 and ONC206 treatments were consistent with that of patient-derived organoids. DIQ (0.5 and 1 μ M), ONC201 (1 and 2 μ M), and ONC206 (0.1 and 0.5 μ M) elicited a statistically significant decrease in the growth of cell line-derived organoids (Figure 48 and 49). The count of the organoids was remarkably decreased upon treatment as compared to control conditions. DAPI/phalloidin staining was performed to determine the morphology of actin filaments upon treatments, which are involved in the regulation of cell shape and polarity (Figure 47).

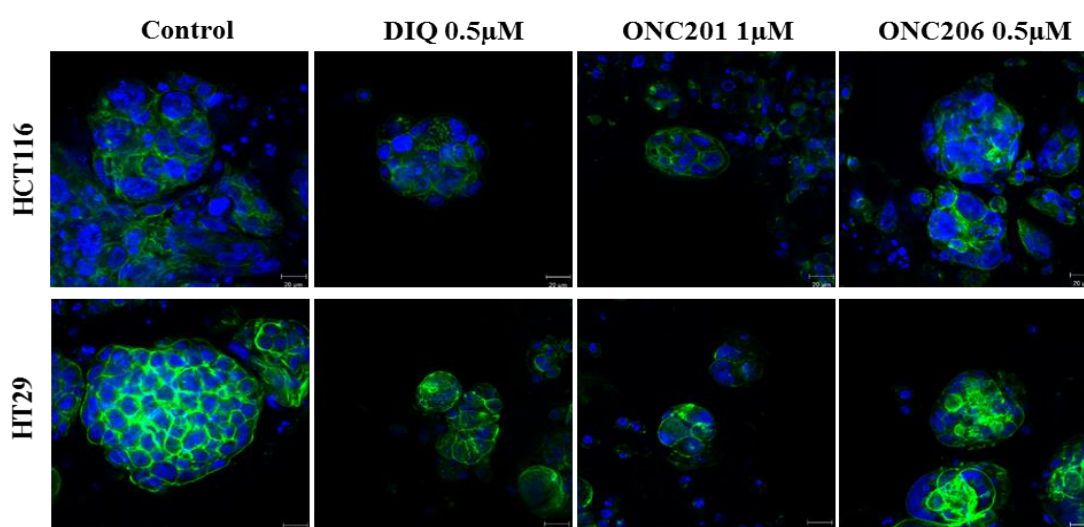


Figure 47. The morphology of the cell-derived organoids from HCT116 and HT29 cells upon DIQ, ONC201 and ONC206 treatments. Immunofluorescent images of organoids derived from HCT116 and HT29 cell lines at G1 in the presence and absence of DIQ (0.5 μ M), ONC201 (1 μ M), and ONC206 (0.5 μ M) stained with phalloidin. The nuclei were stained with anti-fade Fluorogel II with DAPI. Representative confocal microscopy images were acquired using a Zeiss LSM 710 laser scanning confocal microscope. Scale bar 20 μ m.

HCT116-derived Organoids

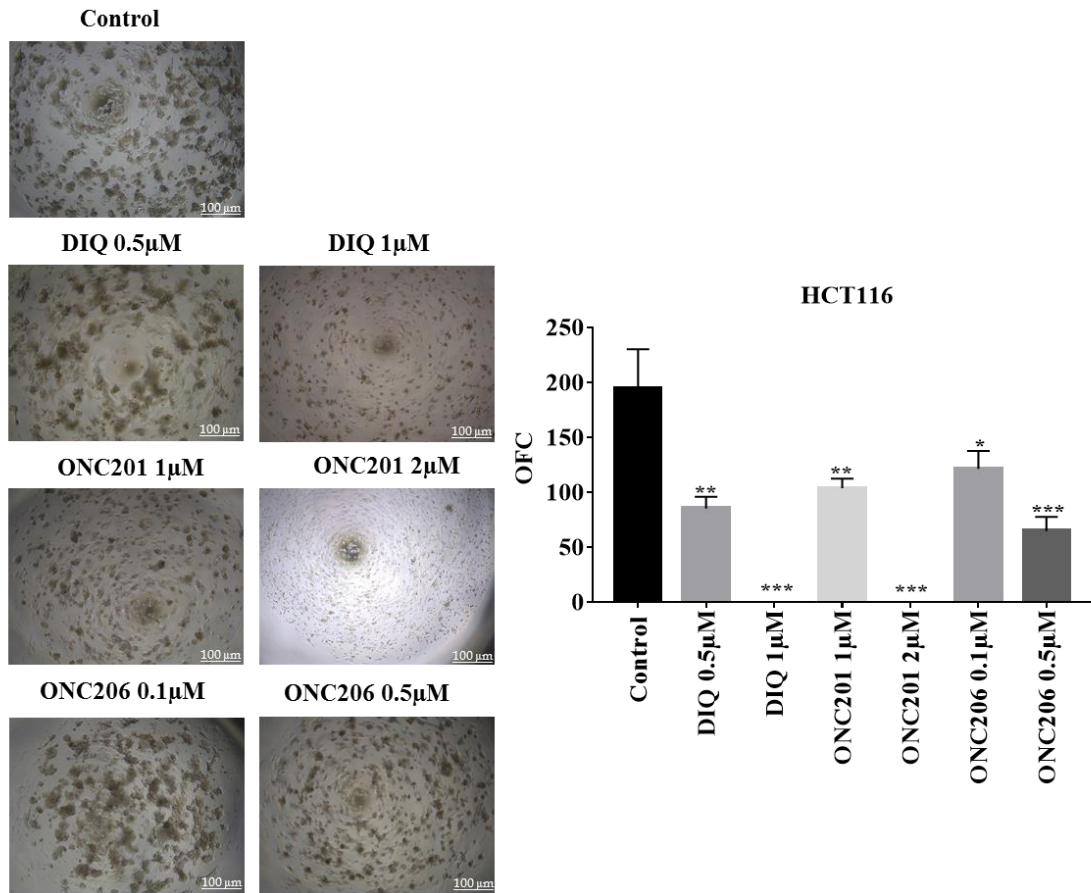


Figure 48. DIQ, ONC201 and ONC206 reduce the growth of the cell-derived organoids from HCT116 cells. Representative bright field images of G1 organoids derived from the colorectal HCT116 cell lines grown with or without DIQ (0.5 μM), ONC201 (1 μM), and ONC206 (0.5 μM) . Scale bar 100 μm. OFC was calculated in duplicate wells per condition. All mean values were reported as mean ± SEM (*P < 0.05, **P < 0.01, ***P < 0.001).

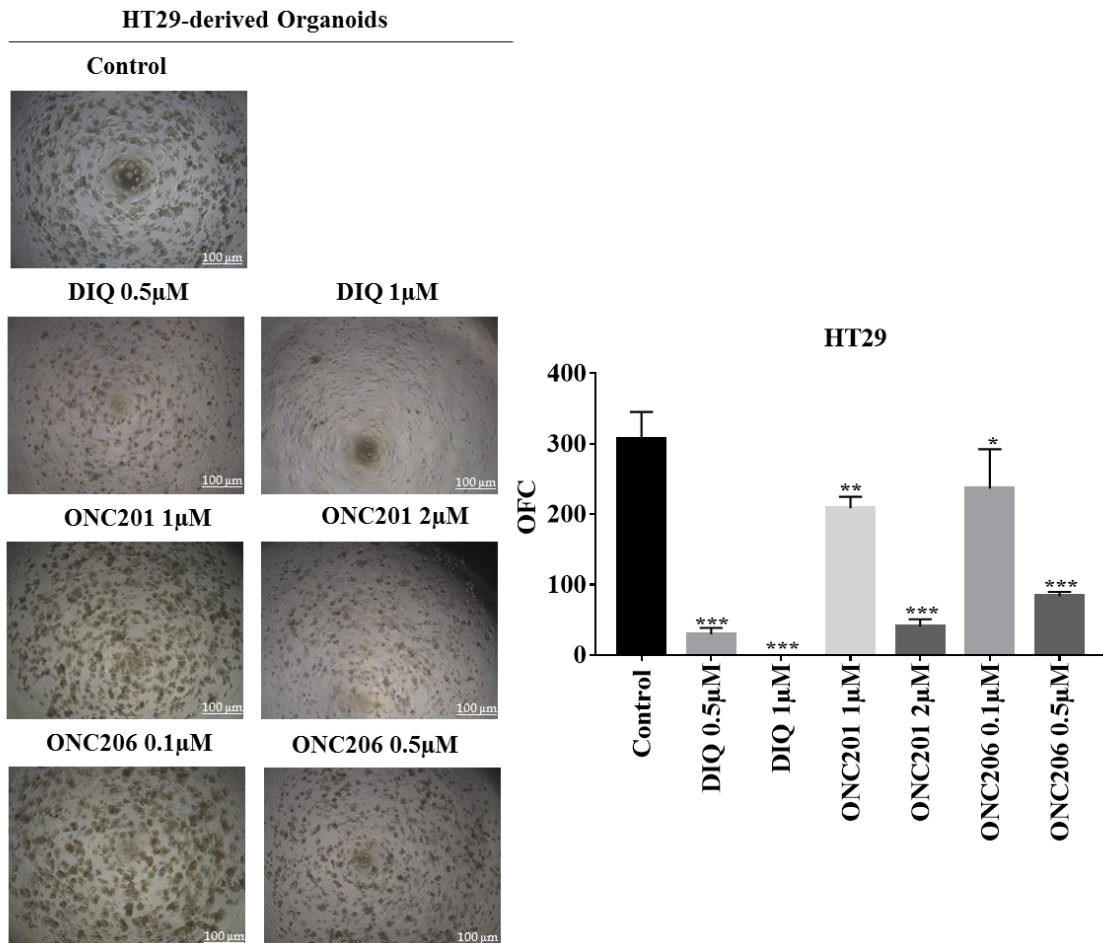


Figure 49. DIQ, ONC201 and ONC206 reduce the growth of the cell-derived organoids from HT29 cells. Representative bright field images of G1 organoids derived from the colorectal HT29 cell lines grown with or without DIQ (0.5 μM), ONC201 (1 μM), and ONC206 (0.5 μM) . Scale bar 100 μm. OFC was calculated in duplicate wells per condition. All mean values were reported as mean ± SEM (*P < 0.05, **P < 0.01, ***P < 0.001).

3. DIQ Assessment on Patient-Derived Organoids from a Different Solid Tumor

Prostate Cancer

We have also assessed the effect of DIQ on prostate patient-derived organoids from prostate (PC) cancer, another solid tumor, following the protocol used in the laboratory of Dr. Abou-Kheir. Knowing that my colleague Katia Cheaito at Dr. Abou-Kheir's laboratory has succeeded in optimizing the organoids culture protocol and establishing PC patient-derived organoids. PC human tissue samples were freshly

collected from patients who underwent radical prostatectomy at AUBMC, minced into small pieces using sterile scalpel blades, then enzymatically digested and cultured using specific human prostate organoids growth medium and successfully established into prostate organoid cultures at day 21. The effect of different concentrations of DIQ (0.5 and 1 μ M) was assessed on 6 different prostate cancer patients belonging to different Gleason groups. DIQ displayed the potential to affect the growth of prostate-derived organoids from tumor tissue samples (Figure 50 and 51). In patients 1, 3, 5 and 6, the OFC was significantly decreased upon DIQ treatment as compared to control condition. DIQ effect was more pronounced in patient 1 at G2; eradication of organoids took place at G2 upon DIQ treatment.

In patient 2, DIQ treatment showed effect only on the size of the organoids at G1; however, the OFU was remarkably decreased at G2 upon 1 μ M DIQ and increased upon 0.5 μ M DIQ.

Interestingly, for patient 4, the addition of 0.5 μ M DIQ resulted in a significant increase in the count and a significant decrease in the size of organoids, while the tumor organoids size and count did not change in the presence of 1 μ M DIQ.

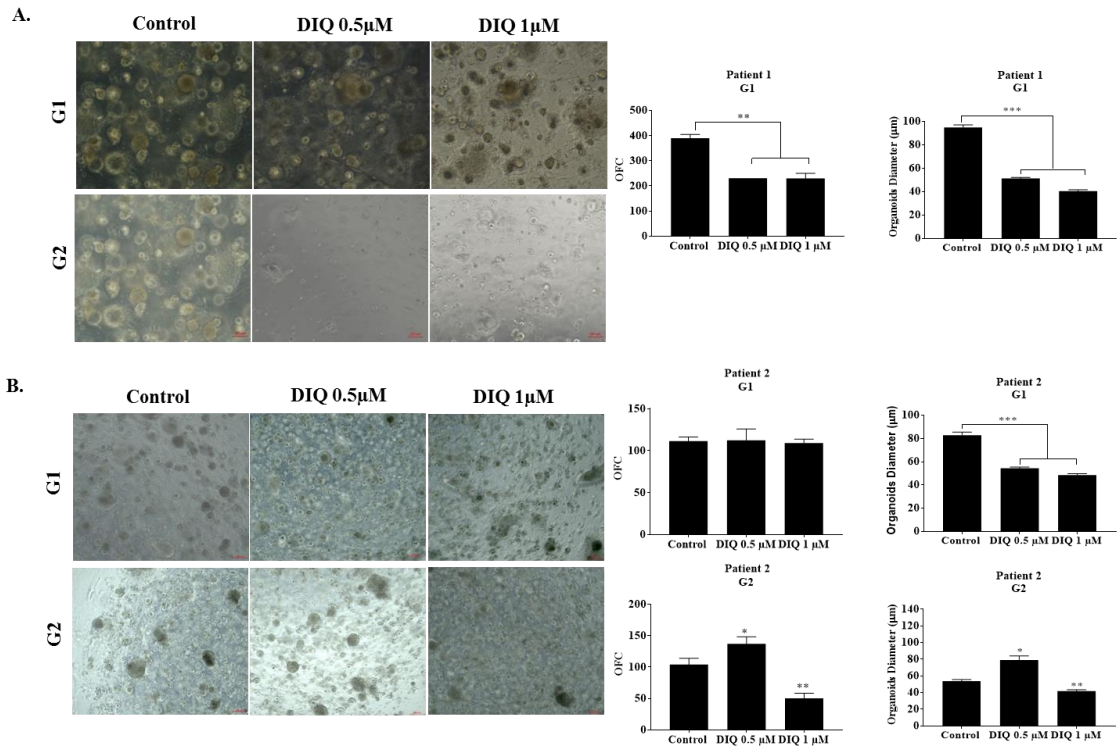


Figure 50. DIQ reduces the growth of the patient-derived organoids from different prostate cancer patients. Representative bright field images of organoids derived from prostate cancer patients 1 and 2 grown with or without DIQ treatment. OFC was calculated in duplicate wells per condition. The quantification of the average diameter was calculated. The average mean of OFC and size are presented in two separate graphs. All mean values were reported as mean \pm SEM (*P < 0.05, **P < 0.01, ***P < 0.001).

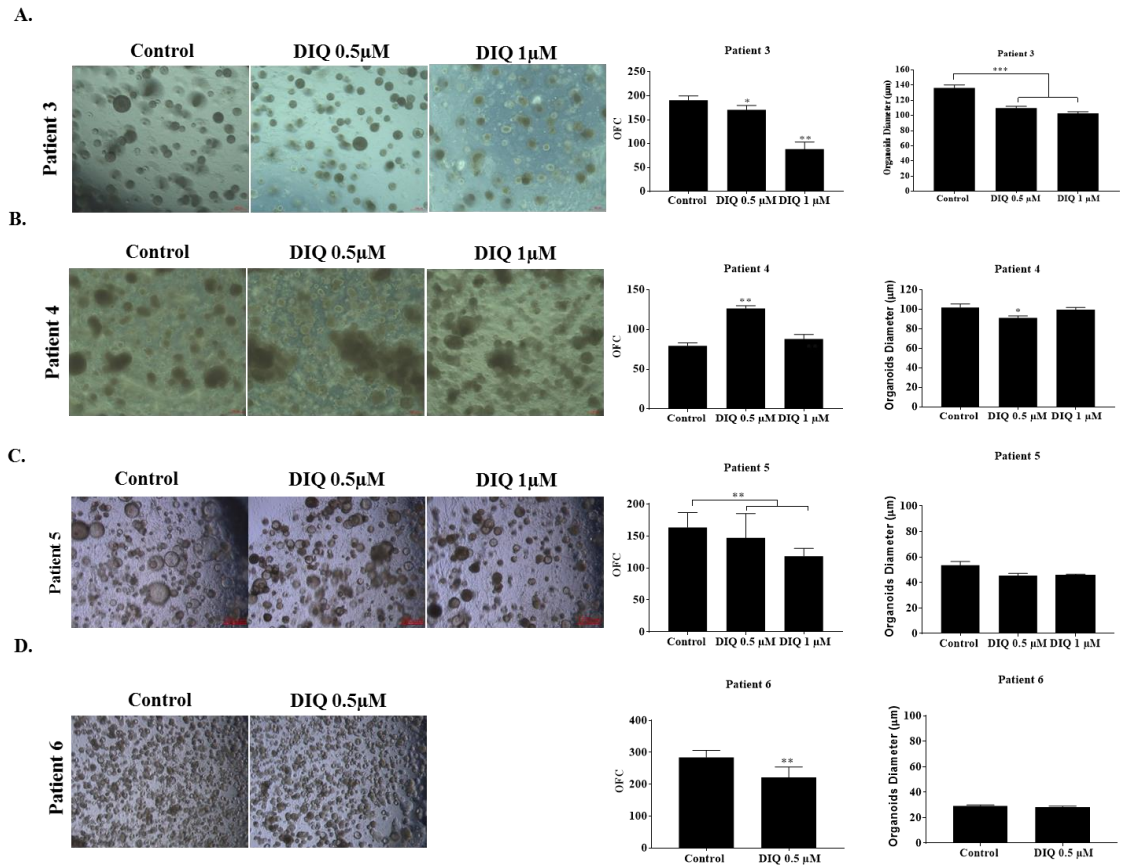


Figure 51. DIQ reduces the growth of the patient-derived organoids from different prostate cancer patients. Representative bright field images of organoids derived from prostate cancer patients 3, 4, 5 and 6 grown with or without DIQ treatment. OFC was calculated in duplicate wells per condition. The quantification of the average diameter was calculated. The average mean of OFC and size are presented in two separate graphs. All mean values were reported as mean \pm SEM (*P < 0.05, **P < 0.01, ***P < 0.001).

CHAPTER IV

DISCUSSION

Colorectal cancer is a multistep genetic disorder caused by sequential mutational events in signal transduction pathways occurring along with progression of the cancer [18]. CRC is one of the most commonly diagnosed and lethal cancers worldwide [1]. High mortality of CRC is mainly correlated to metastasis, treatment resistance and recurrence [135]. Advance in diagnosis and treatment of CRC reveal marginal success in producing favorable clinical outcome, and the disease-free survival of CRC is still limited [136]. 5FU is the standard treatment for CRC; however, it has been ineffective due to drug resistance [100, 137]. The presence of chemotherapy-resistant CSCs, also known as the tumor-initiating cells, has been determined to be one of the most significant causes of treatment failure and tumor recurrence in CRC suggesting that CSCs are a rational target [138, 139]. Therefore, the significant identification of novel therapeutics targeting CSCs in colorectal cancer patients is of high importance for cancer management.

Quinones-containing compounds and imipridone have been reported as one of the promising novel anticancer therapeutics against CRC. The quinone-containing compounds have been found to inhibit colon cancer growth and induce apoptosis both *in vitro* and *in vivo* [96, 97, 100]. We have recently shown that the novel quinone-containing compound DIQ exhibited anticancer effects against colorectal cancer stem-like cells [81]. In addition, ONC201 and its analogue ONC206 which belong to imipridone molecular family have been demonstrated as promising cancer chemotherapeutic agents [121, 123, 128, 130]. ONC201 is currently being investigated in phase I/II clinical trials of patients with hematological malignancies and solid tumors,

and ONC206 demonstrated cytotoxic and apoptotic effects in CRC cell lines [140]. However, limited research exists on the effects of ONC201 targeting the CSC population within bulk tumor cells in colorectal cancer, and there are no studies on the antitumor effects of ONC206 targeting the stemness characteristics of CSCs. Thus, their effects on colorectal CSCs has not been extensively investigated yet.

Our study was designed to investigate the anticancer potential of novel therapeutics DIQ, ONC201 and ONC206 in 2D and 3D model systems of colorectal cancer. To our knowledge, this is the first research that investigated the effects of these therapeutic agents against colorectal cancer and determined their ability to target the self-renewal capacity of CSCs.

In this study, we used PDOs in addition to two different human CRC cell lines HCT116 and HT29. Considering their widespread use, HCT116 and HT29 cell lines included in this study had different mutations and varied in appearance and growth characteristics. The significant finding of this study was the reduction of the sphere-forming and self-renewal ability of colorectal cancer HCT116 and HT29 stem cells by DIQ, ONC201 and ONC206 treatments and eradication of the propagated spheres at sub-toxic doses. Mechanistically, DIQ and ONC206 targeted CSCs by reducing the proliferation marker Ki67 and CRC stem cell markers CD44 and CK19, as well as inducing DNA damage through decreasing γ -H2AX expression and downregulating the main components of stem cell-related β -catenin, AKT and ERK oncogenic signaling pathways. DIQ, ONC201 and ONC206 displayed a highly significant decrease in both the count and the size of the organoids derived from colon cancer patients as compared to control and 5FU conditions. Furthermore, in 2D culture, DIQ, ONC201 and ONC206 significantly inhibited cell proliferation, migration, and invasion of HCT116 and HT29

cell lines. These treatments also induced apoptosis along with an accumulation of cells in the sub-G1 region and an increase in ROS.

In our first aim, we assessed the effect of DIQ, ONC201 and ONC206 on HCT116 and HT29 cells in 2D culture before exploring their effects in the 3D culture system. Our 2D results clearly demonstrated that DIQ, ONC201 and ONC206 have a potent antitumor action against HCT116 and HT29 colorectal cancer cells. DIQ, ONC201 and ONC206 reduced the growth of these two cell lines in a time- and dose-dependent manner, and interestingly were relatively non-toxic to non-tumorigenic FHS74Int cells. These data were consistent with previous findings [81, 127, 129, 141]. Being non-toxic to non-tumorigenic FHS74Int cells makes these therapeutic agents somewhat selective to cancer cells, which is the most essential aspect sought after in anticancer drugs. The potent inhibitory effect of DIQ and ONC206 treatments was accompanied with a significant decrease in cell migration and invasion along with dual reduction in the expression of AKT and ERK and downregulation of PCNA, subsequently suggesting suppression of CRC metastasis by these novel therapeutics.

Our major focus in this study was to evaluate the ability of DIQ, ONC201 and ONC206 to target CSCs in HCT116 and HT29 cells using a 3D sphere formation assay. The increase of SFU in both CRC cell lines from G1 up to G5 suggests an enrichment in CSCs upon propagation, thus confirming the advantage of using 3D sphere formation assay. Treatment of HCT116 and HT29 cells with DIQ, ONC201 and ONC206 at concentrations as low as 1, 1 and 0.1 μM respectively targeted the sub-population of stem/progenitor cells over 5 generations as reflected by the drastic decrease in the SFU and the sphere size in both cell lines over five generations. Both CRC cell lines were similarly sensitive to 1 μM ONC201; however, HCT116 cells were generally more

sensitive in response to 0.1 μM ONC206 treatment where we found an eradication of HCT116 spheres at G4. HT29 spheres were more sensitive to 1 μM DIQ and an eradication of HT29 spheres occurred at G3. Our findings regarding ONC201 treatment are in agreement with a study by Prabhu et al, which demonstrated that ONC201 contributed to downregulation of CSC markers in HCT116, DLD1, and SW480 cell lines and decrease of the CSC self-renewal *in vitro* and *in vivo* through the use of colonosphere formation assays [126]. So, our data of ONC201 targeting CSCs in 3D sphere assay provides further insight into the potent anticancer efficacy of ONC201 and further strengthen the preclinical evidence for its potential therapeutic use in clinics on patients with CRC. These findings suggest that DIQ, ONC201 and ONC206 might selectively target CSC in CRC subsequently preventing cancer relapse. Notably, the inhibitory effects in CRC cell lines were observed at much lower concentrations with ONC206 (1 μM in 2D and 0.1 μM in 3D) versus ONC201 (5 μM in 2D and 1 μM in 3D), suggesting that ONC206 was more potent against CRC compared to ONC201. This is why we were interested in investigating ONC206's molecular mechanisms, in addition to DIQ, in CRC.

Multiple signaling pathways such as EGFR/ MAPK, PI3K/AKT, and Wnt, have been reported to be dysregulated and associated with the resistance of CSCs to therapy [44, 45]. Wnt signaling contributes to stem cell development, tumorigenicity, and oncogenesis in CRC [41, 42]. PI3K/AKT activation was suggested to potentiate drug resistance and increase tumorigenicity by increasing the cancer stem-like populations (CD133) [142]. Additionally, PI3K/AKT/mTOR and MAPK/ERK pathways, which are involved in mediating cell proliferation, invasion and tumorigenesis, are aberrantly activated in cancer, inducing unlimited growth and driving

carcinogenesis. Evidence has shown that AKT and ERK are overexpressed in human CRC [45, 143]. The dysregulation of AKT and ERK signaling pathways are nowadays target therapies against cancer as it was documented that the dual inhibition of AKT and ERK decreased cell survival. Studies have shown that ONC201 affected both bulk tumor cells and CSCs, especially in CRC, prostate cancer, glioblastoma, and AML in 3D sphere cultures and patient-derived models. ONC201 action mechanisms in this regard include modulation of stem cell pathways such as Wnt signaling and genes known to regulate self-renewal (ID1, ID2, ID3 and ALDH7A1) [144, 145]. These effects are followed by depletion of CD133, CD44 and Aldefluor-positive CRC stem cells in an Akt/Foxo3a/DR5/TRAIL-dependent manner [23, 25, 26]. The results Since ONC206 is an analogue of ONC201, we proposed that ONC206 would act through similar mechanisms.

To understand what molecular pathways could be targeted by DIQ and ONC206, we focused mainly on the pathways implicated in CSCs. The mechanism of inhibition of colon sphere formation and the decrease in the sphere size were mainly correlated with the observed decrease in expression of proliferation marker Ki67, the CRC stem markers CD44 and CK19 along with downregulation of p-ERK, p-AKT, PCNA and the CRC stem cell marker CD133. The result of western blot analysis showed that the ratio of both phosphorylated AKT to total AKT (p-AKT/AKT) and phosphorylated ERK to total ERK (p-ERK/ERK), which are key players of AKT/ERK pathways, were decreased upon DIQ and ONC206 treatments in CRC spheres. DIQ and ONC206 reduced the activities of AKT and ERK in 3D culture, resulting in reduction in cell proliferation, thus decreasing the self-renewal potential of colon CSCs. These findings suggest that DIQ and ONC206 suppressed sphere growth and formation via

dual inhibition of AKT/ERK dependent signaling pathways. The profile (AKT/ERK) for ONC206 was similar to that of ONC201 in CRC and other cancer types as shown in previous studies [118, 141].

Given that Wnt/ β -catenin and PI3K and ERK signaling pathways are strongly intersected in the maintenance of CSCs [26, 75], we additionally investigated the protein levels of the key stem cell markers in CRC, CD133 and β -catenin, which are involved in chemotherapy resistance. Interestingly, the expression of CD133 and β -catenin were dramatically downregulated after DIQ and ONC206 treatment. Moreover, upon DIQ and ONC206 treatment, there was a significant decrease in the expression of CD44 and CK19 in both CRC cell lines which were highly expressed in control spheres. It is interesting to note that CK19, which is considered a tumor marker in CRC, is specifically and stably expressed in primary and metastatic colorectal cancer cells (9, 10). These results proposed that both DIQ and ONC206 could target a broad range of proposed CSC markers in CRC considering the lack of single specific CRC marker. Altogether, this suggest that DIQ and ONC206 could be considered novel therapeutic compounds for suppressing CSC self-renewal via different oncogenic stemness mechanisms.

We next assessed whether DNA damage was activated in the spheres derived from both cell lines. We evaluated the expression of γ -H2AX, which is a DNA double-strand damage (DBS) biomarker and could be a classical cancer prognostic factor [35, 36]. The loss of DNA damage in CRC is involved in the development of therapeutic resistance [35, 36]. Quinones and oxaliplatin have been shown to induce apoptosis of CRC cells by activating DBS and activating γ -H2AX expression [30, 37]. ONC206 sustained phosphorylated γ -H2AX expression, increased cleaved PARP1 and cleaved-

caspace-3 at 48 and 72 h compared with vehicle-treated cells in MYCN-amplified neuroblastoma cells [128]. Interestingly, DIQ and ONC206 increased the expression of γ -H2AX in both CRC cells as compared to control condition; clearly emphasizing that DIQ and ONC206 are potent inducers of DNA damage in agreement with previous studies.

Consistent with the *in vitro* data, DIQ exhibited lower tumorigenic potential and proliferation reduction *in vivo*. To further experimentally assess the effect of DIQ on CRC tumorigenesis, we injected NOD-SCID mice with HCT116 spheres and treated them with DIQ. Treatment with 20 mg/kg body weight of DIQ significantly inhibited tumor growth in NOD-SCID mice injected with HCT116 spheres. Tumor development happened earlier in NOD-SCID mice injected with spheres as compared to another group injected with 2D equivalent cell density, reflecting the enrichment of CSCs in HCT116 spheres injected. Tumor volume in DIQ-treated group was always lower than that of control all over the period of treatment, indicating a potent inhibitory effect of DIQ on tumor growth.

Additionally, in the present study, we explored the possible anticancer activity of DIQ, ONC201 and ONC206 on HCT116 and HT29 cells by investigating their effects on cell cycle and production of ROS. Our results showed that DIQ, ONC201 and ONC206 induced apoptosis, increased ROS, and caused cell cycle arrest and accumulation of CRC cell lines in sub-G1 phase. Apoptosis, which is a genetically programmed cell death process, prevents the proliferation of damaged cells [37]. A significant increase in sub-G1 population upon DIQ, ONC201 and ONC206 treatments at 72 h was observed indicating that these treatments induced cell death. Annexin V and PI staining results revealed that treated cells were undergoing apoptosis; total (early and

late) apoptotic phases were detected in all treatments. ROS is one of the major inducers of DNA damage. Induction of ROS generation induces increased stress on cancer cells leading to cancer cell death. This was proposed as a mechanism of action of quinones [84]. ONC206 triggered ISR activation, manifested by production of ROS and reduction of mitochondrial membrane potential [129]. Therefore, the data suggests that DIQ and ONC206 have promoted apoptosis by increasing ROS generation.

In general, the overall cell cycle arrest was quite similar between HCT116 and HT29 cells in response to each treatment, although there were some differences in DIQ treatment. These results demonstrated that the activity of these compounds is independent on proteins or genes that are commonly mutated in CRC, such as p53 and KRAS. This is in agreement with previous studies that have demonstrated ONC201 induced cell death and cell cycle arrest by both TRAIL-dependent and TRAIL-independent mechanisms based on the cancer type and independent of p53 activation [128, 146]. The results of our study revealed that DIQ caused G1 arrest in HCT116 and S phase arrest in HT29 cells along with upregulation of p21 protein expression in both cell lines, suggesting that DIQ-mediated apoptosis and inhibition of cell cycle progression may be dependent on the upregulation of p21, was an effect that is mediated through p53-dependent pathway in HCT116 but not in HT29 cells. Additionally, p21, which is a known tumor suppressor [31], promotes ROS accumulation, binds to proliferating cell nuclear antigen (PCNA) [32], and inhibits cell cycle progression. Cell cycle assessment also showed that ONC201 and ONC206 induced S phase arrest and sub-G1 population accumulation in the tested CRC lines. Interestingly, ONC206 downregulated protein levels of p53 and p21. The findings that ONC206 reduced the level of p53 protein in CRC cell lines suggests its contribution to S-phase arrest and

apoptosis. Due to excessive DNA damage in CRC cells upon ONC206 treatment, apoptosis is favored by downregulating p21. Co-localization studies showed that p21 levels are downregulated in cells with high γ -H2AX staining suggesting that cells with excessive DNA damage were diverted towards cell death by reducing the levels of p21.

In our second aim, we demonstrated effects of DIQ, ONC201 and ONC206 in a patient-derived model. This model which closely recapitulates tissue architecture and cellular composition is used to assess the self-renewal and differentiation capacities of the organoid CSC, including growth kinetics and drug sensitivity [11, 12]. The application of colon patient-derived organoid model is an effective tool that holds great promise for personalized medicine and exhibits a significant potential to predict patient response and connect compound screening and clinical trials [42, 43]. Since drug resistance to chemotherapy is a serious challenge in treating solid tumors, drug exposure studies on the patient-derived organoids help in choosing specific chemotherapy regimens for patients with malignant disease. Consequently, we collected fresh tissue specimens from consented treatment-naïve patients undergoing radical colectomy at AUBMC, to establish and test the effects of the DIQ, ONC201 and ONC206 in targeting CSCs in organoids derived from human colon cancer patients. Regarding the morphology of organoids, the majority consisted of solid organoids as detected by bright-field microscopy. The established colon organoids expressed the CRC epithelial marker lineage CK19 and the CSC cell marker CD44. This observed co-expression recapitulates the architecture and the characteristics of colon tissues. Notably, the self-renewal capacity of CSCs was also reduced upon all treatments in the PDO assay. DIQ, ONC201 and ONC206 significantly reduced the count and the size of the organoids as compared to control condition. Their effects were either more or as potent as that of

5FU. The results of response of HCT116 and HT29 cell-derived organoids to DIQ, ONC201 and ONC206 treatments were consistent with that of patient-derived organoids. Interestingly, DIQ also caused a prominent significant inhibitory effect on growth of organoids from different prostate cancer patients showing differential responses between the patients and emphasizing its potential antitumor potential in cancer patients. We, therefore, for the first time, revealed that DIQ targeted the CSC in patient-derived colon and prostate cancer, thus making DIQ an interesting compound that targets CSC in solid tumors.

Despite the many advantages and potential uses of 3D technology, the present study has several limitations. The limited presence of stromal and lack of native microenvironment components restricts the communication of stem cells with their niches and fail at faithfully recapitulating the *in vivo* microenvironment. the inability to mimic *in vivo* growth signaling gradients in Matrigel matrix and resemble biomechanical forces that stem cells come across *in vivo* is another limitation. With regards to organoids establishment, one major challenge was the availability of tissues at the time of the study and the small size of patient tissue samples. Also, as a clinical study, the patient sample size was relatively small and the percentage success rate of deriving colon patient derived organoids was not more than 42% (as only 5 out of 12 specimens were successfully established as colon organoids). This could possibly be due to low tissue quality as well. A larger cohort is still required to further investigate and evaluate the effects of DIQ, ONC201 and ONC206 in translational medicine.

In conclusion, we demonstrated for the first time that DIQ, ONC201 and ONC206 reduced the self-renewal capacity of colorectal tumors and prevented therapy resistance in patient-derived organoids through interfering with the stem cell Wnt/ β -

catenin, and AKT and ERK pathways that are involved in CRC tumorigenesis. Also, DIQ, ONC201 and ONC206 effects were involved in the major cell-fate responses including apoptosis, cell-cycle arrest, and ROS. These treatments inhibited the key processes of CRC tumorigenesis, including cell growth, proliferation, migration, and invasion. Our findings strongly suggest that DIQ, ONC201 and ONC206 could be promising novel therapeutics for the treatment of CRC patients. These compounds could be clinically used as non-toxic agents for targeting human colon cancer stem/progenitor cells.

BIBLIOGRAPHY

- [1] H. Sung, J. Ferlay, R.L. Siegel, M. Laversanne, I. Soerjomataram, A. Jemal, F. Bray, Global Cancer Statistics 2020: GLOBOCAN Estimates of Incidence and Mortality Worldwide for 36 Cancers in 185 Countries, *CA: a cancer journal for clinicians*, 71 (2021) 209-249.
- [2] P. Kahai, P. Mandiga, C.J. Wehrle, S. Lobo, Anatomy, Abdomen and Pelvis, Large Intestine, StatPearls, StatPearls Publishing
Copyright © 2021, StatPearls Publishing LLC., Treasure Island (FL), 2021.
- [3] F. Arvelo, F. Sojo, C. Cotte, Biology of colorectal cancer, *Ecancermedalscience*, 9 (2015) 520.
- [4] L.L. Azzouz, S. Sharma, Physiology, Large Intestine, StatPearls, StatPearls Publishing
Copyright © 2021, StatPearls Publishing LLC., Treasure Island (FL), 2021.
- [5] C. Crosnier, D. Stamataki, J. Lewis, Organizing cell renewal in the intestine: stem cells, signals and combinatorial control, *Nature reviews. Genetics*, 7 (2006) 349-359.
- [6] S. Umar, Intestinal stem cells, *Current gastroenterology reports*, 12 (2010) 340-348.
- [7] N. Barker, J.H. van Es, J. Kuipers, P. Kujala, M. van den Born, M. Cozijnsen, A. Haegebarth, J. Korving, H. Begthel, P.J. Peters, H. Clevers, Identification of stem cells in small intestine and colon by marker gene *Lgr5*, *Nature*, 449 (2007) 1003-1007.
- [8] H.J. Snippert, L.G. van der Flier, T. Sato, J.H. van Es, M. van den Born, C. Kroon-Veenboer, N. Barker, A.M. Klein, J. van Rheenen, B.D. Simons, H. Clevers, Intestinal crypt homeostasis results from neutral competition between symmetrically dividing *Lgr5* stem cells, *Cell*, 143 (2010) 134-144.
- [9] T. Sato, J.H. van Es, H.J. Snippert, D.E. Stange, R.G. Vries, M. van den Born, N. Barker, N.F. Shroyer, M. van de Wetering, H. Clevers, Paneth cells constitute the niche for *Lgr5* stem cells in intestinal crypts, *Nature*, 469 (2011) 415-418.
- [10] D.H. Scoville, T. Sato, X.C. He, L. Li, Current view: intestinal stem cells and signaling, *Gastroenterology*, 134 (2008) 849-864.
- [11] D.W. Powell, I.V. Pinchuk, J.I. Saada, X. Chen, R.C. Mifflin, Mesenchymal cells of the intestinal lamina propria, *Annual review of physiology*, 73 (2011) 213-237.
- [12] Y. Li, Y. Liu, B. Liu, J. Wang, S. Wei, Z. Qi, S. Wang, W. Fu, Y.G. Chen, A growth factor-free culture system underscores the coordination between Wnt and BMP signaling in *Lgr5*(+) intestinal stem cell maintenance, *Cell discovery*, 4 (2018) 49.
- [13] K.S. Yan, L.A. Chia, X. Li, A. Ootani, J. Su, J.Y. Lee, N. Su, Y. Luo, S.C. Heilshorn, M.R. Amieva, E. Sangiorgi, M.R. Capecchi, C.J. Kuo, The intestinal stem cell markers *Bmi1* and *Lgr5* identify two functionally distinct populations, *Proceedings of the National Academy of Sciences of the United States of America*, 109 (2012) 466-471.
- [14] P. Zhu, J. Wu, Y. Wang, X. Zhu, T. Lu, B. Liu, L. He, B. Ye, S. Wang, S. Meng, D. Fan, J. Wang, L. Yang, X. Qin, Y. Du, C. Li, L. He, W. Ren, X. Wu, Y. Tian, Z. Fan, *LncGata6* maintains stemness of intestinal stem cells and promotes intestinal tumorigenesis, *Nature cell biology*, 20 (2018) 1134-1144.
- [15] F.J. Abdul Khalek, G.I. Gallicano, L. Mishra, Colon cancer stem cells, *Gastrointestinal cancer research : GCR*, (2010) S16-23.

- [16] A.G. Vaiopoulos, I.D. Kostakis, M. Koutsilieris, A.G. Papavassiliou, Colorectal cancer stem cells, *Stem cells (Dayton, Ohio)*, 30 (2012) 363-371.
- [17] U. Testa, E. Pelosi, G. Castelli, Colorectal cancer: genetic abnormalities, tumor progression, tumor heterogeneity, clonal evolution and tumor-initiating cells, *Medical sciences (Basel, Switzerland)*, 6 (2018).
- [18] K. Tariq, K. Ghias, Colorectal cancer carcinogenesis: a review of mechanisms, *Cancer biology & medicine*, 13 (2016) 120-135.
- [19] U. Nitsche, A. Zimmermann, C. Späth, T. Müller, M. Maak, T. Schuster, J. Slotta-Huspenina, S.A. Käser, C.W. Michalski, K.P. Janssen, H. Friess, R. Rosenberg, F.G. Bader, Mucinous and signet-ring cell colorectal cancers differ from classical adenocarcinomas in tumor biology and prognosis, *Annals of surgery*, 258 (2013) 775-782; discussion 782-773.
- [20] S. Chakrabarti, C.Y. Peterson, D. Sriram, A. Mahipal, Early stage colon cancer: Current treatment standards, evolving paradigms, and future directions, *World journal of gastrointestinal oncology*, 12 (2020) 808-832.
- [21] E.J. Kuipers, W.M. Grady, D. Lieberman, T. Seufferlein, J.J. Sung, P.G. Boelens, C.J. van de Velde, T. Watanabe, Colorectal cancer, *Nature reviews. Disease primers*, 1 (2015) 15065.
- [22] M. De Rosa, U. Pace, D. Rega, V. Costabile, F. Duraturo, P. Izzo, P. Delrio, Genetics, diagnosis and management of colorectal cancer (Review), *Oncology reports*, 34 (2015) 1087-1096.
- [23] A. Varghese, Chemotherapy for Stage II Colon Cancer, *Clinics in colon and rectal surgery*, 28 (2015) 256-261.
- [24] Y.H. Xie, Y.X. Chen, J.Y. Fang, Comprehensive review of targeted therapy for colorectal cancer, *Signal transduction and targeted therapy*, 5 (2020) 22.
- [25] P. Rawla, A. Barsouk, A.V. Hadjinicolaou, A. Barsouk, Immunotherapies and Targeted Therapies in the Treatment of Metastatic Colorectal Cancer, *Medical sciences (Basel, Switzerland)*, 7 (2019).
- [26] B. Bao, A. Ahmad, A.S. Azmi, S. Ali, F.H. Sarkar, Overview of cancer stem cells (CSCs) and mechanisms of their regulation: implications for cancer therapy, *Current protocols in pharmacology*, Chapter 14 (2013) Unit 14.25.
- [27] C. Yu, Z. Yao, Y. Jiang, E.T. Keller, Prostate cancer stem cell biology, *Minerva urologica e nefrologica = The Italian journal of urology and nephrology*, 64 (2012) 19-33.
- [28] F.H. Sarkar, Y. Li, Z. Wang, D. Kong, Pancreatic cancer stem cells and EMT in drug resistance and metastasis, *Minerva chirurgica*, 64 (2009) 489-500.
- [29] N.Y. Frank, T. Schatton, M.H. Frank, The therapeutic promise of the cancer stem cell concept, *The Journal of clinical investigation*, 120 (2010) 41-50.
- [30] W. Luo, S. Li, B. Peng, Y. Ye, X. Deng, K. Yao, Embryonic stem cells markers SOX2, OCT4 and Nanog expression and their correlations with epithelial-mesenchymal transition in nasopharyngeal carcinoma, *PloS one*, 8 (2013) e56324.
- [31] M. Shibata, M.O. Hoque, Targeting Cancer Stem Cells: A Strategy for Effective Eradication of Cancer, *Cancers*, 11 (2019).
- [32] Z. Yu, T.G. Pestell, M.P. Lisanti, R.G. Pestell, Cancer stem cells, *The international journal of biochemistry & cell biology*, 44 (2012) 2144-2151.
- [33] C.A. O'Brien, A. Pollett, S. Gallinger, J.E. Dick, A human colon cancer cell capable of initiating tumour growth in immunodeficient mice, *Nature*, 445 (2007) 106-110.

- [34] L. Ricci-Vitiani, D.G. Lombardi, E. Pilozzi, M. Biffoni, M. Todaro, C. Peschle, R. De Maria, Identification and expansion of human colon-cancer-initiating cells, *Nature*, 445 (2007) 111-115.
- [35] S. Chen, X. Song, Z. Chen, X. Li, M. Li, H. Liu, J. Li, CD133 expression and the prognosis of colorectal cancer: a systematic review and meta-analysis, *PloS one*, 8 (2013) e56380.
- [36] S.Y. Lee, K.A. Kim, C.H. Kim, Y.J. Kim, J.H. Lee, H.R. Kim, CD44-shRNA recombinant adenovirus inhibits cell proliferation, invasion, and migration, and promotes apoptosis in HCT116 colon cancer cells, *International journal of oncology*, 50 (2017) 329-336.
- [37] H.C. Hsu, Y.S. Liu, K.C. Tseng, C.L. Hsu, Y. Liang, T.S. Yang, J.S. Chen, R.P. Tang, S.J. Chen, H.C. Chen, Overexpression of Lgr5 correlates with resistance to 5-FU-based chemotherapy in colorectal cancer, *International journal of colorectal disease*, 28 (2013) 1535-1546.
- [38] B. Pardini, R. Kumar, A. Naccarati, J. Novotny, R.B. Prasad, A. Forsti, K. Hemminki, P. Vodicka, J. Lorenzo Bermejo, 5-Fluorouracil-based chemotherapy for colorectal cancer and MTHFR/MTRR genotypes, *British journal of clinical pharmacology*, 72 (2011) 162-163.
- [39] G. Brandi, S. De Lorenzo, M. Nannini, S. Curti, M. Ottone, F.G. Dall'Olio, M.A. Barbera, M.A. Pantaleo, G. Biasco, Adjuvant chemotherapy for resected colorectal cancer metastases: Literature review and meta-analysis, *World journal of gastroenterology*, 22 (2016) 519-533.
- [40] D.L. Dragu, L.G. Necula, C. Bleotu, C.C. Diaconu, M. Chivu-Economescu, Therapies targeting cancer stem cells: Current trends and future challenges, *World journal of stem cells*, 7 (2015) 1185-1201.
- [41] J. Ma, J. Cheng, Y. Gong, L. Tian, Q. Huang, Downregulation of Wnt signaling by sonic hedgehog activation promotes repopulation of human tumor cell lines, *Disease models & mechanisms*, 8 (2015) 385-391.
- [42] A.H. Nwabo Kamdje, P. Takam Kamga, R. Tagne Simo, L. Vecchio, P.F. Seke Etet, J.M. Muller, G. Bassi, E. Lukong, R. Kumar Goel, J. Mbo Amvene, M. Krampera, Developmental pathways associated with cancer metastasis: Notch, Wnt, and Hedgehog, *Cancer biology & medicine*, 14 (2017) 109-120.
- [43] D.Y. Shen, W. Zhang, X. Zeng, C.Q. Liu, Inhibition of Wnt/ β -catenin signaling downregulates P-glycoprotein and reverses multi-drug resistance of cholangiocarcinoma, *Cancer science*, 104 (2013) 1303-1308.
- [44] C. Braicu, M. Buse, C. Busuioc, R. Drula, D. Gulei, L. Raduly, A. Rusu, A. Irimie, A.G. Atanasov, O. Slaby, C. Ionescu, I. Berindan-Neagoe, A Comprehensive Review on MAPK: A Promising Therapeutic Target in Cancer, *Cancers*, 11 (2019).
- [45] Q. Ye, W. Cai, Y. Zheng, B.M. Evers, Q.B. She, ERK and AKT signaling cooperate to translationally regulate survivin expression for metastatic progression of colorectal cancer, *Oncogene*, 33 (2014) 1828-1839.
- [46] A.A. Merchant, W. Matsui, Targeting Hedgehog--a cancer stem cell pathway, *Clinical cancer research : an official journal of the American Association for Cancer Research*, 16 (2010) 3130-3140.
- [47] M. Young, K.R. Reed, Organoids as a Model for Colorectal Cancer, *Current colorectal cancer reports*, 12 (2016) 281-287.
- [48] S. Breslin, L. O'Driscoll, Three-dimensional cell culture: the missing link in drug discovery, *Drug discovery today*, 18 (2013) 240-249.

- [49] C. Zhang, Z. Yang, D.L. Dong, T.S. Jang, J.C. Knowles, H.W. Kim, G.Z. Jin, Y. Xuan, 3D culture technologies of cancer stem cells: promising ex vivo tumor models, *Journal of tissue engineering*, 11 (2020) 2041731420933407.
- [50] A. Radajewska, O. Przybyszewski, F. Emhemmed, C.D. Muller, E. Barg, H. Moreira, Three dimensional in vitro culture systems in anticancer drug discovery targeted on cancer stem cells, *American journal of cancer research*, 11 (2021) 4931-4946.
- [51] X.-L. Ma, Y.-F. Sun, B.-L. Wang, M.-N. Shen, Y. Zhou, J.-W. Chen, B. Hu, Z.-J. Gong, X. Zhang, Y. Cao, B.-s. Pan, J. Zhou, J. Fan, W. Guo, X.-R. Yang, Sphere-forming culture enriches liver cancer stem cells and reveals Stearoyl-CoA desaturase 1 as a potential therapeutic target, *BMC cancer*, 19 (2019) 760.
- [52] J. He, L. Xiong, Q. Li, L. Lin, X. Miao, S. Yan, Z. Hong, L. Yang, Y. Wen, X. Deng, 3D modeling of cancer stem cell niche, *Oncotarget*, 9 (2018) 1326-1345.
- [53] D.D. Fang, Y.J. Kim, C.N. Lee, S. Aggarwal, K. McKinnon, D. Mesmer, J. Norton, C.E. Birse, T. He, S.M. Ruben, P.A. Moore, Expansion of CD133(+) colon cancer cultures retaining stem cell properties to enable cancer stem cell target discovery, *British journal of cancer*, 102 (2010) 1265-1275.
- [54] S. Wang, D. Kanojia, P.-K. Lo, V. Chandrashekar, X. Duan, F. Berger, Q. Wang, H. Chen, Enrichment and Selective Targeting of Cancer Stem Cells in Colorectal Cancer Cell Lines, *Human Genetics & Embryology*, 01 (2012).
- [55] A. Fatehullah, S.H. Tan, N. Barker, Organoids as an in vitro model of human development and disease, *Nature cell biology*, 18 (2016) 246-254.
- [56] M. Huch, J.A. Knoblich, M.P. Lutolf, A. Martinez-Arias, The hope and the hype of organoid research, *Development (Cambridge, England)*, 144 (2017) 938-941.
- [57] T. Sato, R.G. Vries, H.J. Snippert, M. van de Wetering, N. Barker, D.E. Stange, J.H. van Es, A. Abo, P. Kujala, P.J. Peters, H. Clevers, Single Lgr5 stem cells build crypt-villus structures in vitro without a mesenchymal niche, *Nature*, 459 (2009) 262-265.
- [58] T. Sato, D.E. Stange, M. Ferrante, R.G. Vries, J.H. Van Es, S. Van den Brink, W.J. Van Houdt, A. Pronk, J. Van Gorp, P.D. Siersema, H. Clevers, Long-term expansion of epithelial organoids from human colon, adenoma, adenocarcinoma, and Barrett's epithelium, *Gastroenterology*, 141 (2011) 1762-1772.
- [59] J.F. Dekkers, C.L. Wiegerinck, H.R. de Jonge, I. Bronsveld, H.M. Janssens, K.M. de Winter-de Groot, A.M. Brandsma, N.W. de Jong, M.J. Bijvelds, B.J. Scholte, E.E. Nieuwenhuis, S. van den Brink, H. Clevers, C.K. van der Ent, S. Middendorp, J.M. Beekman, A functional CFTR assay using primary cystic fibrosis intestinal organoids, *Nature medicine*, 19 (2013) 939-945.
- [60] N. Barker, M. Huch, P. Kujala, M. van de Wetering, H.J. Snippert, J.H. van Es, T. Sato, D.E. Stange, H. Begthel, M. van den Born, E. Danenberg, S. van den Brink, J. Korving, A. Abo, P.J. Peters, N. Wright, R. Poulsom, H. Clevers, Lgr5(+ve) stem cells drive self-renewal in the stomach and build long-lived gastric units in vitro, *Cell stem cell*, 6 (2010) 25-36.
- [61] M. Huch, C. Dorrell, S.F. Boj, J.H. van Es, V.S. Li, M. van de Wetering, T. Sato, K. Hamer, N. Sasaki, M.J. Finegold, A. Haft, R.G. Vries, M. Grompe, H. Clevers, In vitro expansion of single Lgr5+ liver stem cells induced by Wnt-driven regeneration, *Nature*, 494 (2013) 247-250.

- [62] M. Plodinec, C.A. Schoenenberger, Spatial organization acts on cell signaling: how physical force contributes to the development of cancer, *Breast cancer research : BCR*, 12 (2010) 308.
- [63] M. Matano, S. Date, M. Shimokawa, A. Takano, M. Fujii, Y. Ohta, T. Watanabe, T. Kanai, T. Sato, Modeling colorectal cancer using CRISPR-Cas9-mediated engineering of human intestinal organoids, *Nature medicine*, 21 (2015) 256-262.
- [64] L. Zhou, G. Huang, S. Wang, J. Wu, W.G. Lee, Y. Chen, F. Xu, T. Lu, Advances in cell-based biosensors using three-dimensional cell-encapsulating hydrogels, *Biotechnology journal*, 6 (2011) 1466-1476.
- [65] W. Tan, T.A. Desai, Layer-by-layer microfluidics for biomimetic three-dimensional structures, *Biomaterials*, 25 (2004) 1355-1364.
- [66] M.S. Kim, J.H. Yeon, J.K. Park, A microfluidic platform for 3-dimensional cell culture and cell-based assays, *Biomedical microdevices*, 9 (2007) 25-34.
- [67] J.B. Kim, Three-dimensional tissue culture models in cancer biology, *Seminars in cancer biology*, 15 (2005) 365-377.
- [68] D. Khaitan, S. Chandna, M.B. Arya, B.S. Dwarakanath, Establishment and characterization of multicellular spheroids from a human glioma cell line; Implications for tumor therapy, *Journal of translational medicine*, 4 (2006) 12.
- [69] M. Zietarska, C.M. Maugard, A. Filali-Mouhim, M. Alam-Fahmy, P.N. Tonin, D.M. Provencher, A.M. Mes-Masson, Molecular description of a 3D in vitro model for the study of epithelial ovarian cancer (EOC), *Molecular carcinogenesis*, 46 (2007) 872-885.
- [70] J. Lee, M.J. Cuddihy, N.A. Kotov, Three-dimensional cell culture matrices: state of the art, *Tissue engineering. Part B, Reviews*, 14 (2008) 61-86.
- [71] D. Loessner, K.S. Stok, M.P. Lutolf, D.W. Hutmacher, J.A. Clements, S.C. Rizzi, Bioengineered 3D platform to explore cell-ECM interactions and drug resistance of epithelial ovarian cancer cells, *Biomaterials*, 31 (2010) 8494-8506.
- [72] H. Karlsson, M. Fryknäs, R. Larsson, P. Nygren, Loss of cancer drug activity in colon cancer HCT-116 cells during spheroid formation in a new 3-D spheroid cell culture system, *Experimental cell research*, 318 (2012) 1577-1585.
- [73] I. Serebriiskii, R. Castelló-Cros, A. Lamb, E.A. Golemis, E. Cukierman, Fibroblast-derived 3D matrix differentially regulates the growth and drug-responsiveness of human cancer cells, *Matrix biology : journal of the International Society for Matrix Biology*, 27 (2008) 573-585.
- [74] J.L. Horning, S.K. Sahoo, S. Vijayaraghavalu, S. Dimitrijevic, J.K. Vasir, T.K. Jain, A.K. Panda, V. Labhasetwar, 3-D tumor model for in vitro evaluation of anticancer drugs, *Molecular pharmaceuticals*, 5 (2008) 849-862.
- [75] D.M. Walker, G. Boey, L.A. McDonald, The pathology of oral cancer, *Pathology*, 35 (2003) 376-383.
- [76] K.L. Sodek, M.J. Ringuette, T.J. Brown, Compact spheroid formation by ovarian cancer cells is associated with contractile behavior and an invasive phenotype, *International journal of cancer*, 124 (2009) 2060-2070.
- [77] G.E. Moore, E. Ito, K. Ulrich, A.A. Sandberg, Culture of human leukemia cells, *Cancer*, 19 (1966) 713-723.
- [78] R. Edmondson, J.J. Broglie, A.F. Adcock, L. Yang, Three-dimensional cell culture systems and their applications in drug discovery and cell-based biosensors, *Assay and drug development technologies*, 12 (2014) 207-218.

- [79] M. Kapalczyńska, T. Kolenda, W. Przybyła, M. Zajączkowska, A. Teresiak, V. Filas, M. Ibbs, R. Bliźniak, Ł. Łuczewski, K. Lamperska, 2D and 3D cell cultures - a comparison of different types of cancer cell cultures, *Archives of medical science : AMS*, 14 (2018) 910-919.
- [80] N. Chaicharoenaudomrung, P. Kunhorn, P. Noisa, Three-dimensional cell culture systems as an in vitro platform for cancer and stem cell modeling, *World journal of stem cells*, 11 (2019) 1065-1083.
- [81] A. Monzer, N. Jabotian, F. Ballout, J.S. Zhu, M.J. Kurth, M.J. Haddadin, H. Gali-Muhtasib, Novel 2-(5-Imino-5H-isoquinolones[3,4-b]quinoxalin-7-ylmethyl)-benzonitrile (DIQ3) and Other Related Derivatives Targeting Colon Cancer Cells: Syntheses and in Vitro Models, *ACS omega*, 4 (2019) 3205-3212.
- [82] R.N. Kharwar, A. Mishra, S.K. Gond, A. Stierle, D. Stierle, Anticancer compounds derived from fungal endophytes: their importance and future challenges, *Natural product reports*, 28 (2011) 1208-1228.
- [83] J.L. Bolton, T. Dunlap, Formation and Biological Targets of Quinones: Cytotoxic versus Cytoprotective Effects, *Chemical Research in Toxicology*, 30 (2017) 13-37.
- [84] R.W. Grady, S.H. Blobstein, S.R. Meshnick, P.C. Ulrich, A. Cerami, J. Amirmoazzami, E.M. Hodnett, The in vitro trypanocidal activity of N-substituted p-benzoquinone imines: assessment of biochemical structure-activity relationships using the Hansch approach, *Journal of cellular biochemistry*, 25 (1984) 15-29.
- [85] E.M. Malik, C.E. Müller, Anthraquinones As Pharmacological Tools and Drugs, *Medicinal research reviews*, 36 (2016) 705-748.
- [86] P.S. Guin, S. Das, P.C. Mandal, Electrochemical Reduction of Quinones in Different Media: A Review, *International Journal of Electrochemistry*, 2011 (2011) 816202.
- [87] G. Powis, Metabolism and reactions of quinoid anticancer agents, *Pharmacology & therapeutics*, 35 (1987) 57-162.
- [88] D. Salazar, S.A. Cohen, Multiple tumoricidal effector mechanisms induced by adriamycin, *Cancer research*, 44 (1984) 2561-2566.
- [89] N.R. Bachur, S.L. Gordon, M.V. Gee, H. Kon, NADPH cytochrome P-450 reductase activation of quinone anticancer agents to free radicals, *Proceedings of the National Academy of Sciences of the United States of America*, 76 (1979) 954-957.
- [90] G.A. Zissimou, A. Kourtellaris, M. Manoli, P.A. Koutentis, Redox Active Quinoidal 1,2,4-Benzotriazines, *The Journal of organic chemistry*, 83 (2018) 9391-9402.
- [91] L.J. Keane, S.I. Mirallai, M. Sweeney, M.P. Carty, G.A. Zissimou, A.A. Berezin, P.A. Koutentis, F. Aldabbagh, Anti-Cancer Activity of Phenyl and Pyrid-2-yl 1,3-Substituted Benzo[1,2,4]triazin-7-ones and Stable Free Radical Precursors, *Molecules (Basel, Switzerland)*, 23 (2018).
- [92] N.B. Rumie Vittar, L. Comini, I.M. Fernandez, E. Agostini, S. Nuñez-Montoya, J.L. Cabrera, V.A. Rivarola, Photochemotherapy using natural anthraquinones: Rubiadin and Soranjidiol sensitize human cancer cell to die by apoptosis, *Photodiagnosis and photodynamic therapy*, 11 (2014) 182-192.
- [93] X. Dong, J. Fu, X. Yin, S. Cao, X. Li, L. Lin, J. Ni, Emodin: A Review of its Pharmacology, Toxicity and Pharmacokinetics, *Phytotherapy research : PTR*, 30 (2016) 1207-1218.

- [94] Z. Chen, L. Zhang, J. Yi, Z. Yang, Z. Zhang, Z. Li, Promotion of adiponectin multimerization by emodin: a novel AMPK activator with PPAR γ -agonist activity, *Journal of cellular biochemistry*, 113 (2012) 3547-3558.
- [95] H.J. Kwak, M.J. Park, C.M. Park, S.I. Moon, D.H. Yoo, H.C. Lee, S.H. Lee, M.S. Kim, H.W. Lee, W.S. Shin, I.C. Park, C.H. Rhee, S.I. Hong, Emodin inhibits vascular endothelial growth factor-A-induced angiogenesis by blocking receptor-2 (KDR/Flk-1) phosphorylation, *International journal of cancer*, 118 (2006) 2711-2720.
- [96] I.T. Saunders, H. Mir, N. Kapur, S. Singh, Emodin inhibits colon cancer by altering BCL-2 family proteins and cell survival pathways, *Cancer cell international*, 19 (2019) 98.
- [97] Y. Li, F. Guo, Y. Guan, T. Chen, K. Ma, L. Zhang, Z. Wang, Q. Su, L. Feng, Y. Liu, Y. Zhou, Novel Anthraquinone Compounds Inhibit Colon Cancer Cell Proliferation via the Reactive Oxygen Species/JNK Pathway, *Molecules (Basel, Switzerland)*, 25 (2020).
- [98] M.M. Mehanna, R. Saredidine, J.K. Alwattar, R. Chouaib, H. Gali-Muhtasib, Anticancer Activity of Thymoquinone Cubic Phase Nanoparticles Against Human Breast Cancer: Formulation, Cytotoxicity and Subcellular Localization, *International journal of nanomedicine*, 15 (2020) 9557-9570.
- [99] E.M. Guler, B.H. Sisman, A. Kocyigit, M.A. Hatiboglu, Investigation of cellular effects of thymoquinone on glioma cell, *Toxicology reports*, 8 (2021) 162-170.
- [100] F. Ballout, A. Monzer, M. Fatfat, H.E. Ouweini, M.A. Jaffa, R. Abdel-Samad, N. Darwiche, W. Abou-Kheir, H. Gali-Muhtasib, Thymoquinone induces apoptosis and DNA damage in 5-Fluorouracil-resistant colorectal cancer stem/progenitor cells, *Oncotarget*, 11 (2020) 2959-2972.
- [101] Z. Fatfat, M. Fatfat, H. Gali-Muhtasib, Therapeutic potential of thymoquinone in combination therapy against cancer and cancer stem cells, *World journal of clinical oncology*, 12 (2021) 522-543.
- [102] W. Wang, E.R. Rayburn, S.E. Velu, D. Chen, D.H. Nadkarni, S. Murugesan, D. Chen, R. Zhang, A novel synthetic iminoquinone, BA-TPQ, as an anti-breast cancer agent: in vitro and in vivo activity and mechanisms of action, *Breast cancer research and treatment*, 123 (2010) 321-331.
- [103] F. Wang, S.J. Ezell, Y. Zhang, W. Wang, E.R. Rayburn, D.H. Nadkarni, S. Murugesan, S.E. Velu, R. Zhang, FBA-TPQ, a novel marine-derived compound as experimental therapy for prostate cancer, *Investigational new drugs*, 28 (2010) 234-241.
- [104] N.S. Madhukar, P.K. Khade, L. Huang, K. Gayvert, G. Galletti, M. Stogniew, J.E. Allen, P. Giannakakou, O. Elemento, A Bayesian machine learning approach for drug target identification using diverse data types, *Nature communications*, 10 (2019) 5221.
- [105] R. Benjamin Free, C. Cuoco, V. Prabhu, B. Willette, M. Day, L. Anantharaman, C. Sulli, E. Davidson, S. Deacon, J. Rucker, N. Charter, B. Doranz, W. Oster, M. Stogniew, J. Robert Lane, D. Sibley, J. Allen, EXTH-33. RECEPTOR PHARMACOLOGY OF ONC201: THE FIRST BITOPIC DRD2 ANTAGONIST FOR CLINICAL NEURO-ONCOLOGY, *Neuro-Oncology*, 21 (2019) vi89-vi89.
- [106] S.P. Caragher, R.R. Hall, R. Ahsan, A.U. Ahmed, Monoamines in glioblastoma: complex biology with therapeutic potential, *Neuro Oncol*, 20 (2018) 1014-1025.
- [107] S.P. Caragher, J.M. Shireman, M. Huang, J. Miska, F. Atashi, S. Baisiwala, C. Hong Park, M.R. Saathoff, L. Warnke, T. Xiao, M.S. Lesniak, C.D. James, H. Meltzer, A.K. Tryba, A.U. Ahmed, Activation of Dopamine Receptor 2 Prompts Transcriptomic

and Metabolic Plasticity in Glioblastoma, *The Journal of neuroscience : the official journal of the Society for Neuroscience*, 39 (2019) 1982-1993.

[108] H.W. Cheng, Y.H. Liang, Y.L. Kuo, C.P. Chuu, C.Y. Lin, M.H. Lee, A.T. Wu, C.T. Yeh, E.I. Chen, J. Whang-Peng, C.L. Su, C.Y. Huang, Identification of thioridazine, an antipsychotic drug, as an antiglioblastoma and anticancer stem cell agent using public gene expression data, *Cell death & disease*, 6 (2015) e1753.

[109] J. Li, S. Zhu, D. Kozono, K. Ng, D. Futalan, Y. Shen, J.C. Akers, T. Steed, D. Kushwaha, M. Schlabach, B.S. Carter, C.H. Kwon, F. Furnari, W. Cavenee, S. Elledge, C.C. Chen, Genome-wide shRNA screen revealed integrated mitogenic signaling between dopamine receptor D2 (DRD2) and epidermal growth factor receptor (EGFR) in glioblastoma, *Oncotarget*, 5 (2014) 882-893.

[110] E.J. Meredith, M.J. Holder, A. Rosén, A.D. Lee, M.J. Dyer, N.M. Barnes, J. Gordon, Dopamine targets cycling B cells independent of receptors/transporter for oxidative attack: Implications for non-Hodgkin's lymphoma, *Proceedings of the National Academy of Sciences of the United States of America*, 103 (2006) 13485-13490.

[111] A. Rosas-Cruz, N. Salinas-Jazmín, M.A.V. Velázquez, Dopamine Receptors in Cancer: Are They Valid Therapeutic Targets?, *Technology in cancer research & treatment*, 20 (2021) 15330338211027913.

[112] S.M. DeWire, S. Ahn, R.J. Lefkowitz, S.K. Shenoy, Beta-arrestins and cell signaling, *Annual review of physiology*, 69 (2007) 483-510.

[113] V.V. Prabhu, N.S. Madhukar, C. Gilvary, C.L.B. Kline, S. Oster, W.S. El-Deiry, O. Elemento, F. Doherty, A. VanEngelenburg, J. Durrant, R.S. Tarapore, S. Deacon, N. Charter, J. Jung, D.M. Park, M.R. Gilbert, J. Rusert, R. Wechsler-Reya, I. Arrillaga-Romany, T.T. Batchelor, P.Y. Wen, W. Oster, J.E. Allen, Dopamine Receptor D5 is a Modulator of Tumor Response to Dopamine Receptor D2 Antagonism, *Clinical cancer research : an official journal of the American Association for Cancer Research*, 25 (2019) 2305-2313.

[114] C.L.B. Kline, M.D. Ralff, A.R. Lulla, J.M. Wagner, P.H. Abbosh, D.T. Dicker, J.E. Allen, W.S. El-Deiry, Role of Dopamine Receptors in the Anticancer Activity of ONC201, *Neoplasia (New York, N.Y.)*, 20 (2018) 80-91.

[115] P.R. Graves, L.J. Aponte-Collazo, E.M.J. Fennell, A.C. Graves, A.E. Hale, N. Dicheva, L.E. Herring, T.S.K. Gilbert, M.P. East, I.M. McDonald, M.R. Lockett, H. Ashamalla, N.J. Moorman, D.S. Karanewsky, E.J. Iwanowicz, E. Holmuhamedov, L.M. Graves, Mitochondrial Protease ClpP is a Target for the Anticancer Compounds ONC201 and Related Analogues, *ACS chemical biology*, 14 (2019) 1020-1029.

[116] Y.E. Greer, N. Porat-Shliom, K. Nagashima, C. Stuelten, D. Crooks, V.N. Koparde, S.F. Gilbert, C. Islam, A. Ubaldini, Y. Ji, L. Gattinoni, F. Soheilian, X. Wang, M. Hafner, J. Shetty, B. Tran, P. Jailwala, M. Cam, M. Lang, D. Voeller, W.C. Reinhold, V. Rajapakse, Y. Pommier, R. Weigert, W.M. Linehan, S. Lipkowitz, ONC201 kills breast cancer cells in vitro by targeting mitochondria, *Oncotarget*, 9 (2018) 18454-18479.

[117] A. Ashkenazi, Targeting death and decoy receptors of the tumour-necrosis factor superfamily, *Nature reviews. Cancer*, 2 (2002) 420-430.

[118] J.E. Allen, G. Krigsfeld, P.A. Mayes, L. Patel, D.T. Dicker, A.S. Patel, N.G. Dolloff, E. Messaris, K.A. Scata, W. Wang, J.Y. Zhou, G.S. Wu, W.S. El-Deiry, Dual inactivation of Akt and ERK by TIC10 signals Foxo3a nuclear translocation, TRAIL

- gene induction, and potent antitumor effects, *Science translational medicine*, 5 (2013) 171ra117.
- [119] J.Y. Yang, C.S. Zong, W. Xia, H. Yamaguchi, Q. Ding, X. Xie, J.Y. Lang, C.C. Lai, C.J. Chang, W.C. Huang, H. Huang, H.P. Kuo, D.F. Lee, L.Y. Li, H.C. Lien, X. Cheng, K.J. Chang, C.D. Hsiao, F.J. Tsai, C.H. Tsai, A.A. Sahin, W.J. Muller, G.B. Mills, D. Yu, G.N. Hortobagyi, M.C. Hung, ERK promotes tumorigenesis by inhibiting FOXO3a via MDM2-mediated degradation, *Nature cell biology*, 10 (2008) 138-148.
- [120] J. Ishizawa, K. Kojima, D. Chachad, P. Ruvolo, V. Ruvolo, R.O. Jacamo, G. Borthakur, H. Mu, Z. Zeng, Y. Tabe, J.E. Allen, Z. Wang, W. Ma, H.C. Lee, R. Orłowski, D. Sarbassov dos, P.L. Lorenzi, X. Huang, S.S. Neelapu, T. McDonnell, R.N. Miranda, M. Wang, H. Kantarjian, M. Konopleva, R.E. Davis, M. Andreeff, ATF4 induction through an atypical integrated stress response to ONC201 triggers p53-independent apoptosis in hematological malignancies, *Science signaling*, 9 (2016) ra17.
- [121] C.L. Kline, A.P. Van den Heuvel, J.E. Allen, V.V. Prabhu, D.T. Dicker, W.S. El-Deiry, ONC201 kills solid tumor cells by triggering an integrated stress response dependent on ATF4 activation by specific eIF2 α kinases, *Science signaling*, 9 (2016) ra18.
- [122] H. Ait Ghezala, B. Jolles, S. Salhi, K. Castrillo, W. Carpentier, N. Cagnard, A. Bruhat, P. Fafournoux, O. Jean-Jean, Translation termination efficiency modulates ATF4 response by regulating ATF4 mRNA translation at 5' short ORFs, *Nucleic acids research*, 40 (2012) 9557-9570.
- [123] X. Yuan, D. Kho, J. Xu, A. Gajan, K. Wu, G.S. Wu, ONC201 activates ER stress to inhibit the growth of triple-negative breast cancer cells, *Oncotarget*, 8 (2017) 21626-21638.
- [124] J. Wagner, C.L. Kline, L. Zhou, V. Khazak, W.S. El-Deiry, Anti-tumor effects of ONC201 in combination with VEGF-inhibitors significantly impacts colorectal cancer growth and survival in vivo through complementary non-overlapping mechanisms, *Journal of experimental & clinical cancer research : CR*, 37 (2018) 11.
- [125] J.E. Allen, R.N. Crowder, W.S. El-Deiry, First-In-Class Small Molecule ONC201 Induces DR5 and Cell Death in Tumor but Not Normal Cells to Provide a Wide Therapeutic Index as an Anti-Cancer Agent, *PloS one*, 10 (2015) e0143082.
- [126] V.V. Prabhu, J.E. Allen, D.T. Dicker, W.S. El-Deiry, Small-Molecule ONC201/TIC10 Targets Chemotherapy-Resistant Colorectal Cancer Stem-like Cells in an Akt/Foxo3a/TRAIL-Dependent Manner, *Cancer research*, 75 (2015) 1423-1432.
- [127] Z.Z. Jin, W. Wang, D.L. Fang, Y.J. Jin, mTOR inhibition sensitizes ONC201-induced anti-colorectal cancer cell activity, *Biochemical and biophysical research communications*, 478 (2016) 1515-1520.
- [128] S. El-Soussi, R. Hanna, H. Semaan, A.-R. Khater, J. Abdallah, W. Abou-Kheir, T. Abou-Antoun, A Novel Therapeutic Mechanism of Imipridones ONC201/ONC206 in MYCN-Amplified Neuroblastoma Cells via Differential Expression of Tumorigenic Proteins, *Frontiers in Pediatrics*, 9 (2021).
- [129] Y. Zhang, Y. Huang, Y. Yin, Y. Fan, W. Sun, X. Zhao, K. Tucker, A. Staley, S. Paraghamian, G. Hawkins, V. Prabhu, J.E. Allen, C. Zhou, V. Bae-Jump, ONC206, an Imipridone Derivative, Induces Cell Death Through Activation of the Integrated Stress Response in Serous Endometrial Cancer In Vitro, *Frontiers in oncology*, 10 (2020) 577141.
- [130] J. Jung, T. Dowdy, E. Tabouret, B. Reynolds, J. Allen, M. Larion, M. Gilbert, D. Park, EXTH-58. ONC206, AN IMIPRIDONE FAMILY MEMBER, SUPPRESSES

- GLIOBLASTOMA CELLS VIA BLOCKING CANCER STEMNESS PATHWAYS, *Neuro-Oncology*, 20 (2018) vi97-vi97.
- [131] T.H. Mouhieddine, A. Nokkari, M.M. Itani, F. Chamaa, H. Bahmad, A. Monzer, R. El-Merahbi, G. Daoud, A. Eid, F.H. Kobeissy, W. Abou-Kheir, Metformin and Ara-a Effectively Suppress Brain Cancer by Targeting Cancer Stem/Progenitor Cells, *Frontiers in neuroscience*, 9 (2015) 442.
- [132] W. Abou-Kheir, P.G. Hynes, P. Martin, J.J. Yin, Y.N. Liu, V. Seng, R. Lake, J. Spurrier, K. Kelly, Self-renewing Pten^{-/-} TP53^{-/-} protospheres produce metastatic adenocarcinoma cell lines with multipotent progenitor activity, *PloS one*, 6 (2011) e26112.
- [133] K. Boehnke, P.W. Iversen, D. Schumacher, M.J. Lallena, R. Haro, J. Amat, J. Haybaeck, S. Liebs, M. Lange, R. Schäfer, C.R. Regembrecht, C. Reinhard, J.A. Velasco, Assay Establishment and Validation of a High-Throughput Screening Platform for Three-Dimensional Patient-Derived Colon Cancer Organoid Cultures, *Journal of biomolecular screening*, 21 (2016) 931-941.
- [134] K. Cheaito, H.F. Bahmad, O. Hadadeh, H. Msheik, A. Monzer, F. Ballout, C. Dagher, T. Televizian, N. Saheb, A. Tawil, M. El-Sabban, A. El-Hajj, D. Mukherji, M. Al-Sayegh, W. Abou-Kheir, Establishment and characterization of prostate organoids from treatment-naïve patients with prostate cancer, *Oncology letters*, 23 (2022) 6.
- [135] Y. Zhou, L. Xia, H. Wang, L. Oyang, M. Su, Q. Liu, J. Lin, S. Tan, Y. Tian, Q. Liao, D. Cao, Cancer stem cells in progression of colorectal cancer, *Oncotarget*, 9 (2018) 33403-33415.
- [136] P. Rawla, T. Sunkara, A. Barsouk, Epidemiology of colorectal cancer: incidence, mortality, survival, and risk factors, *Przegląd gastroenterologiczny*, 14 (2019) 89-103.
- [137] L.C. Phua, M. Mal, P.K. Koh, P.Y. Cheah, E.C. Chan, H.K. Ho, Investigating the role of nucleoside transporters in the resistance of colorectal cancer to 5-fluorouracil therapy, *Cancer chemotherapy and pharmacology*, 71 (2013) 817-823.
- [138] L.T.H. Phi, I.N. Sari, Y.G. Yang, S.H. Lee, N. Jun, K.S. Kim, Y.K. Lee, H.Y. Kwon, Cancer Stem Cells (CSCs) in Drug Resistance and their Therapeutic Implications in Cancer Treatment, *Stem cells international*, 2018 (2018) 5416923.
- [139] A. Mitra, L. Mishra, S. Li, EMT, CTCs and CSCs in tumor relapse and drug-resistance, *Oncotarget*, 6 (2015) 10697-10711.
- [140] J. Wagner, C.L. Kline, M.D. Ralff, A. Lev, A. Lulla, L. Zhou, G.L. Olson, B.R. Nallaganchu, C.H. Benes, J.E. Allen, V.V. Prabhu, M. Stogniew, W. Oster, W.S. El-Deiry, Preclinical evaluation of the imipridone family, analogs of clinical stage anti-cancer small molecule ONC201, reveals potent anti-cancer effects of ONC212, *Cell cycle (Georgetown, Tex.)*, 16 (2017) 1790-1799.
- [141] C.T. Ishida, Y. Zhang, E. Bianchetti, C. Shu, T.T.T. Nguyen, G. Kleiner, M.J. Sanchez-Quintero, C.M. Quinzii, M.A. Westhoff, G. Karpel-Massler, V.V. Prabhu, J.E. Allen, M.D. Siegelin, Metabolic Reprogramming by Dual AKT/ERK Inhibition through Imipridones Elicits Unique Vulnerabilities in Glioblastoma, *Clinical cancer research : an official journal of the American Association for Cancer Research*, 24 (2018) 5392-5406.
- [142] A. Dubrovskaya, S. Kim, R.J. Salamone, J.R. Walker, S.M. Maira, C. García-Echeverría, P.G. Schultz, V.A. Reddy, The role of PTEN/Akt/PI3K signaling in the maintenance and viability of prostate cancer stem-like cell populations, *Proceedings of the National Academy of Sciences of the United States of America*, 106 (2009) 268-273.

- [143] D.A. Altomare, J.R. Testa, Perturbations of the AKT signaling pathway in human cancer, *Oncogene*, 24 (2005) 7455-7464.
- [144] V.V. Prabhu, S. Morrow, A. Rahman Kawakibi, L. Zhou, M. Ralff, J. Ray, A. Jhaveri, I. Ferrarini, Y. Lee, C. Parker, Y. Zhang, R. Borsuk, W.I. Chang, J.N. Honeyman, F. Tavora, B. Carneiro, A. Raufi, K. Huntington, L. Carlsen, A. Louie, H. Safran, A.A. Seyhan, R.S. Tarapore, L. Schalop, M. Stogniew, J.E. Allen, W. Oster, W.S. El-Deiry, ONC201 and imipridones: Anti-cancer compounds with clinical efficacy, *Neoplasia (New York, N.Y.)*, 22 (2020) 725-744.
- [145] V.V. Prabhu, A.R. Lulla, N.S. Madhukar, M.D. Ralff, D. Zhao, C.L.B. Kline, A.P.J. Van den Heuvel, A. Lev, M.J. Garnett, U. McDermott, C.H. Benes, T.T. Batchelor, A.S. Chi, O. Elemento, J.E. Allen, W.S. El-Deiry, Cancer stem cell-related gene expression as a potential biomarker of response for first-in-class imipridone ONC201 in solid tumors, *PloS one*, 12 (2017) e0180541.
- [146] J. Wagner, C.L. Kline, L. Zhou, K.S. Campbell, A.W. MacFarlane, A.J. Olszanski, K.Q. Cai, H.H. Hensley, E.A. Ross, M.D. Ralff, A. Zloza, C.B. Chesson, J.H. Newman, H. Kaufman, J. Bertino, M. Stein, W.S. El-Deiry, Dose intensification of TRAIL-inducing ONC201 inhibits metastasis and promotes intratumoral NK cell recruitment, *The Journal of clinical investigation*, 128 (2018) 2325-2338.